

**Role of proteolipid protein (PLP/Dm20) and polyunsaturated fatty acids
in normal and pathological central nervous system**

Inaugural-Dissertation

zur

Erlangung des Doktorgrades

der Mathematisch-Naturwissenschaftlichen Fakultät

der Universität zu Köln



vorgelegt von

Raju Chintha

aus Warangal, India

Köln, 2012

The present work has been done in the Molecular Neuroscience Laboratory of Medical Faculty
of the University of Cologne/Köln under the direct supervision of
Prof. Dr. Dr. Dr. h.c. mult. Wilhelm Stoffel.

REFEREES/ BERICHTERSTATTER

1. Berichterstatter: Prof. Dr. Dr. Dr. h.c. mult. Wilhelm Stoffel
2. Berichterstatter: Prof. Dr. Günter Schwarz

Vorsitzender: Prof. Dr. Siegfried Roth

Tag der mündlichen Prüfung: 04 December 2012

I thank Professor Dr. Dr. Dr. h.c. mult. Wilhelm Stoffel for giving this opportunity to do my PhD thesis under him and for the very interesting PhD thesis topic. I am also very thankful for his generous support, patience and for his immense guidance and comments throughout my PhD work.

My sincere thanks to Prof. Dr. Günter Schwarz for evaluating my PhD thesis work and being in my PhD thesis committee, and I also thank Prof. Dr. Siegfried Roth for being in my PhD thesis committee and for evaluating my PhD thesis work credentials.

My sincere thanks and gratitude towards all my lab members: Frau Erika Binczek, Frau Brigitte Handwerk, Frau Barbara Holz, Frau Britta Jenke, Dr. Ina Hammels und Frau Inga Schmidt-Soltau for creating wonderful atmosphere in the lab.

Once again, I am grateful to Dr. Ina Hammels for friendly in depth subject discussions, unending chats, and for German language help during my PhD. I would like to thank Frau Erika Binczek for her incredible teachings and discussions on molecular biology and biochemical protocols and techniques. I thank Frau Britta Jenke for Pronuclear Injections, Frau Barbara and Frau Inga Schmidt-Soltau for helping me in the cell culture laboratory, and last but not least Frau Brigitte Handwerk for caring my laboratory mice in the animal house.

I also thank to our collaborators at Institute for Anatomy in helping us by giving access to their electron microscope and in supplying behavioral physiology protocols, I am thankful to Milteny Biotech (Bergisch Gladbach, Cologne) for Macs Kits and wonderful technical comments and assistance when ever needed. I thank Ingo Voigt, Max-Planck Institute for Ageing, Cologne, for his assistance in pronuclear and blastocyst injections, and I also thank Analytical department, CMMC Institute, Cologne, for DNA sequencing

My heartily, personal thanks to Dr. Praveen Mamidala, Ohio University, USA, for being as my well wisher in all respects of my professional life and helping me in accomplishing my PhD goal. I also thank him for giving me his wonderful in time suggestions whenever I needed.

I thank Dr. Rehan Villani, CMMC, University of Cologne, Germany, for critically reading some parts of my thesis and for her valuable comments.

I also thank Jun. Prof. Dr. Thalapalli Shirisha Sai for her invaluable time to time discussions on organic chemistry and on lipid chemistry related topics, and for the immense support.

Last but not least, I thank my sweet family especially to the little girl Madella Jeevana Priya Mani Goud, for their incredible constant moral support and never ending unconditional love.

*Dedicated to my beloved
father Chintha Venkataswamy Goud and
mother Kalavathi*

Index

1 Introduction.....	1
1.1 Central nervous system.....	1
1.2 Oligodendrocytes.....	2
1.2.1 Targeting of myelin components in oligodendrocytes.....	3
1.2.2 Nestin and MBP expression.....	4
1.3 CNS Myelin.....	5
1.4 CNS Myelin; Proteolipid protein (PLP).....	9
1.4.1 PLP gene transcripts and isoproteins.....	10
1.4.2 Cys residues and hydrophobic properties.....	11
1.4.3 PLP related myelin disorders; PMD and SPG2.....	13
1.5 CNS Myelin; Phospho- and sphingolipids.....	14
1.5.1 Fatty acid composition of phospholipids.....	16
1.5.2 Classification of fatty acids and the polyunsaturated fatty acids (PUFAs) synthesis cascade.....	18
1.5.3 PUFAs in the CNS.....	20
1.5.4 Retinal morphology.....	21
1.5.5 Fads2 knock-out mouse (PUFAs deficient mouse model).....	22
1.6 Transgenic mouse models.....	22
1.6.1 Gene targeting.....	22
1.6.2 Pronuclear microinjection.....	23
1.7 Site-directed mutagenesis.....	24
2 Aim of the thesis.....	25
3 Results.....	26
3.1 Construction of mutant cDNA pool of PLP and Dm20.....	26
3.1.1 Site-directed mutagenesis (SDM) and Overlap extension PCR.....	26
3.1.2 DNA sequencing.....	28
3.2 <i>In silico</i> Kyte-Doolittle hydropathy plots.....	30
3.3 EGFP fused WT-PLP, Mut-PLP, and Mut-Dm20; Intracellular trafficking.....	33
3.3.1 Cloning and validation of WT-PLP-EGFP, Mut-PLP-EGFP and Mut- Dm20- EGFP.....	33
3.3.2 Mut-PLP-EGFP and Mut-Dm20-EGFP compared to WT-PLP-EGFP trafficking in COS-7	34
3.3.3 WT-PLP-EGFP and Mut-PLP-EGFP trafficking in PLP null oligodendrocytes.....	37
3.3.3.1 Isolation and transfection of PLP-null murine oligodendrocytes.....	37
3.3.3.2 WT-PLP-EGFP and Mut-PLP-EGFP membrane targeting in oligodendrocytes.....	37
3.4 Mut-PLP expression under the control of Nestin-enhancer; generation of a transgenic mutant.....	39
3.4.1 Validation of Nestin enhancer function in OLN93 cells.....	39
3.4.2 Trans-gene cloning and pronuclear injection.....	41
3.5 Generation of knock-in mouse mutant of PLP/Dm20 devoid of di-sulfide bridges.....	43
3.5.1 Knock-in targeting construct and targeting strategy.....	43

3.5.2	ES cells electroporation and ES clones screening.....	45
3.5.3	Verification of a positive ES clone.....	46
3.5.4	Mutated Cys residues validation by DNA sequencing.....	47
3.5.5	Karyotyping of positive ES clone.....	48
3.5.6	Embryo manipulation... ..	48
3.5.7	Chimera validation and breeding.....	49
3.6	PLP and PUFAs pivotal role in the CNS.....	50
3.6.1	Generation of plp-/-fads2-/- double mutant mouse (DM).....	50
3.6.2	Genotyping and validation of DM.....	51
3.6.3	Phenotyping of DM.....	53
3.6.4	Gene expression analysis by semi-quantitative RT-PCR.....	55
3.6.5	Brain and myelin protein analysis.....	56
3.6.6	Myelin quantification.....	57
3.6.7	Immunohistochemical stainings.....	58
3.6.8	Lipid analysis.....	60
3.6.8.1	Brain lipid analysis.....	60
3.6.8.2	Brain fatty acid profile.....	61
3.6.8.3	Brain phospholipids and glycosphingolipids fatty acid profile	63
3.6.8.4	Myelin lipid and fatty acid profile analysis.....	64
3.6.9	Morphology of the myelin sheath.....	66
3.6.10	Retinal morphology and function.....	67
3.6.11	Behavioral physiology.....	69
3.6.11.1	Rotarod Task (Wallace <i>et al.</i> , 1980).....	69
3.6.11.2	Horizontal-Rod Task (Wallace <i>et al.</i> , 1980).....	70
3.6.11.3	Grid Task.....	71
3.6.11.4	Open field Task (Barclay <i>et al.</i> , 1982).....	72
3.6.11.5	T-Maze Task	72
3.6.11.6	Morris Water-Maze Task (Morris <i>et al.</i> , 1984).....	73
4	Summary of Results.....	76
5	Discussion.....	80
5.1	Cys residues are critical for PLP and Dm20 targeting to the Cell surface.....	80
5.1.1	Similar trafficking of Mut-PLP and Mut-Dm20 in COS-7 cells and PMD.....	81
5.1.2	Differential trafficking <i>in vitro</i> and <i>in vivo</i>	81
5.1.3	Cys-mut PLP (Mut-PLP) expression in early CNS developmental stages.....	82
5.1.3.1	Validation of Nestin enhancer regulation of Mut-PLP.....	82
5.1.3.2	Generation of a transgenic mouse expressing Mut-PLP regulated by the Nestin enhancer region.....	82
5.2	Knock-in mouse mutant of PLP/Dm20-lacking disulfide bridges.....	83
5.3	The role of PLP and PUFA in the CNS.....	84
6	Materials and methods.....	88
6.1	Cell culture methods.....	88
6.1.1	Oligodendrocytes preparation and transfection	88
6.1.2	ES cell culture.....	88

6.1.3	Electroporation and Selection of ES cells.....	89
6.1.4	Karyotyping of ES cells.....	90
6.1.5	Cryopreservation of ES cells and COS-7 cells.....	91
6.1.6	Thawing and expansion of ES-cells and COS-cells.....	91
6.1.7	COS-7 cell culture and transfection.....	91
6.1.8	Embryonic fibroblasts culture.....	91
6.1.9	Lipofection (DNA-Lipofectamine 2000), Electroporation of COS-7 and OLN93 cells.....	92
6.1.10	Stable selection of COS-7 or OLN93 cells.....	92
6.2	Molecular biology methods.....	92
6.2.1	Plasmid-DNA preparation.....	92
6.2.2	Extraction of DNA from agarose gels.....	93
6.2.3	DNA isolation from ES cells or COS-7 cells.....	93
6.2.4	Genomic DNA isolation from mouse tail.....	93
6.2.5	Restriction analysis/digestion.....	94
6.2.6	Ligation.....	94
6.2.7	Preparation of Competent Cells and transformation of plasmid DNA.....	94
6.2.8	Polymerase chain reaction (PCR).....	95
6.2.9	DNA sequencing and Synthesis of oligonucleotide.....	96
6.2.10	RNA preparation.....	96
6.2.11	RT-PCR (Reverse transcription-PCR).....	96
6.2.12	Radioactive DNA labeling.....	97
6.3	Biochemical methods.....	97
6.3.1	Protein quantification.....	97
6.3.2	SDS-polyacrylamide gel electrophoresis (SDS-PAGE).....	98
6.3.3	Myelin preparation (Based on sucrose gradient separation).....	98
6.3.4	Lipid analysis.....	98
6.3.5	Gas Chromatography–Mass Spectrometry (GC-MS).....	99
6.4	Immunological methods.....	100
6.4.1	Western blotting.....	100
6.4.2	Immunostaining of cells.....	101
6.4.3	Mouse brain fixation for cryo-sectioning.....	101
6.4.3.1	Cryo-sections immunohistochemical staining.....	102
6.4.4	Mouse brain fixation for paraffin sectioning.....	102
6.4.4.1	Paraffin sections immunohistochemical and hematoxylin-eosin staining.....	103
6.5	Electron microscopy.....	103
6.6	Methods for generating mice mutants (Transgenic and Knock-in mutants).....	103
6.6.1	Mice maintenance.....	103
6.6.2	Microinjection.....	104
6.6.3	Vasectomized males.....	104
6.6.4	Blastocyst injection.....	104
6.7	Behavioral physiology.....	105
6.7.1	Rotarod.....	105
6.7.2	Horizontal rod and Grid task.....	105
6.7.3	T-maze.....	106

6.7.4 Open field.....	106
6.7.5 Morris water maze (Morris <i>et al.</i> , 1984).....	106
6.8 Bioinformatic programs and servers.....	107
7 Appendix.....	108
7.1 Plasmids used in the present study.....	108
7.2 Oligonucleotides.....	108
7.3 Abbreviations.....	110
8 References.....	113
Zusammenfassung (Abstract in German language).....	126
Abstract.....	128

1 Introduction

1.1 Central nervous system

The CNS of vertebrates consists of the brain, spinal cord and retina. The brain is made up of extensive and complex networks of neurons and their supporting cells termed as glial cells. Neurons are interconnected by synaptic junctions and are involved mainly in conduction of rapid action potential signals along their axons. Compared to neurons, glial cells are more abundant in the CNS i.e., accounting for approximately 65% of cells in rodent brain and 90% in humans (Pfrieger und Barres, 1995). Virchow in 1846 for the first time described glial cells as neuroglia and later they were more extensively described by Ramon y Cajal and Rio-Hortega in 1913. Glial cells are predominantly involved in supporting neurons and maintaining metabolic homeostasis in the CNS. They are broadly classified into astrocytes, oligodendrocytes, and microglia, based on their functional significance. Glial cells including astrocytes and oligodendrocytes are derived from ectodermal tissue of the developing embryo, whereas microglial cells are derived from hematopoietic precursors.

Astrocytes are star shaped cells and are majorly populated among the glial cell population within the brain. They are distributed in the grey and white matter of the brain. Immature astrocytes are called radial glia, which play a major role in neuronal migration during fetal development. Astrocytes are mainly involved in regulating the external chemical environment in the brain such as recycling neurotransmitters released during synaptic transmission, and also provide growth factors to neurons. Astrocytes contact blood capillaries and the nodes of Ranvier (Figure 1) and are also involved in angiogenesis (Montgomery *et al.*, 1994). Microglia functions as brain macrophages of the CNS and account for 15% of total glial cells. They are mainly involved in phagocytosis (Compston *et al.*, 1997) and are typically in the resting state and are activated under conditions like CNS inflammation, trauma, and infections. Microglial cells are the resident macrophages in the brain. Oligodendrocytes are involved in the myelination of axons in the CNS, whereas Schwann cells are involved in PNS.

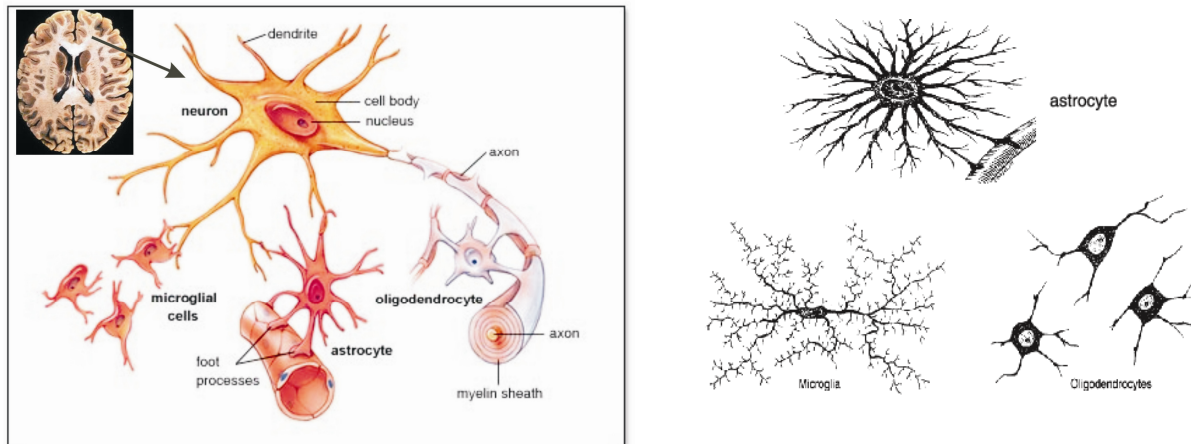


Figure 1: Neuron and glial cells in the brain. Left; Oligodendrocytes wrapping myelin sheath around neuronal axons, astrocytes are attached to blood capillaries, neurons and microglial cells, Right; Individual glial cells i.e., astrocytes, microglia and oligodendrocytes (modified from MHHE science resource)

1.2 Oligodendrocytes

Rio-Hortega first described oligodendrocytes and microglia in 1928. Like neuronal progenitors, early oligodendrocytes progenitors are derived from neuroepithelial precursors of the ventricular zone of the brain and lumen of the spinal cord (Reynolds and Wilkin, 1988; Levine and Goldman, 1988). Mature oligodendrocytes develop from their early progenitors broadly in four stages i.e., early progenitor cells (O2A cells), late progenitor cells (A2B5, O4 cells), premature oligodendrocytes and mature oligodendrocytes (Figure 2). All these differentiation stages undergo several morphological changes starting from single or bipolar to multiple projections, and express cell specific antigen markers such as NG2, O4, GalC, MBP, and PLP (Figure 2) along with several other intracellular changes (Wia Baron, 2003). The early glial progenitors exhibit lineage plasticity such as neural stem cell like features of differentiation into neuronal or any of the glial cell types (Kondo and Raff, 2000c), whereas O4 progenitors (OL-progenitors) are the start of the committed oligodendrocyte lineage. Immature-oligodendrocytes express galactocerebrosides and other myelinating proteins such as MBP and Dm20 which are transported and enriched at the filopodial-like projections of the plasma membrane, whereas they are not capable of myelinating axons. Pre or mature-oligodendrocytes are involved in myelinating axons with their plasma membrane derived filopodia-like structures. Oligodendrocytes are also capable of expressing myelin genes and develop filopodia-like projections in the devoid of external neuronal signals under *in vitro* conditions (Pfeiffer *et al.*, 1993).

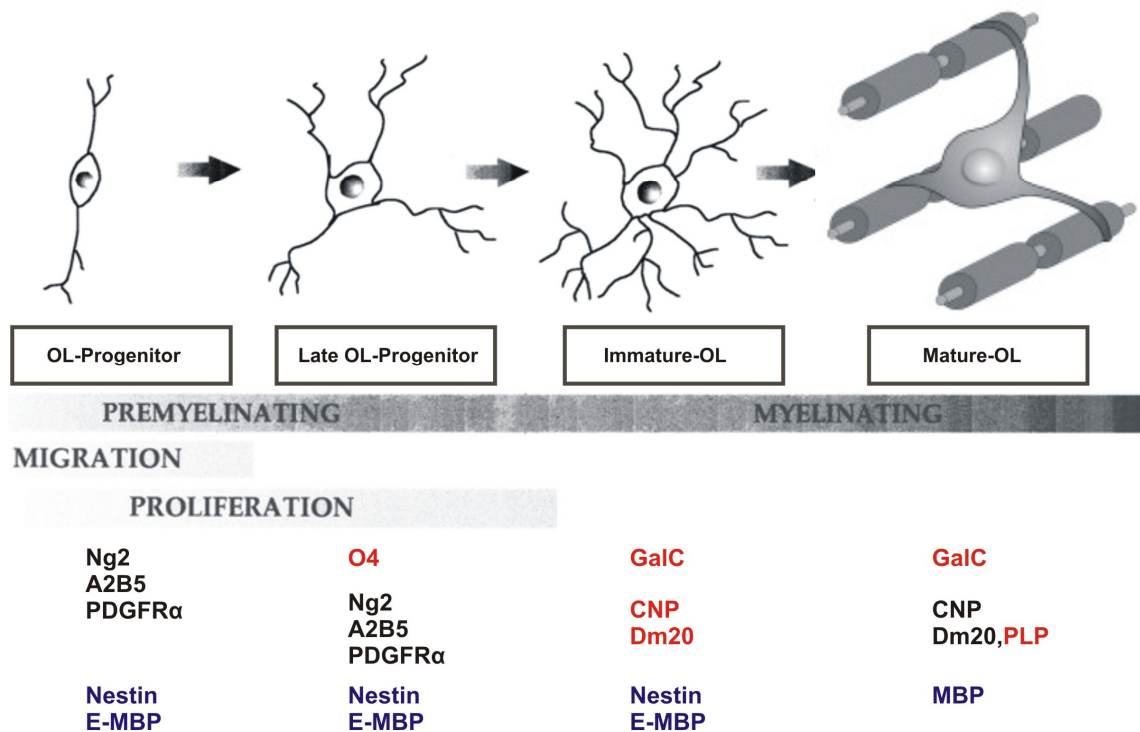


Figure 2: Developmental stages of oligodendrocytes from early progenitors. Different cell specific gene markers expressed during oligodendrocyte maturation; OL=Oligodendrocyte. (Modified from Back SA *et al.*, 2007)

1.2.1 Targeting of myelin components in oligodendrocytes

Oligodendrocytes have highly specialized mechanisms for sorting and targeting myelin protein and lipid components to the growing polarized plasma membrane/myelin membrane. Oligodendrocytes share similarities with polarized epithelial cells, such as MDCK cells, in the underlying mechanisms of protein trafficking to the plasma membrane (Kramer *et al.*, 2001). Polarized cells like MDCKs are therefore suitable *in vitro* cell culture models for studying the underlying mechanisms of myelin proteins trafficking. For instance, transfection studies in MDCK cells showed differential trafficking among myelin proteins; PLP is sorted to the apical membrane and MOG sorted to the basolateral membrane (Kroepfl and Gardinier, 2001). Among the two isoforms of MAG i.e., S-MAG and L-MAG, L-MAG is targeted to both apical and basolateral compartments, whereas S-MAG is targeted only to the apical domain (Minuk and Braun, 1996).

In oligodendrocytes, PLP is transported from the ER to the cell surface via mechanisms including vesicular transport, endosome, and transcytosis. Polarized trafficking of myelin proteins and lipids, such as PLP and GalC, may include initial sorting at trans-Golgi or in endosomes accordingly and then transported to specific plasma membrane domains directly or via cytoskeleton anchored transport in a spatial and temporal manner. MBP and MOBP's mRNA isoforms are transported near to the plasma membrane where actually their protein translation is initiated (Barbarese *et al.*, 1995). CNP is transported anchored to the cytoskeleton, such as actin filaments and microtubules, to the non-compact myelin membrane regions (Laezza *et al.*, 1997). The exact trafficking routes of myelin components, especially mutated myelin proteins, and their mechanisms of plasma membrane targeting are still under investigation.

1.2.2 Nestin and MBP expression

Nestin protein is an intermediate filament protein that is specifically expressed in neural tube, neuroepithelium stem cells and in glial precursors (Lendahl *et al.*, 1990). Nestin is also expressed in neural stem cells and in its subsequent generations of neuronal progenitors and glial progenitors (Zimmerman *et al.*, 1994, Johansson *et al.*, 2002). In the oligodendroglial lineage, nestin expression levels are gradually down-regulated from immature-oligodendrocyte to mature oligodendrocytes (Vittorio Gallo and Regina C Armstrong, 1995). The nestin gene contains four exons and three introns and is highly conserved among human, rat and mouse (Lendhal U *et al.*, 1990; Lothian *et al.*, 1999). The second-intron enhancer of the nestin gene is particularly critical as it contains regulatory elements proposed to regulate gene expression specifically in the neural stem cells and in subsequent oligodendrocyte progenitors (Zimmermann *et al.*, 1994, Lothian *et al.*, 1999).

Of the two major myelin proteins synthesized in oligodendrocytes, PLP and MBP, MBP has a stronger promoter for transcription initiation than PLP. 1.5kb of intron-I and partial-exon-I of MBP gene sequence containing the MBP promoter has been well characterized in a transgenic mouse mutant (Kimura *et al.*, 1989). Although MBP is a marker for mature-oligodendrocytes, an MBP isoform is also detected in early embryonic developmental stages, on both the protein and mRNA level, and is called embryonic-MBP or E-MBP (Mathisen *et al.*, 1993; Nakajima *et al.*, 1993). As characterized in wild-type mice, E-MBP expression is observed in early embryonic stages, postnatal day-7, day-20 (active-myelination phase) and day-60 (matured-myelination phase) (kimura *et al.*, 1989).

1.3 CNS Myelin

Myelin has been first described and termed by Rudolf Virchow in 1854 and its ultra structure first studied by Sjostrand in 1947 by electronic microscopy. Myelin is a highly regulated plasma membrane extension of oligodendrocytes in the CNS, and Schwann cells in the PNS. In the CNS, the plasma membrane of oligodendrocytes or myelin is spirally wrapped around the axons of neurons in multiple locations termed internodes (Figure 3.A). Periodic interruptions between two internodes that leave the axon unmyelinated are termed nodes of Ranvier (N), and the edges of the internode are termed paranodes (PN) (Figure 3 C, B).

Internodes and myelin compaction

Spirally wrapped internodal myelin layers are compacted due to van der Waals, and electrostatic forces between polar head groups of phospho- and sphingolipids, as well as interactions of phospholipids with cytosolic MBP and integral membrane proteins such as PLP. In electron micrographs myelin layers appear as periodic structures of electron dense lines termed major-dense lines (MDL) and less electron-dense lines termed intraperiod lines (IPL) (Figure 3.D). MDLs represent the tight opposition of cytoplasmic sides while IPLs represent the extracellular side of the myelin membrane. Myelin proteins such as PLP, MAG and MOG are integrated into the cholesterol-phospho- and sphingolipid bilayer of the myelin membrane (Figure 3D). The periodicity distance between two IPL is $170 \pm 7 \text{ \AA}$. Occasionally the compact cytoplasm, i.e. MDL, is interrupted and compaction is lost, forming funnel like longitudinal structures along the MDL, called Schmidt-Lanterman clefts however these are very rare in CNS and more abundant in PNS.

Paranodes and junctions

Paranodes are the end points of internode (Figure 3 C, B). The periaxonal space of the myelin is sealed from the outside milieu and connected to the axon via septate-like junctions (Einheber *et al.*, 1997; Saher *et al.*, 2011) (Figure 3B). The paranodal loops or junctions are connected with the axons by tight junction proteins such as OSP or Claudin-11 (Figure 3 B). Paranodal junctions are critical for efficient action potential propagation and in ion channel clustering (Schafer *et al.*, 2004). The outer most part of paranode is termed juxtaparanodal (JPN) region.

Nodes of Ranvier

Louis-Antoine Ranvier discovered regularly spaced unmyelinated gaps (approximately 1 μm in length) termed nodes of Ranvier (Figure 3.B). They harbor voltage-gated sodium (Na^+) ion channels that are engaged in conduction of action potentials. Myelinated axons have salutatory conduction in the range of 1 m/s to over 100 m/s, 0.5m/s to 15 m/s in unmyelinated axons (Mutschler, 1991), thus enhancing the conductance 10-fold compared to unmyelinated axons.

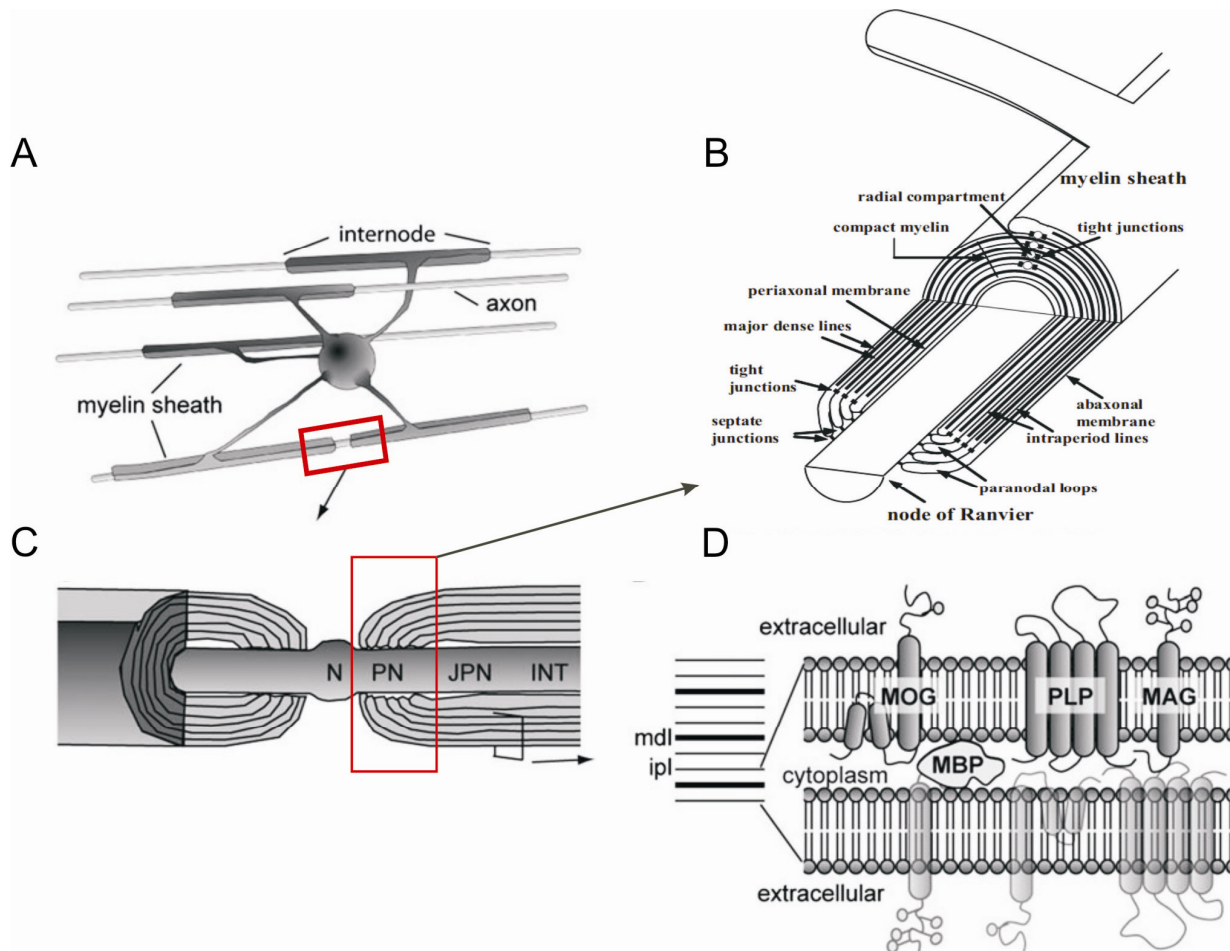


Figure 3: Schematic representation of CNS myelin. A. An oligodendrocyte myelinating multiple axons. B. Zoomed view depicting paranodal junction and its molecular arrangement C. Zoomed view representing node of Ranvier (N), paranodal junction (PN) juxtaparanodal junction (JPN) and internode (INT), and D. Zoomed view of myelin membrane extracellular side and cytoplasmic arrangement, intraperiod lines (IPL), myelin dense line (MDL), and embedded myelin proteins in the myelin membrane. (Adapted and modified from Potter *et al.*, 2010)

Myelin proteins

Myelin accounts for 30% of the dry weight of the brain. Myelin is a lipid rich membrane, with 70-80% lipids and 20-30% proteins. The myelin membrane is composed of unusual sphingolipid classes and high cholesterol and myelin specific proteins.

The most abundant proteins of myelin are proteolipid protein (PLP) and myelin basic protein (MBP) constituting 50% and 30%, respectively, together making 80% of whole myelin protein composition. PLP and MBP localization in the myelin membrane was first identified based on immunolocalization studies (Hartman *et al.*, 1982). Other myelin proteins are: 2', 3'-cyclic nucleotide-3'-phosphodiesterase (CNP) 4-5%, myelin associated glycoprotein (MAG) 1%, and myelin oligodendrocyte glycoprotein (MOG) and myelin-oligodendrocyte basic protein (MOBP) >1% each (S. A. Kalwy and Ross Smith, 1994). Recently several hundreds of distinct proteins of low range concentrations were detected in the myelin through gel based proteome analysis (Werner *et al.*, 2007).

Proteolipid protein (PLP) is further discussed in section 1.4.

Myelin basic protein (MBP)

MBP has several splice variants which differ in different species, four in humans, and six in mice, with protein sizes ranging from 14 to 24kDa (Newman *et al.*, 1987). MBP contains a high number of basic amino acid residues and is a hydrophilic protein localized in the cytoplasm of the myelin membrane (MDL) (figure 3 D). As MBP is highly positively charged, it may interact with the cytoplasmic side myelin membrane, thereby contributing to compaction and stabilization of the myelin membrane (Figure 3 D) (Morell *et al.*, 1994). Although MBP null mice (shiverer mutant or myelin deficient mutants) show compact myelin around the axons, its hypomyelination causes severe neurological defects including tremors and seizures (Bird *et al.*, 1978). Several types of post-translational modifications occur on MBP such as acetylation, phosphorylation, methylation and citrullination (Wood and Moscarello, 1989). Furthermore methylation of MBP might be important for compaction of myelin sheath (Campagnoni *et al.*, 1993). MBP is also present in PNS which accounts for 5-15 % of total proteins.

Myelin-associated glycoprotein (MAG)

MAG is an integral membrane glycoprotein with a molecular mass of 100 kDa. It has two isoforms; L-MAG and S-MAG. MAG is involved in axon-glial contacts and signaling, and axonal maintenance (Poltorak *et al.*, 1987). The majority of MAG is located in periaxonal regions of myelin (Webster *et al.*, 1983). Its structural role in the myelin sheath is not clear.

Myelin-oligodendrocyte glycoprotein (MOG) and other proteins

MOG is an integral membrane glycoprotein which was first identified as one of the antigens in experimental autoimmune encephalomyelitis (EAE). MOG is highly glycosylated and is believed to act as an adhesion molecule. MOG is also involved in signal transduction pathways, and lipid-protein sorting (Kim and Pfeiffer, 1999).

Other myelin proteins such as: CNP is located in the cytoplasm and one of the earliest expressed proteins during myelination. Although CNP is named after its function and believed to have a structural role, its functional role in CNS remains to be elucidated. Adult CNP null mice showed axonal swellings and axonal degeneration. The double mutant *plp^{-/-}cnp^{-/-}* mice showed progressive axonal loss (J.M. Edgar *et al.*, 2009). Other myelin proteins such as myelin-associated oligodendrocytic basic protein (MOBP) and tight junction proteins like oligodendrocyte specific protein (OSP)/Claudin-11 are minor components among myelin proteins with undefined functions. Due to various transgenic mouse mutants, it is now clear that the tight junction proteins including OSP protein are important in proper CNS myelination and function.

Myelin proteins and respective phenotypes

Myelin is a complex unique membrane, and many proteins are specific to myelin. Many studies have been made during the past two decades also by employing transgenic mice. Various myelin proteins, respective knockout mouse mutants, and their phenotypes are summarized in the table 1.

Myelin Protein	Location and function	Null-mouse mutants and their myelin phenotype
PLP/Dm20 (Hydrophobic and Integral membrane spanning protein)	Localized to myelin membrane internodes, involved in myelin compaction and long term axonal stabilization.	Loss of myelin compaction (Dissociation of outer surface, IDL); Late onset of axonal degeneration (Boison and Stoffel, 1994; Griffiths <i>et al.</i> , 1998)
MBP (Hydrophilic and Peripheral membrane protein)	Localized in cytoplasm (MDL), and might be also involved in compaction of myelin	Hypomyelination but myelin remains compact, Increased number of oligodendrocytes (Bird <i>et al.</i> , 1978; Nagara <i>et al.</i> , 1983)
MAG (Glycoprotein and Integral membrane protein)	Present at periaxonal membrane, and involved in maintenances of periaxonal collar	Reduced cytoplasmic collar, multiple myelin sheaths (CNS). (Li <i>et al.</i> , 1994)
CNP (Membrane associated protein)	Localized to cytoplasmic channels, paranodal loops, and axon-glia interactions	Early axonal degeneration (Lee <i>et al.</i> , 2005; Rasband <i>et al.</i> , 2005)
OSP/Claudin11 Integral membrane protein, and belongs to claudin tight junction protein family	Majorly localized to paranodal septet junctions and radial compartment	Loss of tight junctions at paranodal loops, and mild motor impairments (Gow <i>et al.</i> , 1999)

Table 1: Summary of the major myelin proteins and their functional significance in myelin

1.4 CNS Myelin; Proteolipid Protein (PLP)

In 1951 Folch and Lees isolated PLP, the major protein accounting approximately 50% of total brain myelin protein. PLP cDNA has been cloned in 1986 in our laboratory (Schaich *et al.*, 1986).

1.4.1 PLP gene transcripts and isoforms

The PLP (*plp1*) gene is 16 kb (Diehl *et al.*, 1986) and is located on the X-chromosome, Xq22 in human and H2C in mice. The PLP gene is comprised of seven exons (Diehl *et al.*, 1986; Stoffel *et al.*, 1985) and has a protein coding region of 828 bps that encodes 276 amino acids (Stoffel *et al.*, 1982). PLP has a splice variant called Dm20. Dm20 mRNA lacks the last 105 bps of exon 3 of PLP mRNA and thereby 35 amino acids in the cytosolic loop of PLP (Nave *et al.*, 1987). PLP is expressed primarily in oligodendrocytes where it is integrated into the plasma membrane. PLP has been extensively studied for more than 20 years, on the molecular and structural level, and regarding its role in myelin morphology specifically in relation towards CNS myelin disorders. PLP is highly conserved. Specific point mutations in PLP result in the severe form of Pelizaeus–Merzbacher disease (PMD) (Weimbs *et al.*, 1990) or spastic paraplegia type 2 (SPG2) (Koeppen and Robitaille, 2002), whereas the absence of PLP does not result in PMD nor in myelin defects but only in loss of myelin compaction (Boison and Stoffel, 1994) and axonal degeneration in adults (Griffith *et al.*, 1998). Strikingly, the wild-type PLP gene over-expression in mouse models (i.e., PLP transgenic mouse model) revealed that PLP over-expression alone imparts toxicity in the oligodendrocytes and thus causes myelin defects that could result in PMD condition, demonstrating the importance of PLP gene dosage (Karim *et al.*, 2007).

In addition to the classical PLP and its isoform Dm20, Bongarzone *et al.*, 1999 showed an additional exon and translational site between exon-I and exon-II of the classical PLP gene. The derived mRNA can also be alternatively spliced into two new isoforms called sr.PLP and sr.Dm20. Their corresponding protein products contain an additional 11 amino acids. These novel isoforms (i.e., sr.PLP and sr.Dm20) accounts to 2% of total myelin protein composition, restricted to the somata of oligodendrocytes and neurons, and not detected nor trafficked to the myelin membrane.

Structure and Protein conservation

PLP is the highly hydrophobic and integral transmembrane protein of the myelin membrane. The complete topology of PLP was unraveled by biochemical studies by Weimbs and Stoffel, 1992 and Wahle and Stoffel, 1998. PLP contains four transmembrane spanning hydrophobic domains connected by three hydrophilic loops in which two loops (EC-I and EC-II) are located in the extra-cytosolic space and one loop in the cytosolic space. The NH₂ and COOH terminal domains are located on the cytosolic side (Weimbs and Stoffel, 1992; Gow *et al.*, 1994; Greer *et al.*, 1996). PLP is phylogenetically highly conserved (Schliess and Stoffel, 1991), and is identical at amino acid level among human, mice and rat (Figure 4). PLP from birds and amphibians also show approximately 85% homology with mammalian PLP (Schliess and Stoffel, 1991). PLP and

Dm20 and other proteins such as M6 glycoproteins share, to a certain extent, homology in their transmembrane domains and Cys positions (Greer *et al.*, 2001). PLP amino acid residues are conserved especially with regard to their point mutations among mammals and other species (Schliess and Stoffel, 1991).

1.4.2 Cys residues and hydrophobic properties

Of fourteen Cys residues in PLP, six at amino acid positions 5, 6, 9, 108, 138 and 140 are involved in post-transacylation modification, four Cys residues are involved in formation of disulfide bridges i.e., Cys183-Cys227 and Cy200-Cys219, and the remaining four Cys residues at amino acid positions 24, 32, 34 and 168 are located in the hydrophobic domains in the myelin membrane (Weimbs and Stoffel, 1992; Wahle and Stoffel, 1998).

PLP is also soluble in organic solvents such as chloroform/methanol due to its strong hydrophobic nature. It is composed of more than 50% of apolar (hydrophobic) residues that are spanned in the phospholipid bilayer as four hydrophobic membrane domains (Wahle and Stoffel, 1998; Stoffel *et al.*, 1984; Weimbs and Stoffel, 1992). PLP also undergoes post-translational modification i.e., acylation where fatty acid (usually palmitic acid) is covalently bound to thiol groups of Cys residues of PLP. Acylated fatty acids of PLP might interact with the adjacent myelin phospholipid bilayer and also contribute to the hydrophobic nature of PLP (Weimbs and Stoffel, 1992). Alterations in PLP such as point mutations, deletions, duplication, missense mutation, over-expressions lead to disturbance in the PLP topology or conformation and abnormal targeting in oligodendrocytes. PLP misfolding may result in oligodendrocytes apoptosis and thus myelin disorders such as PMD and SPG2.

Multi-alignment of human, mouse and rat's PLP CDNA sequence

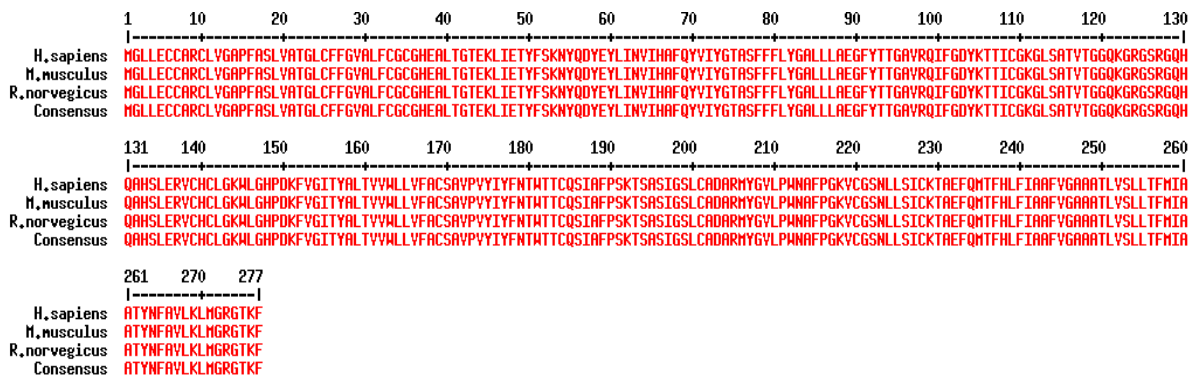


Figure 4: Alignment of human, mouse and rat protein sequences. 100% homology (consensus) is

observed among human (*H.sapiens*), mouse (*M.musculus*), and Rat (*R. norvegicus*) on protein sequence. ‘Align’ software was used for alignment and respective protein sequences were obtained from ensemble database.

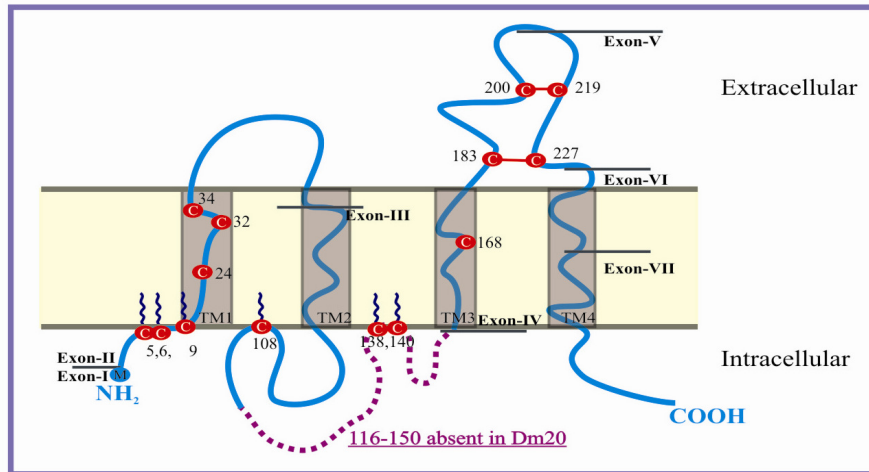


Figure 5: Topology of proteolipid protein (PLP) and its isoform Dm20. Dm20 lacks 35 amino acids from 116 to 150 in the hydrophilic loop of PLP (absence of violet color dashed line). PLP/Dm20 contains four hydrophobic membrane spanning domains, one intracellular and two extracellular loops, two disulphide bridges in the extra-cytosolic-II loop and post-translational modifications (transacylation on Cys residues).

Point mutations, disulfide bonds, and cell surface targeting

PLP/Dm20 is synthesized in oligodendrocytes on membrane bound polysomes and via Golgi vesicular transport it is targeted to the plasma membrane. Calnexin, an ER chaperone, binds to the newly synthesized PLP in the ER and contributes in its proper folding and ER quality control (Swanton *et al.*, 2003). Properly folded PLP exits the ER and interacts with lipid rafts for vesicular transportation to the cell surface, whereas misfolded PLP (due to point mutations) is stably coupled with calnexin and does not exit the ER. Moreover stable binding of PLP with calnexin chaperone further prohibits ER-protein degradation, thus accumulating PLP in the ER, causing ER stress and further triggering apoptosis via unfolded-protein response (UPR), which in turn may lead to PMD or SPG2. The impairment of the PLP association with lipid rafts, due to its misfolding, might perturb its normal transport leading to a condition called as SPG2 (kraemer-albers *et al.*, 2006). If PLP is in excess quantity, as in the case of PLP duplications,

during its intracellular transport excess PLP constituting lipid rafts are trapped in the lysosome which triggers oligodendrocyte apoptosis, a situation observed in dysmyelination (Simons *et al.* 2002). In less severe forms of PMD or SPG2, PLP is trapped in the ER, but its isoform Dm20 is targeted normally to the cell surface, indicating that PLP and Dm20 are differentially targeted, which correlates with the extent of PMD pathology.

The proximal (Cys183-Cys227) and outer disulphide bridges (Cys200-Cys219), located in EC-II loop of PLP/Dm20 are critical in trafficking. Their functional role under *in vivo* conditions specifically in cell surface trafficking of PLP/Dm20 and in myelin phenotype is still unknown. In the heterologous COS-7 cells of *in vitro* system, PLP, lacking the proximal disulphide bridge, is retained in the ER and is not detected on the cell membrane. Therefore the proximal disulphide bridge is involved in ER quality control. In contrast, PLP lacking the outer disulphide bridge passed ER quality control and appeared on the cell membrane similar to the wild-type PLP. Therefore the outer disulphide bridge is not involved in ER quality control. PLP devoid of both disulphide bridges is ER retained (Dhaunchak and Nave, 2007). Interestingly, there is also a human case report demonstrating naturally occurring point mutation at Cys219Tyr deleting the outer disulfide bridge of PLP. This point mutation traps PLP in the ER and expresses the connatal PMD phenotype (Fukumura *et al.*, 2010).

1.4.3 PLP related myelin disorders; PMD and SPG2

Naturally occurring mouse mutants such as rumpshaker mouse containing a point mutation (I186T) in PLP (Schneider *et al.*, 1992), Jimpy mouse mutant with an A242V point mutation in PLP, and a PLP transgenic mouse with extra PLP copies (Redhead *et al.*, 1994), exhibited severe myelin defects such as dysmyelination and hypomyelination. Some of these myelin defects resulted in PMD or SPG2 diseases. The main molecular mechanism that underlies PMD and SPG2 is impaired targeting of PLP to the oligodendrocyte plasma membrane (Seitelberger, 1995; Werner *et al.*, 1998) and oligodendrocyte apoptosis. The different trafficking of PLP and Dm20 in oligodendrocytes is also a determining factor influencing PMD severity. Both isoforms, when retained in the ER, result in severe forms of connatal PMD. When PLP alone is retained in the ER and Dm20 is targeted normally to the oligodendrocyte cell surface a less severe or classical form of PMD is observed (Gow and Lazzarini, 1996).

PMD or SPG2 mouse models exhibit phenotypes such as neuromotor defects including leg and arm muscle atrophy, seizures, tremors, cognitive and behavioral defects. They die prematurely within few weeks after birth (Yool *et al.*, 2000). The PMD mouse models closely resemble human PMD on the molecular level, such as mutations in PLP. PMD patients exhibit mild to

severe abnormalities starting from their first postnatal year with gradual progression; delayed cognitive development, spasticity or muscle weakness, partially controlled neck and head movements and involuntary eye moments. Patients with the severe form of SPG2 exhibit defects in motor development including partial extent of cognitive defects of PMD.

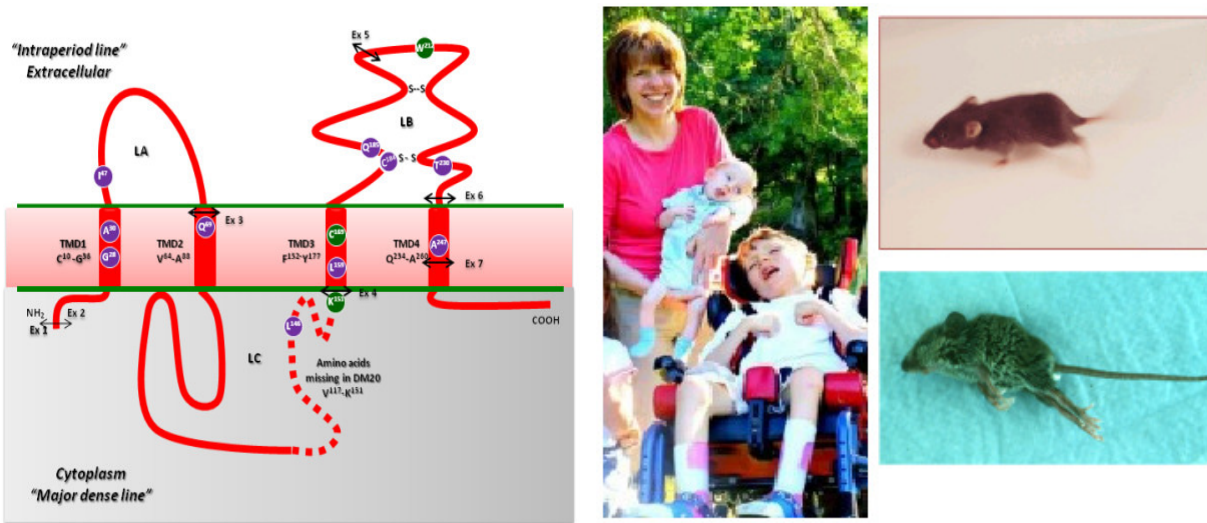


Figure 6: PLP with some of the point mutations which lead to PMD/SPG2. Children effected with PMD, and the severely affected PMD (PLP jimpy, A242V) mouse model. (Pictures adapted and modified from Grossi *et al.*, 2011, CURE-PMD organization).

1.5 CNS Myelin; Phospho- and sphingolipids

Lipids constitute 70% of the total CNS myelin dry mass, with galactocerebrosides (GalC) being the most abundant lipid class. Major lipid types in the whole brain and in myelin (white matter) are cholesterol, phospholipids, and glycosphingolipids which are present in a ratio of 4:3:2 (Norton and Cammer, 1984). Phospholipids of myelin contain 70% phosphatidylethanolamine as plasmalogens compared to 5% in liver. Phospholipids are asymmetrically distributed in the myelin membrane; wherein mostly phosphoglycerides are arranged in the cytoplasmic leaflet of myelin MDL and galactosphingolipids (GalC and sGalC) at the exoplasmic face of the myelin IDL (Figure 3.D). The important role of lipids and proteins in the myelin membrane was verified by several *in vivo* and *in vitro* experiments (Table 2).

Targeted myelin lipid	Disrupted enzyme	Myelin morphology and phenotypes in various null mouse mutants
GalC and Sulfatides (Sulfated GalC) (Bosio <i>et al.</i> ,1996)	UDP-galactose-ceramide galactosyltransferase (CGT)	Perturbed myelin membrane paranodal loops and septate junctions. Impaired salutatory conduction. Showed sever neurological defects
Sulfatides (Honke <i>et al.</i> , 2002)	Cerebroside sulfotransferase (CST)	Perturbed myelin paranodal loops. Similar but with less sever phenotypes to that of CGT null mutant.
Hydroxyl-fatty acid-GalC and Hydroxyl-fatty acid-Sulfatides	Fatty Acid 2-hydrolase (FA2H)	Late onset of myelin degeneration and myelin de-compaction
Cholesterol (Saher <i>et al.</i> , 2005)	Squalene synthase in oligodendrocytes of mice	Myelination defects

Table 2: Important lipids of myelin, their enzymes, and their role in myelin morphology

The retina, a highly organized CNS structure, is rich in phospholipids and is essential for visual functions. Phospholipids of retina consists 54% of phosphatidylethanolamine (PE) and 30-40% phosphatidylcholine (PC), which constitutes mainly PUFA at both sn1 and sn2 positions. Impairment in PUFAs composition may alter visual function. Retina morphology and function, is further discussed in section 1.5.4.

1.5.1 Fatty acid composition of phospholipids

Phosphoglycerides have a glycerol backbone, and sphingolipids have a sphingosine back bone. In phosphoglycerides; two fatty acids, generally a saturated and an unsaturated or polyunsaturated fatty acid (PUFA), are bound as esters at the sn-1 and sn-2 of the glycerol backbone. In sphingolipids; only single fatty acid chain, generally a saturated or un- or polyunsaturated, is linked with an amide bond to the sphingosine back bone. In phosphoglycerides, a polar head group such as choline, ethanolamine, serine and inositol, is linked by a phosphate ester bond to a third carbon (C3) of the phosphoglyceride back bone. Thus, based on the type of polar head group attached, the phosphoglycerides are termed accordingly as phosphatidylcholine, phosphatidylethanolamine, phosphatidylserine, and phosphatidylinositol. Sphingolipids contain polar head groups such as phosphocholine in sphingomyelin, and glucose or galactose polar head groups in cerobroside (GluC/GalC).

The basic structure of membrane phospholipids is depicted in the figure 7.

The appropriate nature and composition of saturated and unsaturated or polyunsaturated fatty acids in phospholipids of cell membranes are critical in maintaining respective membrane conformation, stability, fluidity and dynamics. Besides structural roles, fatty acids also serve in a variety of functions such as energy reserves, precursors of eicosanoids, and regulators of myelin gene expression in the brain. Deficiency or lack of essential fatty acids (EFAs) in mammals causes physiological disorders and is incompatible with life.

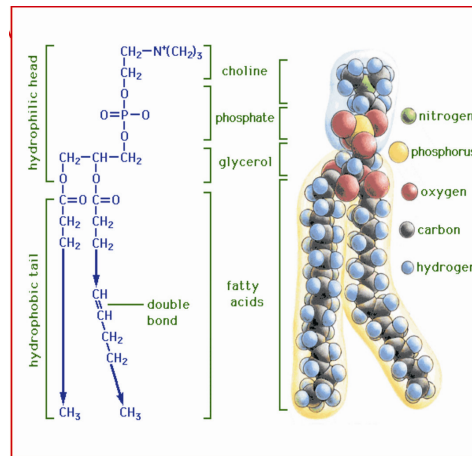
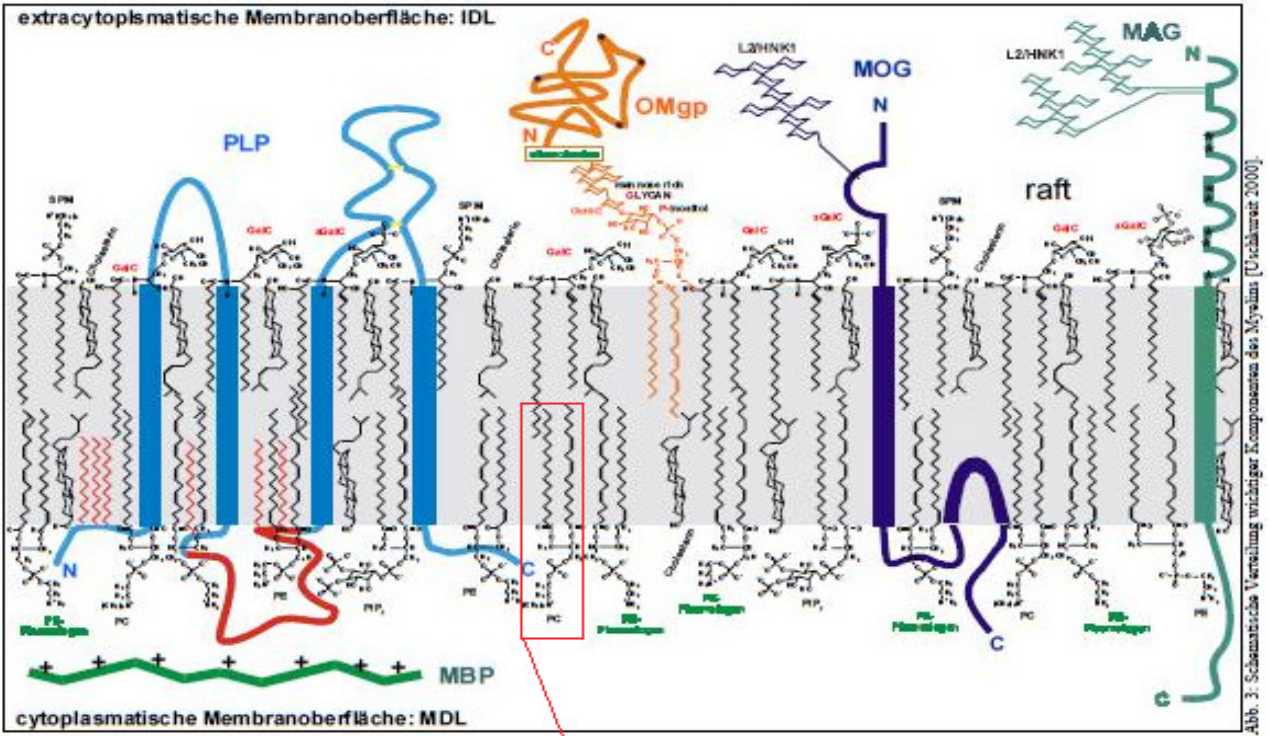


Figure 7: Myelin membrane composed of asymmetrically distributed phospholipids, and major myelin proteins. Zoomed box: depicting a phospholipid; phosphatidylcholine with its saturated and unsaturated hydrophobic fatty acid tails and the hydrophilic choline polar head group (Adopted and modified from Uschkureit, 2000).

1.5.2 Classification of fatty acids and the polyunsaturated fatty acids (PUFAs) synthesis cascade

Fatty acids are broadly classified into saturated and unsaturated fatty acids based on the number of carbon-carbon double bonds. Saturated fatty acids have no carbon-carbon double bonds, e.g. palmitic acid (16:0) and stearic acid (18:0). They are mostly involved in energy storage in the form of triglycerides in adipose tissue and are also major structural components in membrane phospholipids. Unsaturated fatty acids are classified into monounsaturated fatty acids (MUFAs) and polyunsaturated fatty acids (PUFAs). MUFAs contain only a single carbon-carbon double bond, e.g., oleic acid (18:1, n-9). PUFAs are further classified into omega-9, omega-6, and omega-3-fatty acids (Figure 8) and contain more than one carbon-carbon double bond. PUFAs are the important structural constituents of membrane phospholipids; their carbon-carbon double bonds introduce kinks in the membrane phospholipids. The degree of double bonds or unsaturation in the phospholipid fatty acid chains may increase membrane fluidity and decrease membrane melting point and transition temperature. PUFAs such as arachidonic acid (AA), docosahexanoic acid (DHA), are also involved in cell signaling and are precursors for variety of metabolic processes. According to the omega (ω /n) classification system, the carbon-carbon double bond numbering starts from the methyl carbon terminal.

Common name	Systematic name	Abbreviation
Saturates		
myristic	tetradecanoic	14:0
palmitic	hexadecanoic	16:0
stearic	octadecanoic	18:0
arachidic	eicosadecanoic	20:0
Unsaturates		
Monounsaturates		
palmitoleic	<i>cis</i> -9-hexadecenoic*	16:1 n-7**
vaccenic	<i>cis</i> -11-octadecenoic	18:1 n-7
oleic	<i>cis</i> -9-octadecenoic	18:1 n-9
Polyunsaturates		
omega-9		
mead	all- <i>cis</i> -5,8,11-eicosatrienoic	20:3 n-9
omega-6		
α -linoleic	<i>cis,cis</i> -9,12-octadecadienoic	18:2 n-6
γ -linolenic	all- <i>cis</i> -6,9,12-octadecatrienoic	18:3 n-6
No common name	all- <i>cis</i> -8,11,14-eicosatrienoic	20:3 n-6
arachidonic	all- <i>cis</i> -5,8,11,14-eicosatetraenoic	20:4 n-6
No common name	all- <i>cis</i> -4,7,10,13,16-docosapentaenoic	22:5 n-6
omega-3		
α -linolenic	all- <i>cis</i> -9,12,15-octadecatrienoic	18:3 n-3
No common name	all- <i>cis</i> -11,14,17-eicosatrienoic	20:3 n-3
EPA	all- <i>cis</i> -5,8,11,14,17-eicosapentaenoic	20:5 n-3
DHA	all- <i>cis</i> -4,7,10,13,16,19-docosahexaenoic	22:6 n-3

Saturated fatty acids

Monounsaturated fatty acid

Polyunsaturated fatty acids

Figure 8: Fatty acid classification with their common and systematic names and abbreviations. PUFAs classification into omega-9, omega-6 and omega-3, and some fatty acids structures were depicted.

Polyunsaturated fatty acid biosynthesis

In mammals, the majority of PUFAs are acquired from diet and by transforming from their precursors essential fatty acids (EFAs) such as linoleic acid (18:2, n-6) and alpha-linolenic acid (18:3, n-3) endogenously via specific fatty acid synthases, elongases, and desaturases.

In mammals, delta-desaturases such as delta-9, delta-5, and delta-6 introduce double bonds at defined positions in respective fatty acids. Delta-9 desaturases, also called stearoyl-CoA desaturase-1 (SCD), introduce the double bond at the 9, 10 position from the carboxylic terminal in 18:0 fatty acid (Figure 9) thus generating 18:1 (n-9) monounsaturated fatty acid. Four SCD isoforms have been identified in mouse and they are tissue-specific. The SCD1 isoform is expressed in liver whereas SCD2 is brain specific, and SCD3 and SCD4 isoforms are skin and heart specific, respectively. In the PUFA synthesizing cascade, elongase is involved in extending the fatty acid chain.

PUFAs (n-3 and n-6) are synthesized by desaturation from their respective precursor fatty acids in the ER membrane by ER membrane-bound desaturases i.e., delta-5 desaturase also called as Fads1, and delta-6 desaturase also called as Fads2. Fads1 introduces at position 5 the cis double bond in their respective precursor fatty acyl chains, Fads2 at position 6 of EFAs in the initial and further steps of the PUFA biosynthetic pathway (Figure 9). Lack of fads2 enzyme disrupts PUFA biosynthesis, thereby abolishing synthesis of endogenous the major PUFAs such as AA (20:4 n-6), EPA (20:5, n-3), and DHA (22:6, n-3), along with very long chain-PUFAs (Stoffel *et al.*, 2008; Stroud *et al.*, 2009).

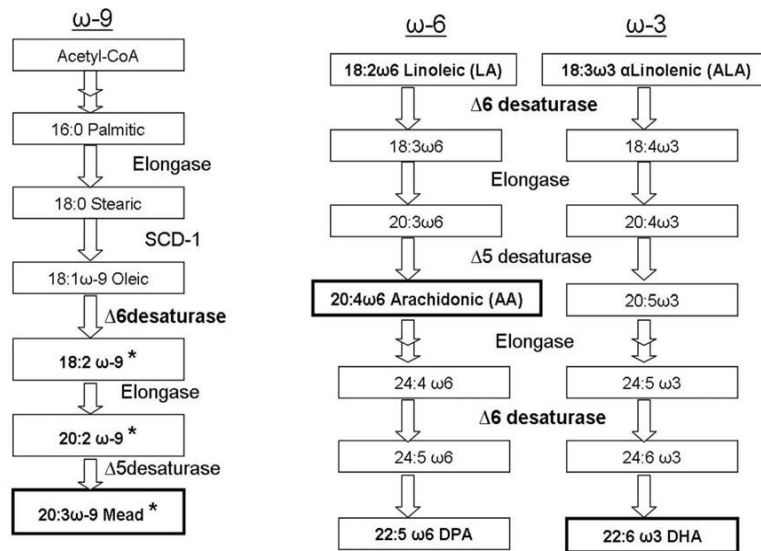


Figure 9: The cascade of PUFA biosynthesis by desaturases and elongases in mammals.

1.5.3 PUFAs in the CNS

PUFAs and very long chain-PUFAs (VL-PUFAs) are the major components in phospholipids of the myelin membrane in the CNS. Among the PUFAs, AA and DHA are the major constituents of the CNS brain and in retinal phospholipids in contrast to other cell membranes. It is known that AA and DHA are highly conserved and are critical for normal physiological functions in the brain and retina (Carrie *et al.*, 2000a). AA and DHA are also precursors of eicosanoids and docosanoids, respectively, and also carry out a myriad of pharmacological functions.

Deficiency of PUFAs may disrupt membrane bilayer conformation, cell polarity and tight junctions, which might in turn disrupt respective physiological functions. This has been shown in Sertoli cell polarity and in blood testis-barrier, and in granulosa cells of ovarian follicles (Stoffel *et al.*, 2008).

The supplementation of omega-3 and omega-6 PUFAs for brain development, especially in early myelin developmental stages, is an active research area in nutritional and brain physiology (Yehuda *et al.*, 2002). Miller *et al.*, 1984 demonstrated that a lack of essential fatty acids (EFAs) results in a decrease of total myelin protein content to 25%, lipid phosphorous content to 22%, brain weight to 7% and a reduction in body weight up to 40%. PUFAs play an important role in myelinogenesis by influencing myelin gene expression levels (Clarke, 2001). Eicosapentaenoic acid (EPA) supplementation to glial cells *in vitro* up-regulated PLP gene expression levels via cAMP-mediated pathways (Salvati *et al.*, 2004), whereas under DHA supplementation PLP gene expression is up-regulated via retinoid X receptor signaling pathway (Jang *et al.*, 2004). *In vivo*, injecting DHA and EPA into rat brain stimulated several myelin proteins such as PLP, MBP, MOG and CNP, via down-regulating CREB (cAMP-response element-binding) activity due to decreased levels of CREB phosphorylation (Salvati *et al.*, 2008). In clinical studies PUFAs supplementation has been promising in remyelination, especially in multiple sclerosis (MS) with demyelinating disorder. PUFAs are also used in minimizing neurotoxin levels in schizophrenia. In mammals, perturbed behavioral physiology such as impaired cognitive ability and motor coordination has been observed in EFA deficient conditions (Vinot *et al.*, 2011; Chengwei He *et al.*, 2009).

Retinal photoreceptor rods and cones outer segments (OS) consist of thousands of vertically stacked membrane disks that are made up of lipoprotein bilayers enriched with DHA and AA (Bazan *et al.*, 1993). Electroretinography (ERG) is used to assess retinal photoreceptor function and retinal photo-transduction cascade which is triggered in response to light (Weisinger *et al.*, 1996a). ERG output is the direct measurement of the visual function of the retina in the presence of light. LC-PUFA deficiency may affect the rod outer membrane and RPE membrane and thus may impair normal visual functions (Jeffrey *et al.*, 2001).

1.5.4 Retinal morphology

In vertebrate embryonic development, the retina and optic nerve originate as an outgrowth of the developing brain. The vital role of the retina is in the conversion of light signals into nerve impulses that are passed along the optic nerve to different visual centers of brain. Outer segments of retinal photoreceptors and retinal synapses are highly enriched in PUFAs, specifically DHA. The retinal pigment epithelium (RPE) is involved in nutrient transport and removal of waste products from photoreceptors by the apical microvilli. The basal surface of the RPE interacts with underlying Bruch membrane (Figure 10). RPE is separated from the choriocapillaris (CC) by Bruch membrane (Figure 10). The outer segments (OS) are made up of sensory cilia and a series of membrane stacks composed of 60% of DHA, which are important in light conduction. DHA depletion may result in retinal degeneration and functional impairments.

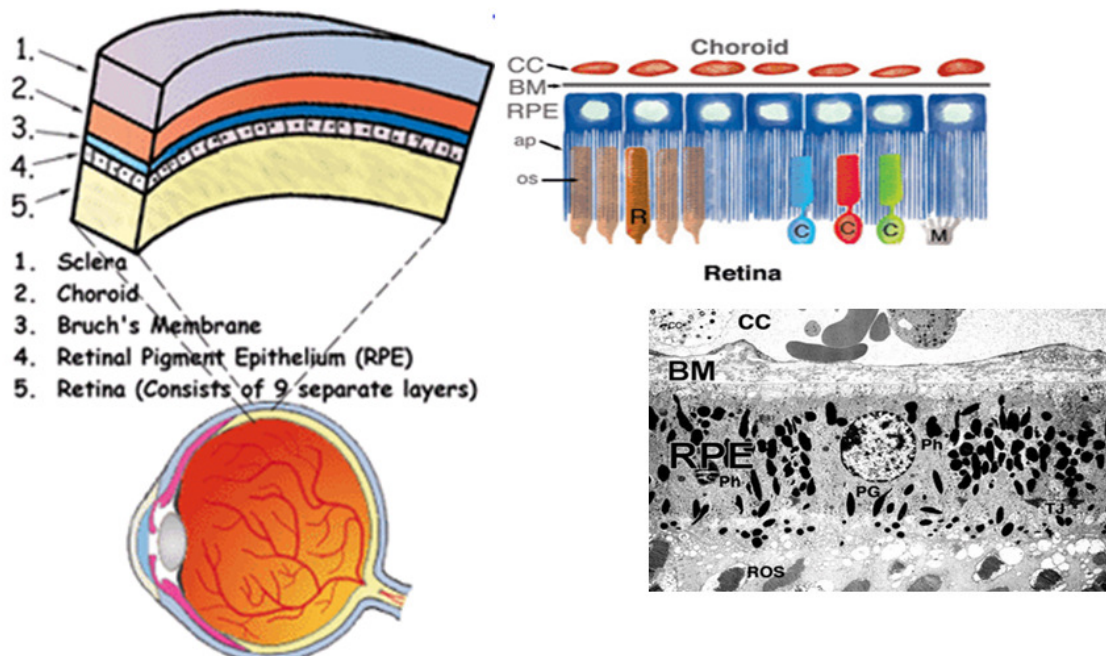


Figure 10: Morphology of the retinal layers (Human). Right upper diagram depicts the layers of the retina: CC, choriocapillaris, BM, Bruch's membrane; RPE, retinal pigment epithelium; ap, apical processes or RPE apical microvilli; os, outer segments; C, cones, R, rods; M, Müller cells. Right lower image: electron micrograph of human retinal RPE region (adapted and modified from Web vision-retina)

1.5.5 Fads2 knock-out mouse (PUFAs deficient mouse model)

The *fads2* (Delta6) null mouse mutant has been generated in our lab (Stoffel *et al.*, 2008) to investigate the functional significance of PUFAs deficiency without depleting their precursor EFAs (LA and ALA). The *fads2* null mouse lack the synthesis of all PUFAs including AA and DHA along with their derivatives such as eicosanoids and LC-PUFA (Stoffel *et al.*, 2008, Stroud *et al.*, 2009). Since DHA and AA are the major representatives among PUFAs in the brain and retina, lack of endogenous PUFAs biosynthesis especially AA and DHA in the *fads2* null mouse mutant enables us to investigate the significance of PUFAs in membrane structure and function focusing on the CNS i.e., brain and retina.

The generation of gene targeted mouse mutants (transgenic mice), in which key enzymes of lipid biosynthesis have been deleted are central to the key strategy to unravel the role of specific lipid functions. These models are similar to the mouse models in which key protein structures of CNS have been deleted.

1.6 Transgenic mouse models

A very important method for analyzing gene function, from its role in normal development to pathology, is possible by generating gene manipulated mouse models, in which a specific gene of interest is deleted, modified or over-expressed. Genetically engineered mouse mutants can be obtained by several ways, such as by gene targeting (Capecchi *et al.*, 1994) in which the endogenous copy of a gene is partly or completely deleted by homologous recombination, or by pronuclear injection technique (Gordon and Ruddle, 1983) where a gene can be over-expressed at random loci in the genome.

1.6.1 Gene targeting

The technique of gene targeting involves the mutation of a specific gene locus by the homologous recombination in embryonic stem cells. It is most often employed for generating gene knock-out or knock-in mutants. In the gene knock-out approach, specific gene function is usually eliminated by deleting partly or completely the endogenous gene by homologous recombination, whereas in a gene knock-in approach, instead of eliminating gene function the gene is manipulated as desired, e.g., by introducing point mutations in specific loci.

In the gene targeting technique, initially a gene-targeting construct with the desired modifications such as point mutations, partial gene deletions, insertion of fluorescent gene markers etc., is engineered. This is then cloned into a gene targeting vector and further transfected into pluripotent ES cells. The mutated homologous gene fragment then recombines with the endogenous gene counterpart in the ES cells (Thomas and Capecchi, 1986). Increased length of the exogenous targeting homologous arms will increase the frequency of homologous recombination with the endogenous locus (Hasty *et al.*, 1991b). The targeting vector also contains one or more selection markers such as a neomycin resistance gene and a thymidine kinase gene from herpes simplex virus (HSV-TK). Positive or negative selection markers allow for screening of homologously recombined clones from a pool of clones (Mansour *et al.*, 1988). Successfully homologously recombined positive ES clones will be verified by PCR and Southern blot hybridization. Positive ES clones are then injected into mouse embryos at the blastocyst stage (Bradley *et al.*, 1984) and re-implanted in to pseudo-pregnant foster mice. Thus obtained chimeric progeny are verified by PCR and DNA sequencing. The verified chimeras can be further bred to generate germ line chimeric heterozygotes and further to homozygous mutants.

1.6.2 Pronuclear Microinjection

The pronuclear micro-injection technique is fast and robust for generating transgenic mouse mutants to investigate gene function *in vivo*. An exogenous gene or cDNA from the appropriate gene, termed transgene, is introduced into the pronucleus of fertilized murine eggs by microinjection. The transgene is a DNA fragment usually containing a tissue-specific enhancer, promoter, and the gene-of-interest (gene or protein coding CDNA). In this technique, multiple transgene copies are stably integrated into the mouse genome at random loci. Pronuclei injection technique can be used to investigate gene gain-of-function (Babinet, 2000), and gene localization by tagging or fusing gene of interest with the appropriate reporter gene such as EGFP or *E. coli* beta-galactosidase. The transgene can also micro-injected into the fertilized eggs from a specific genetic background such as a null-mutant. The main disadvantage of the transgenic technique is the position effect, i.e., the pronuclear injected transgene integrates randomly and therefore may disturb the function of other genes. Hence large numbers of founder mice have to be analyzed to assess the true function of the injected transgene.

1.7 Site-directed mutagenesis

The site-directed mutagenesis (SDM) technique is used to introduce mutations (point or multiple), insertions and deletions at desired positions in a DNA fragment, by using synthetic oligonucleotides (Itakura *et al.*, 1984; Carter, 1986). In SDM, the DNA sequence that has to be manipulated is employed as a template in the PCR reaction with mismatched nucleotide containing primers, and these primers are then extended on the template synthesizing new DNA fragments incorporating the mutations or mismatches. Among various methods of PCR-based mutagenesis, basic strategies employed within this thesis work are conventional PCR mutagenesis, which introduces mutations towards the 5' end and 3' ends of the desired template DNA fragment, and overlap-extension PCR, which introduces mutations at more than one desired location within the target DNA template fragment.

In overlap-extension PCR, multiple mutations are introduced in a single PCR reaction by employing more than one set of primers containing nucleotide mismatches (mutations). It can also be employed by combining two individual DNA fragments at their terminal overlapping sequence.

2 Aim of the thesis

Proteolipid protein (PLP) is a major structural element in the ordered myelin architecture and is an essential component for the maintenance of myelin sheath in CNS. PLP and its isoform Dm20 contain 14 Cys and 12 Cys residues respectively; in which six Cys residues are involved in post-translational thio-acylation modification and four Cys residues in two disulfide bridge formation that are localized in extra cellular loop-II. These Cys-residues may be critical for maintaining the topological structure of PLP in the membrane. It is well known that some point mutations of PLP effects its conformational changes and perturbs the intracellular trafficking of PLP, leading to the apoptosis of oligodendrocytes there by resulting in severe forms of dysmyelinating CNS diseases such as PMD and SPG2.

The primary aim of the present study is to identify the function of Cys residues (Cys-mut-PLP and Cys-mut-Dm20 proteins) in PLP and its isoform Dm20, as structural elements and their role in intracellular trafficking under *in vitro* and *in vivo* conditions. As a part of this, a transgenic mutant mouse expressing a mutant form of PLP (Cys-mut-PLP) under the control of promoters of early neuronal or glial cell lineage markers (MBP promoter and Nestin enhancer) on the PLP null background will be generated. Simultaneously, in order to understand the significance of the two disulfide bridges formed by the four Cys residues in PLP and Dm20, a knock-in mutant mouse lacking the disulfide bridges of endogenous PLP and Dm20 has to be generated by homologous recombination. As the first step, a targeting construct will be generated containing the PLP gene sequence with mutated four Cys residues that are involved in the formation of two disulfide bridges.

The integral membrane protein PLP, and phospholipid's polyunsaturated fatty acids (PUFAs), play significant structural and functional roles in the CNS myelin sheath. The *plp*^{-/-} knock-out mouse generated previously in our laboratory revealed that the lack of PLP resulted in disruption of CNS myelin membrane compaction and long term axonal maintenance but did not show any dysmyelination, hypomyelination or other severe neurological disorders. The *fads2*^{-/-} knock-out mouse that was generated in our laboratory has completely abolished endogenous *in vivo* PUFA synthesis, and even more close observation revealed disrupted gap-junctions in Sertoli cell polarity and blood-testis barrier in addition to the gap junction network between granulosa cells of ovarian follicles. Hence, the generation of a *plp*^{-/-}*fads2*^{-/-} double knock-out mouse would reveal the significant functional and structural roles of two pivotal structures PLP and PUFA in the organization of myelin membrane of CNS.

The second aim of this dissertation is to generate a *plp*^{-/-}*fads2*^{-/-} double knock-out mouse and to characterize the ultra structural phenotype of myelin membrane using biochemical, cellular, and behavioral studies. Since the retina is a part of the CNS and its photoreceptor outer segment membranes are primarily composed of PUFA such as DHA, its structural features along with its functions will also be investigated.

3 Results

3.1 Construction of mutant cDNA pool of PLP and Dm20

3.1.1 Site-directed mutagenesis (SDM) and Overlap extension PCR

In order to study the role of PLP and Dm20 Cys residues in intracellular and plasma membrane trafficking under *in vitro* and *in vivo* conditions, PLP and Dm20 cDNA constructs containing Cys point mutations at desired positions were generated (Table 3).

Total mRNA isolated from adult C57BL/6 mouse brain was used as a template to derive PLP and Dm20 cDNA fragments by RT-PCR. Site-directed mutagenesis (SDM) and overlap extension PCR techniques were performed as follows: two pairs of point mutated primers were used to generate two 5' and 3' incomplete overlapping cDNA fragments in two separate PCR reactions. Subsequently, these two overlapping cDNA fragments were annealed, extended, and amplified to generate full length cDNA fragments with appropriate Cys mutations. Using this method, Cys codons of PLP and Dm20 cDNA were mutated to Ser codons at the desired positions. The lengths of the cDNA fragments were confirmed by agarose gel electrophoresis and the mutations introduced were confirmed by DNA sequencing (Figure 11 and 12).

Similarly, a total of ten PLP cDNA fragments and nine Dm20 cDNA fragments with Cys codons at defined positions mutated to Ser codons were generated. These amplified cDNA fragments were cloned into the PCR2.1 vector (Invitrogen). Thus generated cDNA inserts were used for further cloning steps to generate final vectors for the study of their *in vivo* intracellular targeting properties. cDNA mutations are illustrated in the figure 11 B.

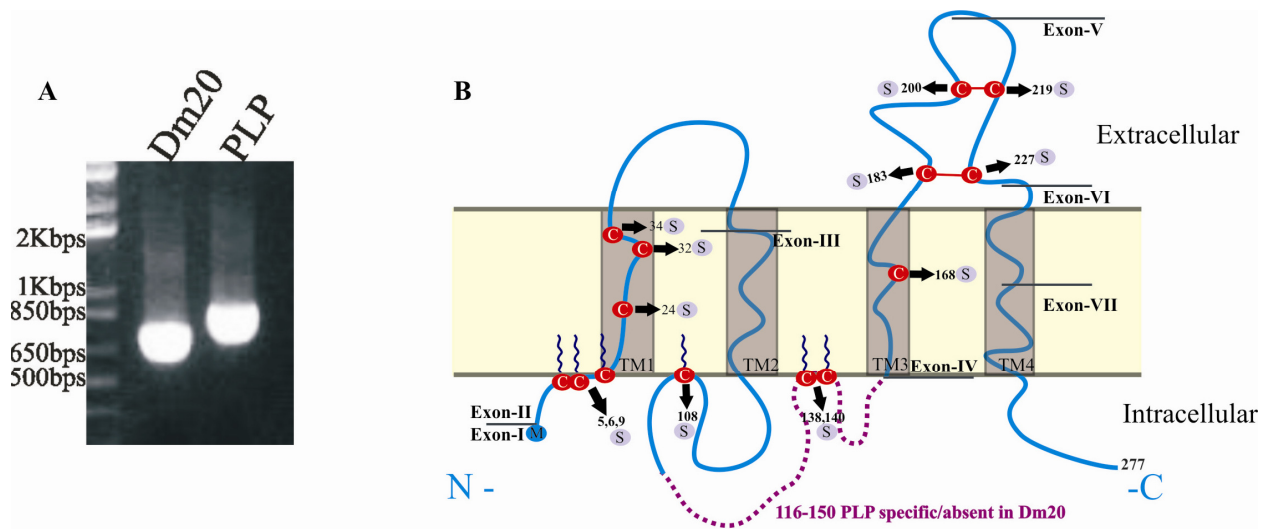


Figure 11: A) Agarose gel electrophoresis of cDNAs of PLP (825bp) and Dm20 (723bp) and DNA Marker (Biolabs). B) PLP and Dm20 transmembrane structure. The intracellular hydrophilic loop of amino acids 116 to 150 are specific to PLP (violet dotted line) but are absent in Dm20. Transmembrane structure: four hydrophobic membrane spanning domains (shaded bars) are connected by five hydrophilic domains (blue lines). Cytosolic domains encoded by partial or complete exons I, II, III, IV, VII, and extracellular domains by partial exons II, IV, V and VI were represented. Positions of Cys residues mutated to Ser residues were represented.

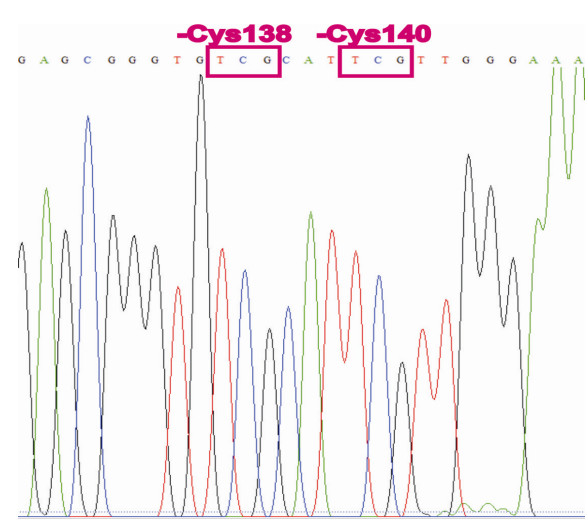
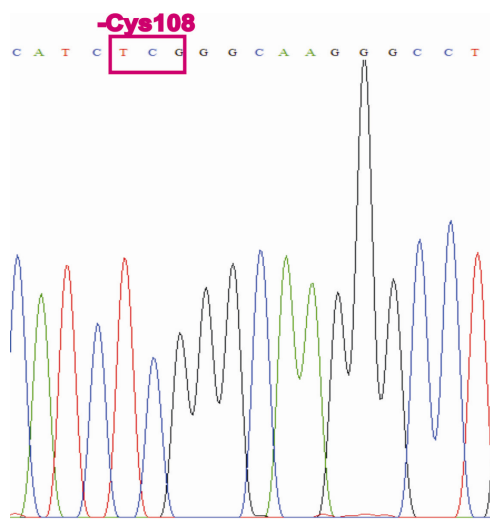
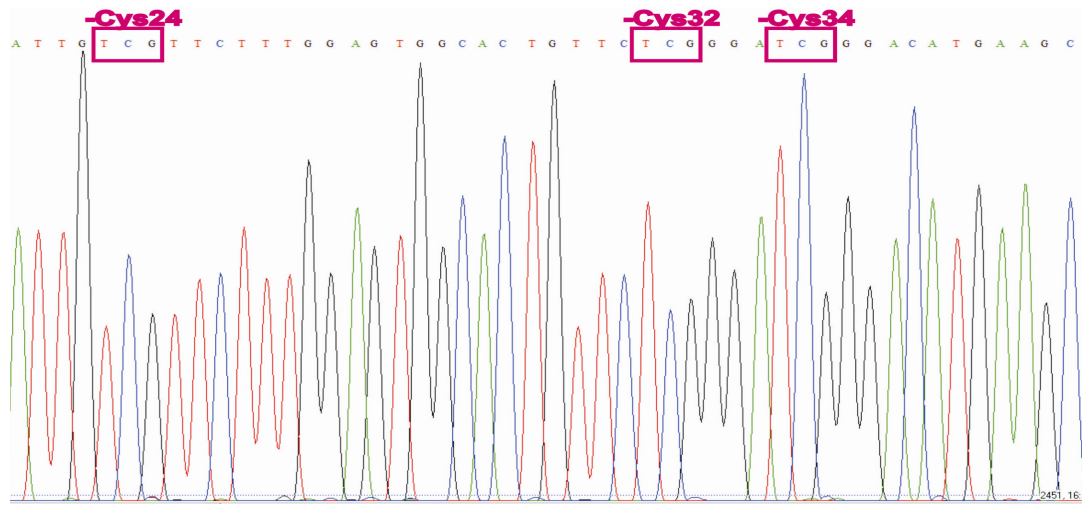
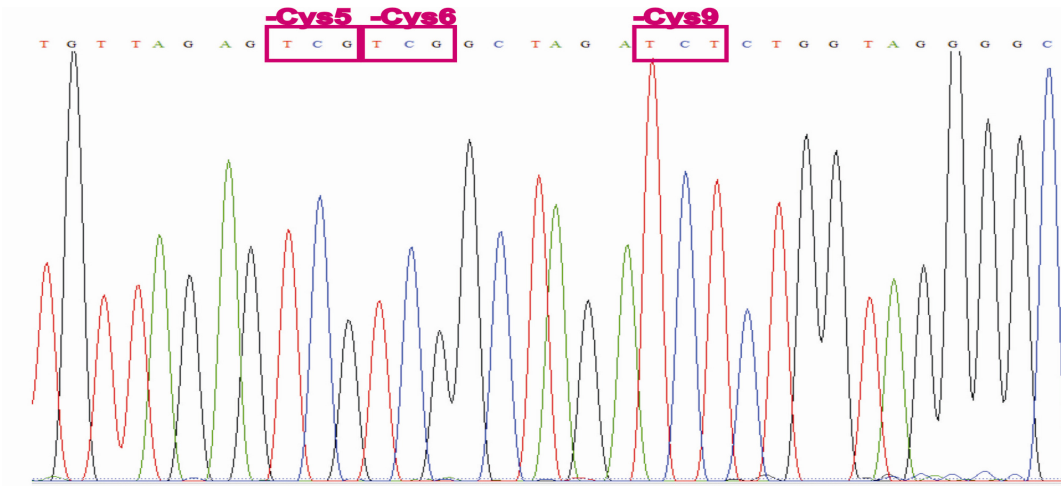
No .	Name of the cDNA Construct	PLP/ Dm20	Mutated Cys codons position, deleted S-acylation or disulfide bridge Cys-codons position	Mutate d Exon	Average Protein Hydrophobic value
1	Wild-type (WT)	PLP	Nil	0	0,550181
2	-ca	PLP	<u>5,6,9</u>	II	
3	-C34	PLP	<u>5,6,9,24,32,34</u>	II	
4	-C108	PLP	<u>5,6,9,24,32,34,108</u>	II,III	
5	-C140	PLP	<u>5,6,9,24,32,34,108,138,140</u>	II,III	
6	-C168	PLP	<u>5,6,9,24,32,34,108,138,140,168</u>	II,III	
7	-C183	PLP	<u>5,6,9,24,32,34,108,138,140,168,183</u> (removed first proximal disulfide bridge)	II,III,IV	
8	-C200	PLP	<u>5,6,9,24,32,34,108,138,140,168,183,200</u> (removed two disulfide bridges)	II,III,IV	
9	-C219	PLP	<u>5,6,9,24,32,34,108,138,140,168,183,200</u>	II,III,IV,	

			<u>.219</u>	V	
10	Mut-PLP (Cys-less PLP)	PLP	All Cys residues mutated to Ser residues <u>5,6,9,24,32,34,108,138,140,168,183,200</u> <u>.219,227</u>	II,III,IV, V	0,38339
11	Wild-type	Dm20	Nil	0	0,780579
12	-ca	Dm20	<u>5,6,9</u>	II	
13	-C34	Dm20	<u>5,6,9,24,32,34</u>	II,III	
14	-C108	Dm20	<u>5,6,9,24,32,34,108</u>	II,III	
15	-C168	Dm20	<u>5,6,9,24,32,34,108,138,140,168</u>	II,III,IV	
16	-C183	Dm20	<u>5,6,9,24,32,34,108,138,140,168,183</u> (Removed first proximal disulfide bridge)	II,III,IV	
17	-C200	Dm20	<u>5,6,9,24,32,34,108,138,140,168,183,200</u> (Removed two disulfide bridges)	II,III,IV	
18	-C219	Dm20	<u>5,6,9,24,32,34,108,138,140,168,183,200</u> <u>.219</u>	II,III,IV	
19	Mut- Dm20 (Cys-less Dm20)	Dm20	All Cys residues mutated to Ser residues <u>5,6,9,24,32,34,108,138,140,168,183,200</u> <u>.219,227</u>	II,III,IV, V	0,616942

Table 3: Generated constructs of PLP and Dm20 cDNA with point mutated Cys codons. Nomenclature representing positions of the mutated Cys residues and their corresponding exons are listed. *In silico* average protein hydrophobicity values (Section 3.2) are indicated. Bold, underlined and italicized numbers indicate mutated Cys positions with deleted S-acylation sites. Bold, underlined and italicized numbers indicate Cys positions involved in of Disulfide bridges.

3.1.2 DNA sequencing

Cys codons mutated to Ser codons in cDNA fragments generated (Section 3.1, Table 3) were confirmed by DNA sequencing. In Mut-PLP and Mut-Dm20 all the Cys codons were mutated to Ser codons.



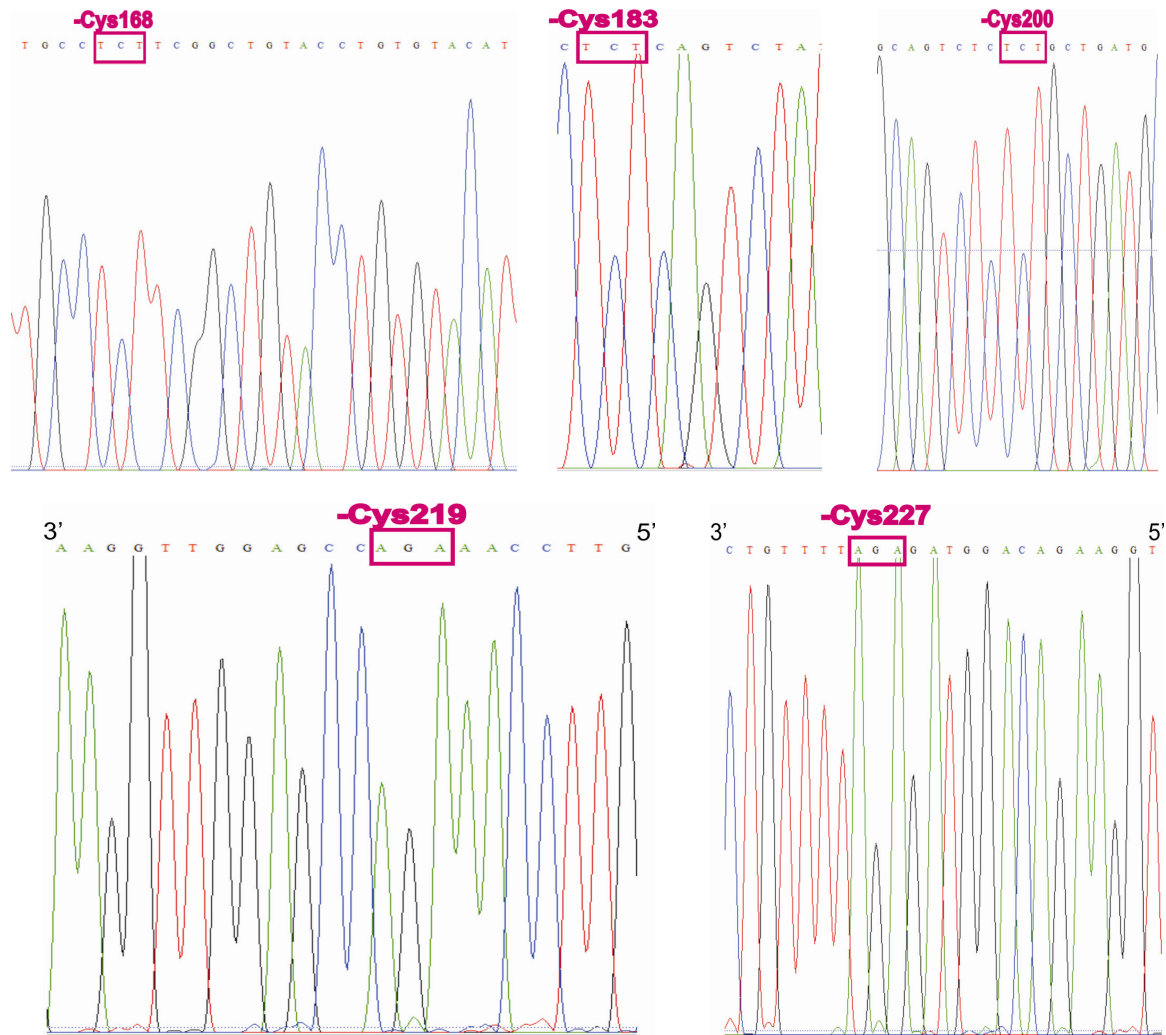


Figure 12: DNA sequencing results of Mut-PLP/Dm20. All 14 Cys codons that were interchanged to Ser codons were verified.

3.2 *In silico* Kyte-Doolittle hydropathy plots

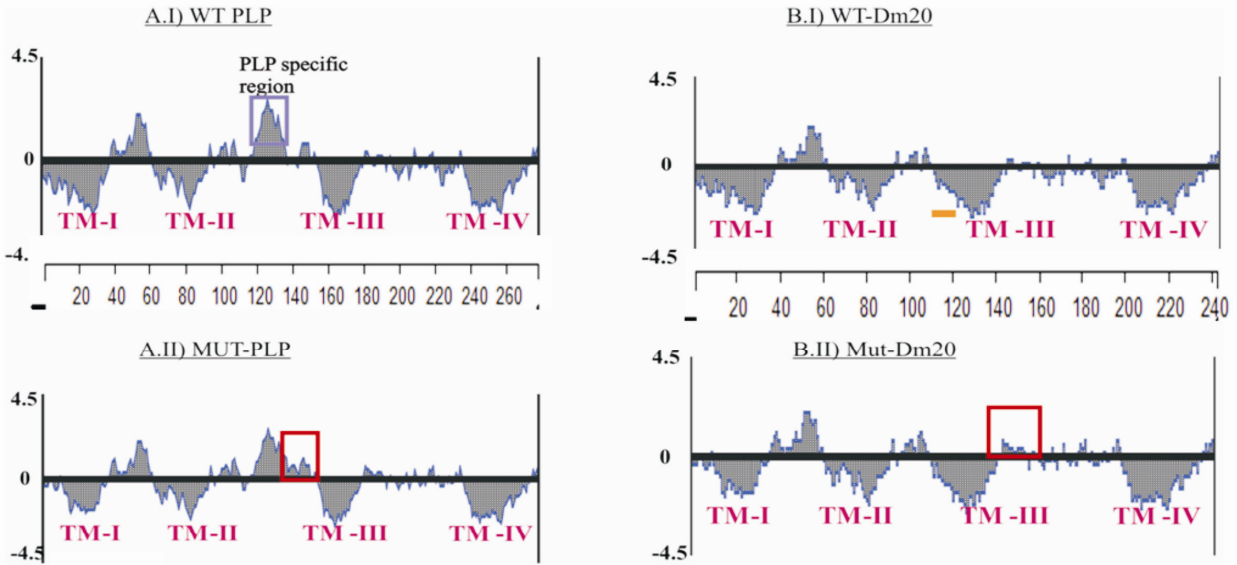
Trafficking of PLP to the plasma membrane depends on factors such as hydrophobic properties and protein lipidation. The shift in hydrophobicity may affect PLP/Dm20 sorting and trafficking to the membrane (Kraemer-Albers *et al.*, 2006).

In silico Kyte-Doolittle hydropathy plots (Kyte and Doolittle 1982) based on amino acid sequences of WT-PLP, Mut-PLP (Cys substituted to Ser PLP), WT-Dm20, and Mut-Dm20 (Cys substituted Ser Dm20) were generated. The DNASTAR Protean program with a minimizing parameter of window 11, as suggested for PLP/Dm20 (Dhaunchak *et al*, 2011) was used. Kyte-Doolittle hydropathy plots can indicate potential transmembrane protein structure and hydrophilic surface regions (Kyte and Doolittle, 1982).

WT-PLP, Mut-PLP, WT-Dm20 and Mut-Dm20 hydropathy plots indicated four hydrophobic transmembrane domains (TM). WT-PLP and Mut-PLP plots also indicated an additional hydrophilic domain of PLP specific (Figure 13 A.I, blue box) in comparison to WT/Mut-Dm20 plots, were in agreement with the biochemical topology studies of PLP by Weimbs and Stoffel, 1992.

Compared with the WT-PLP plot, the Mut-PLP plot showed a partial extended hydrophilic domain into hydrophilic space i.e., in between TM II and III (Figure 13 A.II, red box) which might corresponds to the *in vivo* PLP topology intracellular PLP specific hydrophilic loop. The Mut-Dm20 plot also showed an extended hydrophilic domain into the hydrophilic space (Figure 13 B.II, red box) but not with considerable difference from WT-Dm20. *In silico* amino acid hydropathy index values (Figure 13 C) were obtained from SOSUI program (Mitaku *et al.*, 2002) which predicted reduced hydropathy index values for mutated forms in comparison to the WT forms of PLP and Dm20 (Figure 13 C).

Thus *in silico* prediction of hydrophobic properties i.e. based on hydropathy plots or hydrophilic/hydrophobic structural orientation (Figure 13 A and B), and amino acid hydropathy index (Figure 13 C) suggest that under *in vivo* conditions there might be a considerable decrease of hydrophobicity from WT to mutated forms of PLP and Dm20. Moreover, in Mut-PLP there may be a partial but considerable conformational disturbance within the hydrophilic domain compared to WT-PLP. This might alter normal plasma membrane trafficking of Mut-PLP and Mut-Dm20 compared to WT forms *in vivo*.



C.

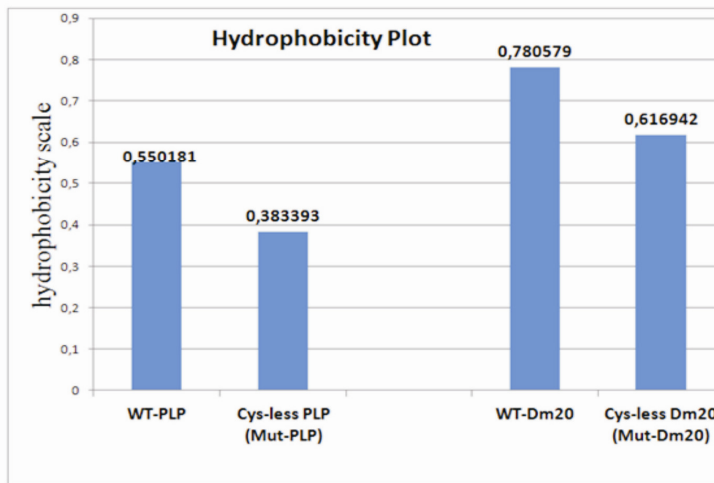


Figure 13: *In silico* Kyte and Doolittle hydrophobicity/hydrophilicity plots of WT-PLP/Dm20, Mut-PLP/Dm20: In the plot, positive values indicate predicted hydrophilic structural orientation whereas negative values indicate predicted hydrophobic structural orientation. All plots, including WT and mutated forms, predict four transmembrane hydrophobic domains with additional features. Plots were generated from the DNASTAR, Protean software with a minimizing window of 11, with amino acid sequence as input.

A. I) The WT-PLP plot depicting four hydrophobic domains (TM-I, II, III and IV) in negative values, and also a hydrophilic PLP loop in positive values (blue box in figure A.I) is in agreement to the *in vivo* PLP topology II) In the Mut-PLP plot, the hydrophilic PLP loop specific region is partial disturbed and considerably extends into hydrophilic space (red box figure A, II) in comparison to that of PLP specific region of WT-PLP plot (Figure A, I) demonstrating that Mut-PLP is less hydrophobic and with a partial structural disturbance (red box) in comparison to WT-PLP.

B. I) WT-Dm20 plot; Line - indicates an extension of hydrophobic stretch of TM-III that is absent in WT-PLP plot. II) Mut-Dm20 showing an extended loop after TM-III in hydrophilic space (Red Box) in comparison with WT-Dm20 plot which predicts that Mut-DM20 is partially altered with no considerable differences.

C. Hydropathy index values obtained from SOSUI program. Hydrophobicity values obtained for individual proteins is depicted; WT-Dm20 > Mut-Dm20 > WT-PLP > Mut-PLP.

3.3 EGFP fused WT-PLP, Mut-PLP, and Mut-Dm20; Intracellular trafficking

EGFP fused WT-PLP, Mut-PLP (Cys-less PLP), and Mut-Dm20 (Cys-less Dm20) cloning and their intracellular trafficking were studied *in vitro* in non-glial cell line (i.e., COS-7 cells) and *in vivo* in glial cells (i.e., primary oligodendrocytes) as follows.

3.3.1 Cloning and validation of WT-PLP-EGFP, Mut-PLP-EGFP and Mut-Dm20-EGFP

WT-PLP, Mut-PLP and Mut-Dm20 cDNA constructs were obtained from the previously generated cDNA pool (Table 3). These cDNA fragments were used as templates for site-directed mutagenesis (SDM). By SDM, an XhoI restriction site was introduced at the 5' end and a mutated stop codon along with PstI restriction site was introduced at the 3' end of PLP/Dm20 cDNA. Thus prepared WT-PLP and Mut-PLP and Mut-Dm20 cDNA fragments were cloned into the EGFP.N2 expression plasmid (Clonotech) using XhoI and PstI restriction sites. Appropriate directional insertion and Cys mutations were confirmed by restriction analysis and by DNA sequencing.

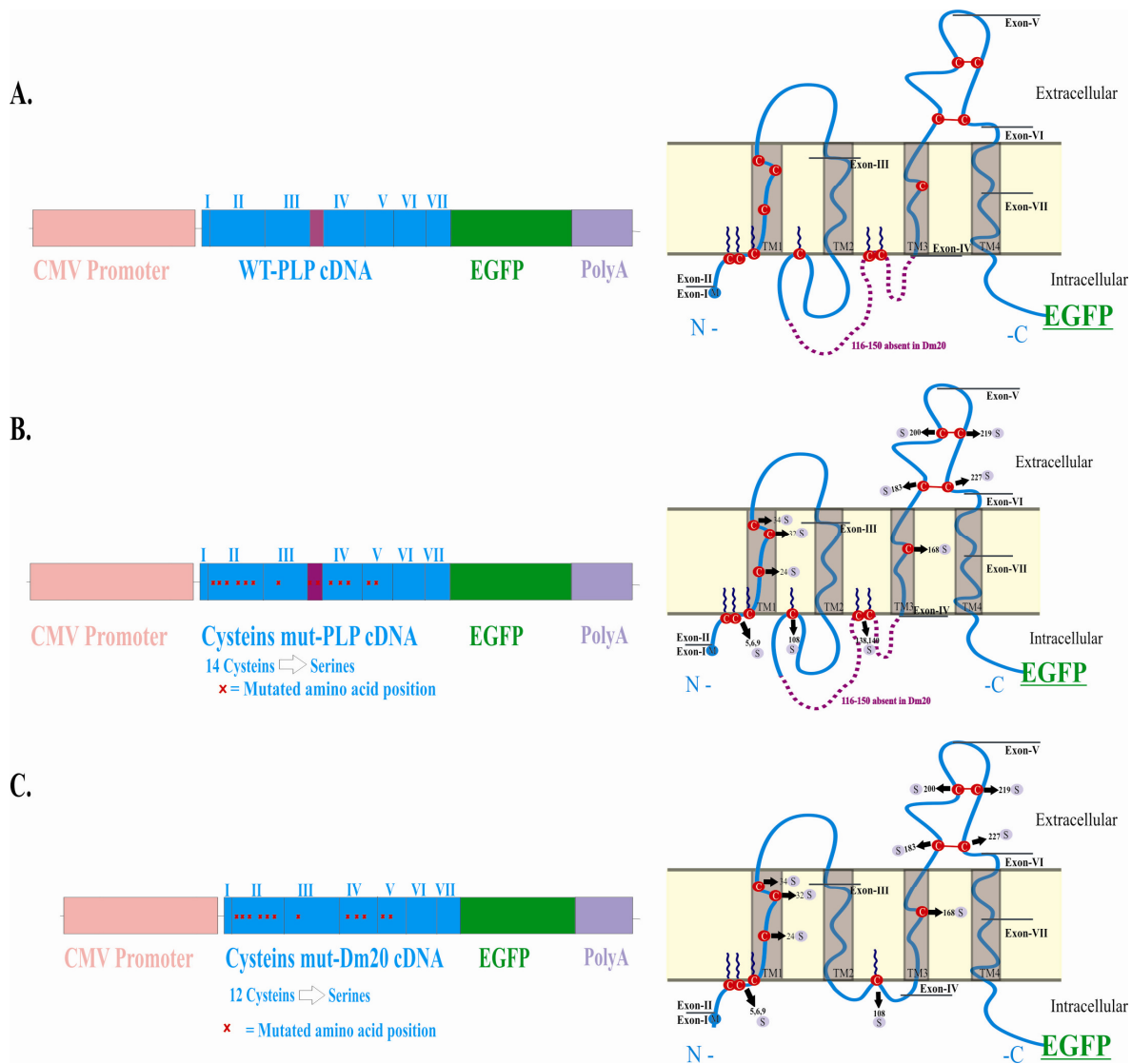


Figure 14: Schematic representation of A. WT-PLP-EGFP, B. Mut-PLP-EGFP and C. Mut-Dm20-EGFP constructs, and their corresponding protein structures including Cys mutations. N terminal CMV promoter, respective cDNA with eliminated stop codon was fused to N terminal EGFP in EGFP.N2 expression plasmid.

3.3.2 Mut-PLP-EGFP and Mut-Dm20-EGFP compared to WT-PLP-EGFP trafficking in COS-7 cells

Intracellular trafficking and plasma membrane targeting of the above cloned constructs WT-PLP-EGFP, Mut-PLP-EGFP, and Mut-Dm20-EGFP were studied *in vitro* in COS-7 cells.

Transfection and immunocytostainings were carried out as described in methods (Section 6.1.9). WT-PLP-EGFP transfected COS-7 cells immunocytostaining revealed that WT-PLP-EGFP (green) co-localizes in the plasma membrane projections (filopodia) and at the plasma membrane with anti-PLP (Cy3-red) staining (Figure 15 A-D and Inset, Figure 16.I A and D (Inset)). These results were consistent with previous results (Koizume *et al.*, 2006). Intriguingly, immunocytostaining of COS-7 cells transfected with Mut-PLP-EGFP and Mut-Dm20-EGFP individually revealed neither Mut-PLP-EGFP (green), Mut-Dm20-EGFP (green) or anti-PLP (CY3-red) staining was detected in the filopodia, at plasma membrane or at the cell surface (Figure 15 E-L and Inset).

Furthermore, the WT-PLP-EGFP, Mut-PLP-EGFP and Mut-Dm20-EGFP (green) were co-localized with the K58 (Golgi marker, Cy3-red) and BiP (ER marker, Cy3-red), (Figure 16.I E-L, Figure 16.II, arrows).

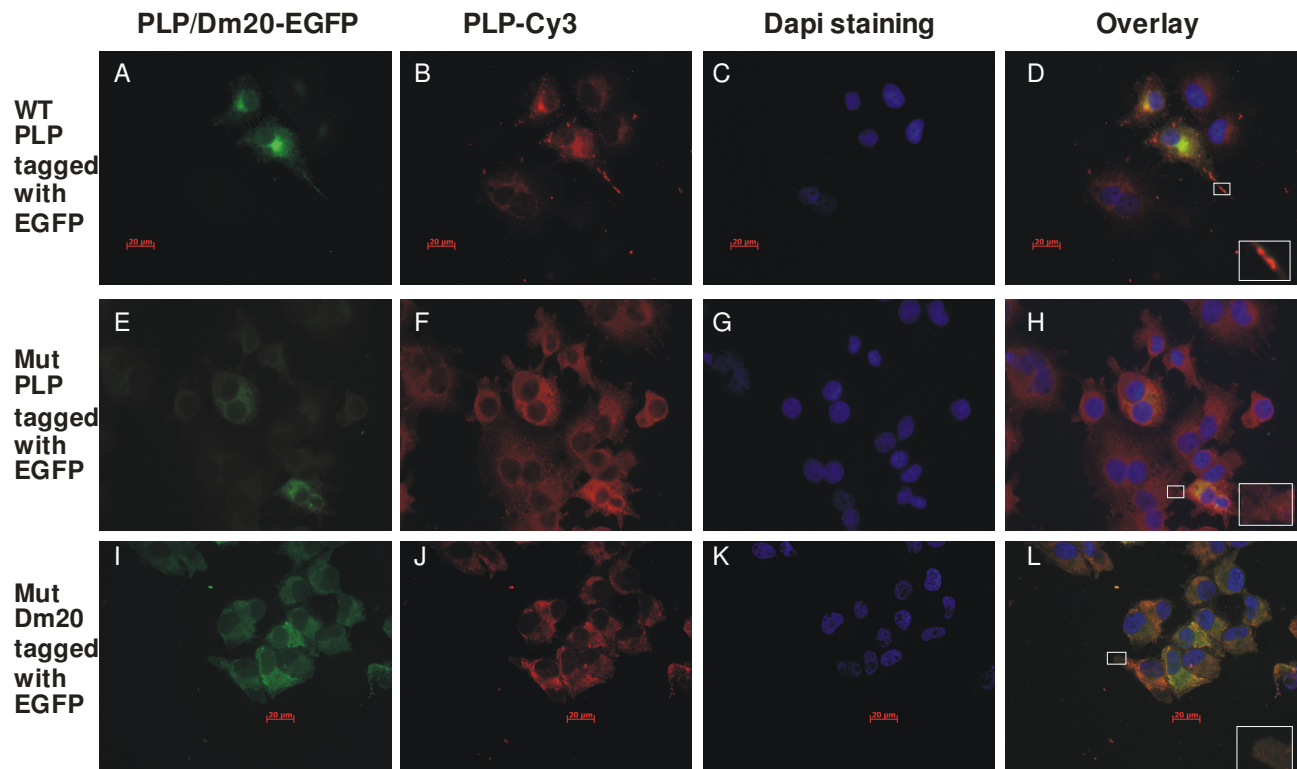


Figure 15: Localization of WT-PLP-EGFP, Mut-PLP-EGFP, and Mut-Dm20-EGFP fusion proteins in COS-7 cells. Immunostaining was performed with anti-PLP (1:200) and Cy3 conjugated secondary antibody (Jackson anti-rabbit-Cy3, 1:800) along with DAPI (for nuclei). Overlay = PLP/Dm20-EGFP (green), anti-PLP-Cy3 (red) and Dapi (blue).

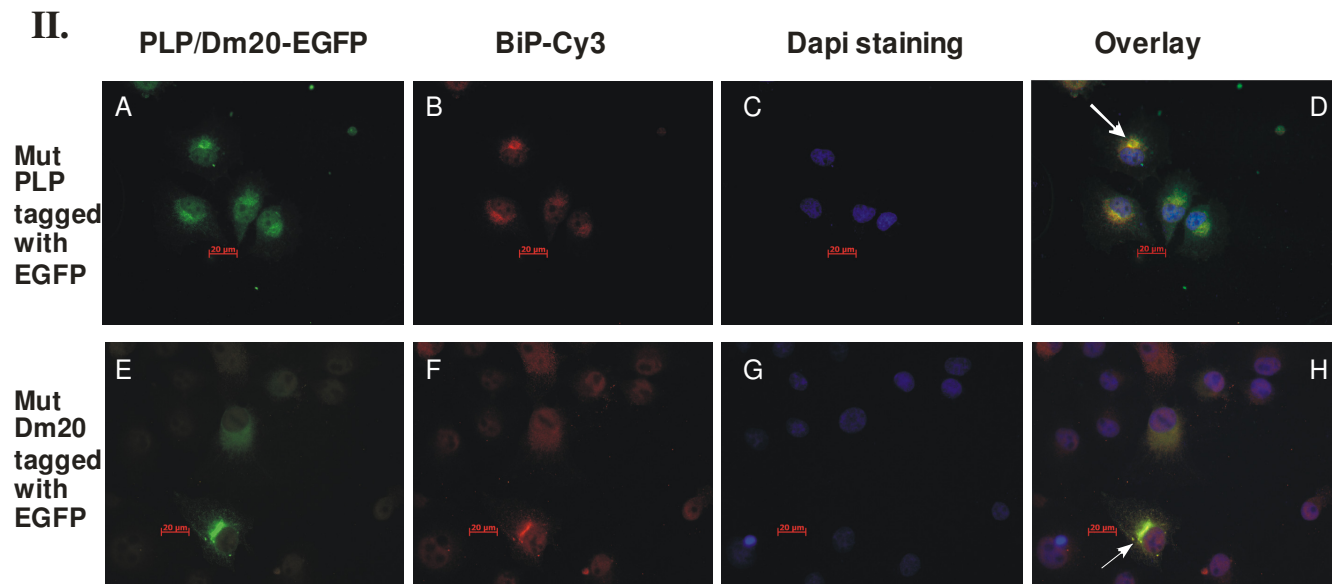
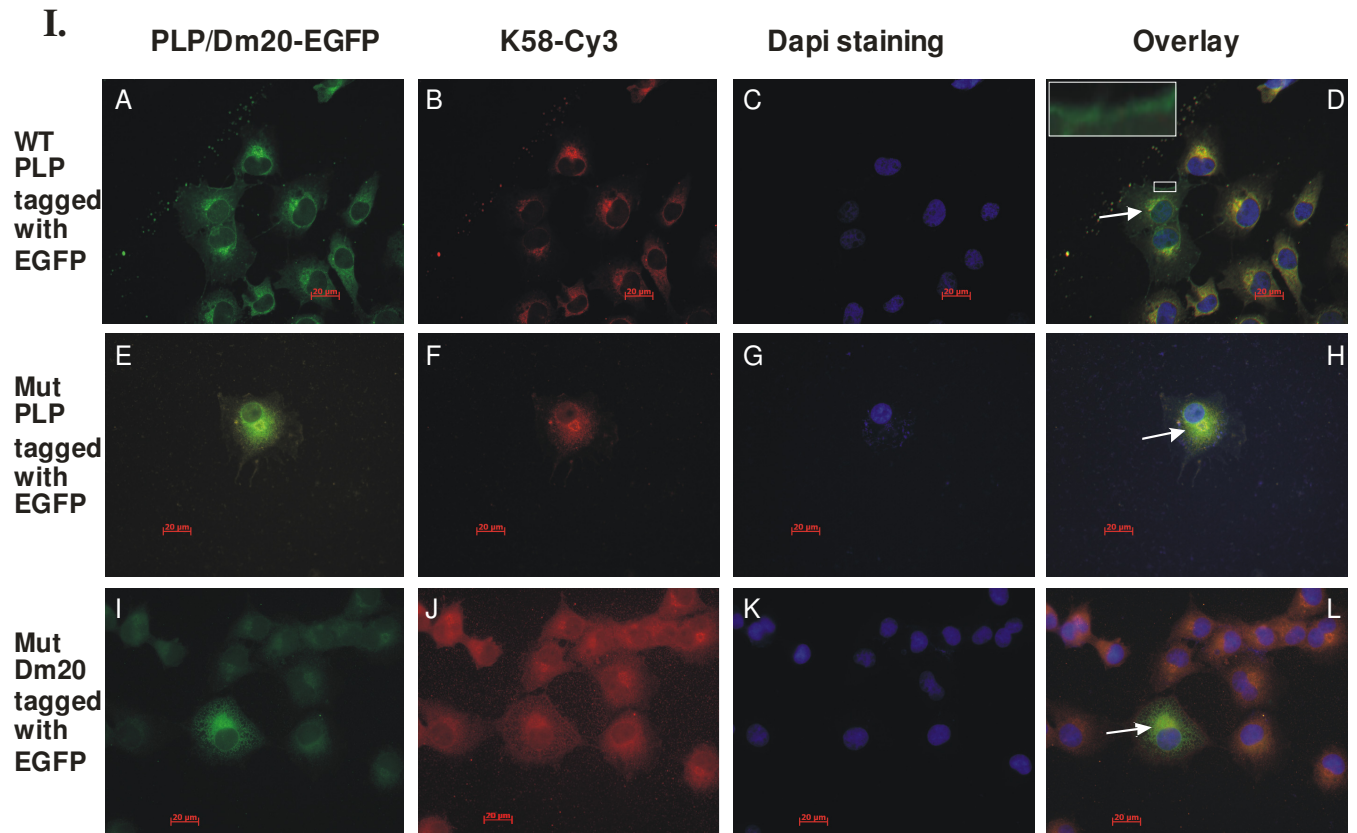


Figure 16: Localization of WT-PLP-EGFP, Mut-PLP-EGFP, and Mut-Dm20-EGFP fusion proteins in COS-7 cells.

The staining was performed with Golgi apparatus and endoplasmic reticulum (ER) specific markers:

I) Staining with K58 (1:100, Sigma) and Cy3 conjugated secondary antibody (Jackson anti-rabbit-Cy3, 1:800) and DAPI. PLP/Dm20-EGFP (green), anti-K58/Cy3 (red) and Dapi (blue). Overlay = EGFP (green) + anti-K58/Cy3 (red) + Dapi (blue).

II) Staining with anti-BiP (1:200, Biomol) and Cy3 conjugated secondary antibody (Jackson anti-rabbit-Cy3, 1:800) and DAPI (blue). PLP/Dm20-EGFP (green), anti-BiP-Cy3 (red) and Dapi (blue). Overlay = EGFP (green) + anti-K58/Cy3 (red) + Dapi (blue).

3.3.3 WT-PLP-EGFP and Mut-PLP-EGFP trafficking in PLP null oligodendrocytes

To understand the intracellular trafficking of WT-PLP-EGFP and Mut-PLP-EGFP under *in vivo* conditions, we employed primary cultures of oligodendrocytes derived from neonatal PLP^{-/-} mice brain. Oligodendrocytes derived from plp^{-/-} mice, lacks endogenous WT-PLP production which has been genetically deleted, and are perfect tissue culture models, which mimic glial lineage.

3.3.3.1 Isolation and transfection of PLP-null murine oligodendrocytes

Progenitor oligodendrocytes or oligodendrocytes were isolated from neonatal PLP^{-/-} mice brain during their early myelination phase p7-p10 (7-10 days old) using Macs-columns (Miltenyi) for oligodendrocyte purification (Miltenyi; Cizkova *et al.*, 2009). Oligodendrocytes were further tested with various oligodendrocyte specific markers for determining the oligodendrocyte quality. Thus derived primary oligodendrocyte cultures were transiently transfected with WT-PLP-EGFP and Mut-PLP-EGFP DNA constructs. Immunocytostainings were carried out 24-46 hours after transfection.

3.3.3.2 WT-PLP-EGFP and Mut-PLP-EGFP membrane targeting in oligodendrocytes

The WT-PLP-EGFP transfected oligodendrocytes revealed that WT-PLP-EGFP (green) was observed in the filopodia and at plasma membrane, which was also confirmed by anti-PLP (cy3-red) immunostaining (Figure 17). On the other hand, Mut-PLP-EGFP transfected

oligodendrocytes revealed that Mut-PLP-EGFP fluorescence (green) was detected only in the cytoplasm and not in filopodia or at the plasma membrane, which was also confirmed by the anti-PLP (Cy3-red) immunostaining (Figure 18).

Although WT and mutant forms of PLP/Dm20 were extensively expressed in the cytoplasm, they show differential sorting, trafficking and integration into the plasma membrane. WT-PLP-EGFP is sorted and integrated into the plasma membrane but Mut-PLP-EGFP failed to be recruited to the plasma membrane. These *in vivo* or native cell type system results are consistent with the plasma membrane trafficking results observed under *in vitro* conditions in COS-7 cells (Section 3.3.2).

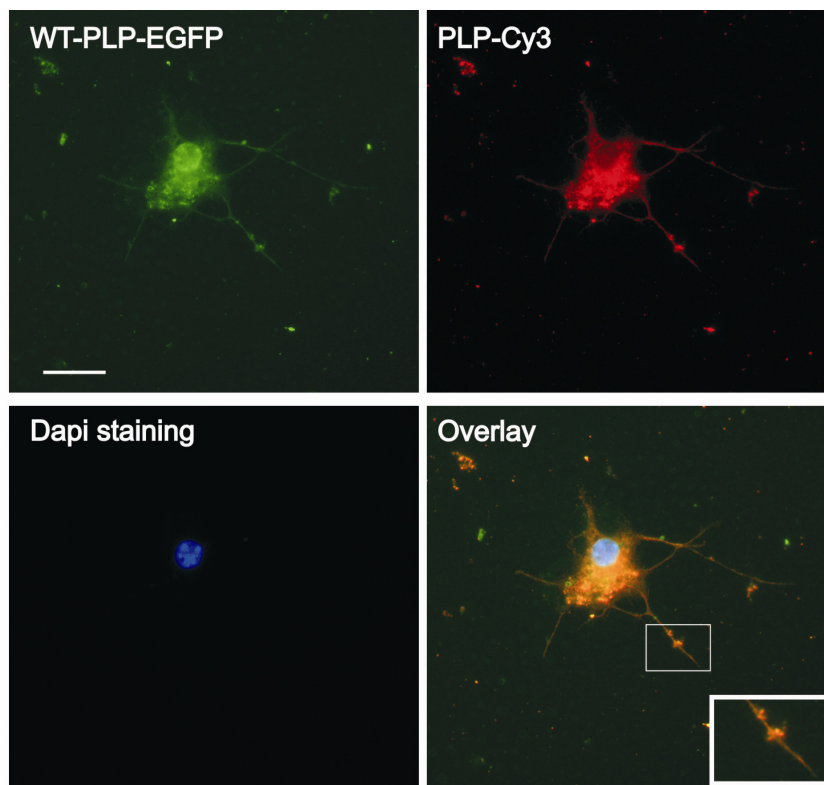


Figure 17: Localization of WT-PLP-EGFP in PLP null oligodendrocytes. WT-PLP-EGFP transfected oligodendrocytes immunostained with anti-PLP (1:200) and a Cy3 conjugated secondary antibody (Jackson anti-rabbit, 1:800) and Dapi; WT-PLP-EGFP (green), anti-PLP (Cy3/red), and nucleus (blue). Overlay= WT-PLP-EGFP (green) + anti-PLP (Cy3/red), + Dapi (blue). 20 μ m scale

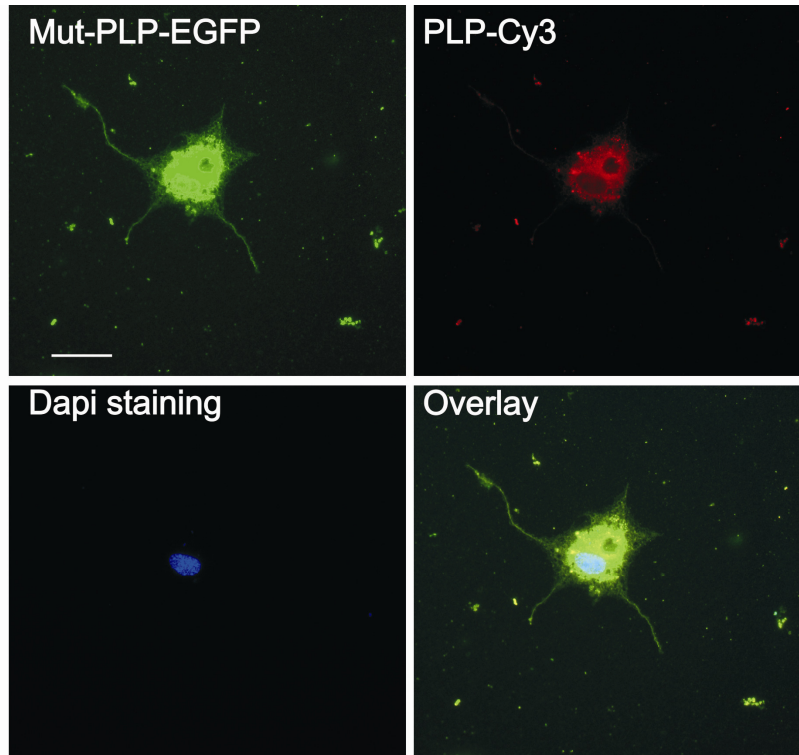


Figure 18: Localization of Mut-PLP-EGFP in PLP null oligodendrocytes. Mut-PLP-EGFP transfected oligodendrocytes immunostained with anti-PLP (1:200) and Cy3 conjugated secondary antibody (Jackson anti-rabbit, 1:800) and Dapi; Mut-PLP-EGFP auto-fluorescence (green), anti-PLP (Cy3/red), nucleus (blue). Overlay=Mut-PLP-EGFP (green) +anti-PLP (Cy3/red) +dapi(blue). 20 μ m scale

3.4 Mut-PLP expression under the control of Nestin-enhancer; generation of a transgenic mutant

3.4.1 Validation of Nestin enhancer function in OLN93 cells

We validated the Nestin enhancer gene element (human nestin gene II-Intron sequence (Lothian and Lendahl, 1997) as a controlling element for regulating the Mut-PLP (Cys-mut PLP) expression, as follows.

Cloning: Nestin enhancer sequence (1.8 kb) with a HSV-TK promoter was obtained from Lothian and Lendahl, and cloned into the pBSKII(+/-) vector. The Mut-PLP cDNA fragment (listed in Section 3.1, Table 3) and a poly (A) tail (Clontech) was engineered at the 3' end of the HSV-TK promoter. Orientation of the individually cloned fragments was confirmed by restriction digestion and by DNA sequencing.

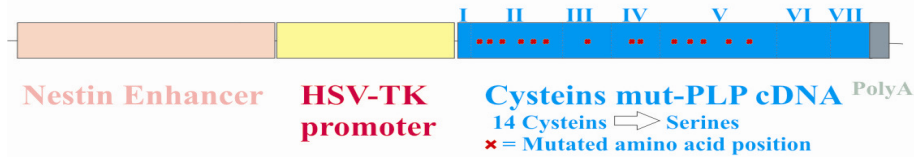


Figure 19: NesMut-PLP construct. From 5' to 3' direction: Nestin enhancer, tk promoter, Mut-PLP cDNA and polyA tail, cloned into the pBSKII(+/-) vector.

Over-expression and semi-quantification of Mut-PLP mRNA over-expression in OLN93

The Nestin-Mut-PLP construct was transfected into OLN93 cells. Expression levels of PLP and Dm20 mRNAs were then quantified with cDNA specific primers.

Total mRNA was isolated from NesMut-PLP transfected OLN93 cell lines (clones 3 and 4) and non-transfected OLN93 cell lines. Isolated mRNA was reverse transcribed with universal primers to generate total cDNA, and PLP and Dm20 cDNA specific primers were used for qRT-PCR. HGPRT cRNA primers were used as a loading control. In contrast to non-transfected OLN93 cells, the NesMut-PLP transfected OLN93 cell clones A and B showed two fold higher expression of PLP mRNA. The Dm20+PLP mRNA levels in clone A and B revealed constant Dm20 mRNA levels (Figure 20). This data suggests that the nestin enhancer can drive Mut-PLP over-expression in OLN93 cells.

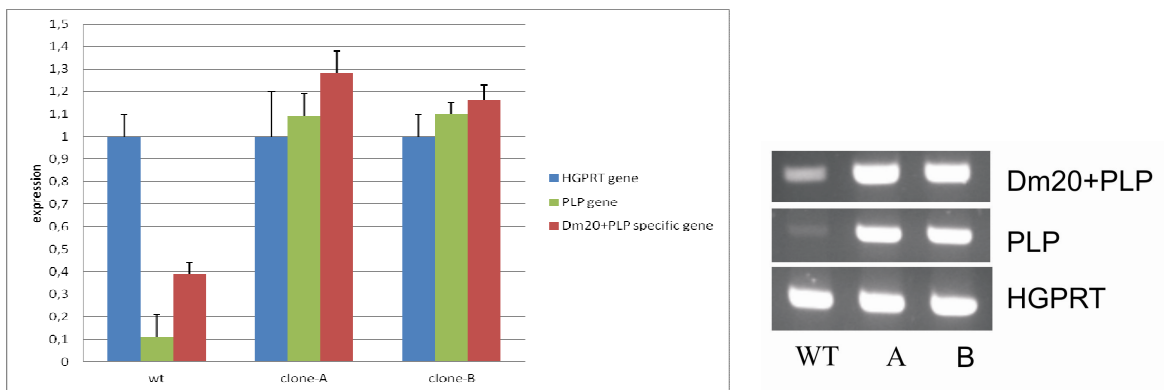


Figure 20: Semi-quantitative RT-PCR: WT (untransfected OLN93 cells), and clone A and B of

NesMutPLP transfected OLN93 cells. Densitometric data from RT-PCR analysis. Data represented from three independent experiments (mean± SEM).

3.4.2 Nh/MBPMut-PLP Transgenic mice generation

Transgenic mice with Nestin enhancer and Mbp promoter driven Mut-PLP has been generated to address the points of 1) Nestin enhancer regulation in early glial precursors i.e., O4 and oligodendrocytes 2) expression and control of MBP promoter plus Nestin enhancer on Mut-PLP 3) the impact of the loss of post-translational S-acylation of PLP on its functional activity in intracellular trafficking, myelinogenesis and in myelin compaction and maintenance, and 5) the role of Mut-PLP in Pelizaeus–Merzbacher disease.

Since it has been shown previously that MBP expression is crucial and specific for myelination and it is expressed in early and mature glial cells we employed the MBP promoter, which has been well characterized in our laboratory (Stefan Meininger, 2004), together with the Nestin enhancer in cloning of the transgene construct.

In the transgene, the enhanced green fluorescent protein sequence together with IRES (internal ribosome entry site) sequence was engineered to the 3' end of the Mut-PLP cDNA.

3.4.2 Trans-gene cloning and pronuclear injection

a. Trans-gene cloning

The HSV-TK promoter of NesMut-PLP construct (Figure 19) was replaced with the 1.2 kb MBP promoter sequence obtained from Meininger, 2004. A 1.8kb EGFP with poly(A) tail DNA (Clontech) was then cloned into the XhoI sites to the 3' end of Mut-PLP. Orientation of the individual fragments was confirmed by restriction digestion and DNA sequencing. The generated Nh/MBPMut-PLP transgene construct (Figure 21) was used for pronuclear injection.

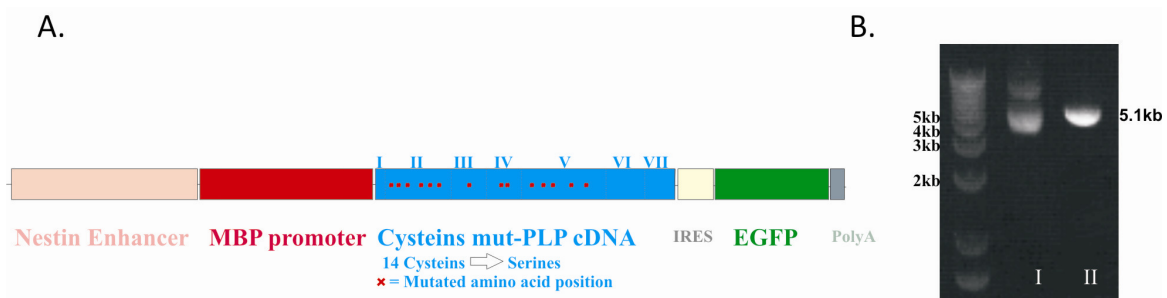


Figure 21: Pronuclear injection (PNI) construct: A. Nh/MBPMut-PLP; 5’ to 3’ direction cloned fragments of Nestin enhancer, MBP promoter, Mut-PLP, IRES and EGFP with a Poly(A) tail. B. Agarose gel depicting the trans-gene construct of 5.1 kb. Lane I: non-linearized construct (as a control), Lane II: linearized trans-gene construct.

b. Pronuclear injection

A transgenic mouse has been generated by pronuclear injection. The Nh/MBPMut-PLP transgene was injected into the pronuclei of oocytes derived from PLP null mutant females.

The ultra purified Nh/MBPMut-PLP transgene DNA fragment was injected into the pronuclei of oocytes or fertilized eggs of *plp*^{-/-} female mice. To obtain fertilized eggs (oocytes), *plp*^{-/-} transgenic female mice were super ovulated and mated with *plp*^{-/-} male mice. From 5 super-ovulated *plp*^{-/-} female mice, 50-60 fertilized eggs were isolated for micro injection of Nh/MBPMut-PLP transgene construct into their male pronuclei.

Pronuclear injection derived mice

S.No	Total No. of <i>plp</i> ^{-/-} oocytes injected with transgene construct	No. of litters born	No. of litters containing transgene construct	Founder/Transgene mice obtained
1	270	6	0	-

Table 4: Summary of the performed pronuclear injection experiments.

3.5 Generation of knock-in mouse mutant of PLP/Dm20 devoid of di-sulfide bridges

Gene-targeted mouse models are approved systems to investigate neurological disorders at the molecular level *in vivo*. In order to study the functional consequences of PLP devoid of the two disulfide bridges (Cys¹⁸³ with Cys²²⁷ and Cys²⁰⁰ with Cys²¹⁹) *in vivo*, a PLP knock-in mouse mutant is being generated via homologous recombination in ES cells.

For selection of homologously recombined ES clones, a positive selection agent G418 (neomycin analogue) and a negative selection agent ganciclovir (Ganc) were used. Positive selection was enabled by expression of the gene coding for neomycin phosphotransferase that inactivates G418 by phosphorylation allowing only homologous recombined ES clones to survive. In the absence of recombination G418 blocks protein synthesis and kills the non-recombined ES cell. A negative selection was obtained by expression of the HSV-TK gene which is located at the 5' end of the linearized targeting construct that does not integrate into the ES cell genome in correct homologous recombination. During non-homologous recombination events the HSV-TK sequence is incorporated into the genome of ES cell and thereby thymidine kinase phosphorylation of GanC inhibits DNA synthesis resulting in ES cell death.

3.5.1 Knock-in targeting construct and targeting strategy

A 5' homology arm of 2.5kb, consisting of PLP gene partial Intron-I to exon-III and partial Intron-III, was cloned using NotI and AvrII restriction sites into the PEFRTGK12 gene targeting vector. The 3' targeting arm of 6.8 Kb fragment, consisting of PLP partial intron-III, exon-IV, exon-V containing four Cys point mutations (C183S, C227S, C200S, and C219S), and exon-IV to partial exon-VII, was cloned via HpaI and XhoI restriction sites. Cys point mutations were introduced by the SDM. The HSV-TK sequence was located at the 3' end of the linearized construct (Figure 22).

All point mutations created by SDM and all cloned exon sequences were verified by DNA sequencing. The organization of the construct is depicted in Figure 22. The PBS246 gene targeting vector with the same 5' and 3' targeting arms of PEFRTGK12 vector was also cloned and used in electroporation.

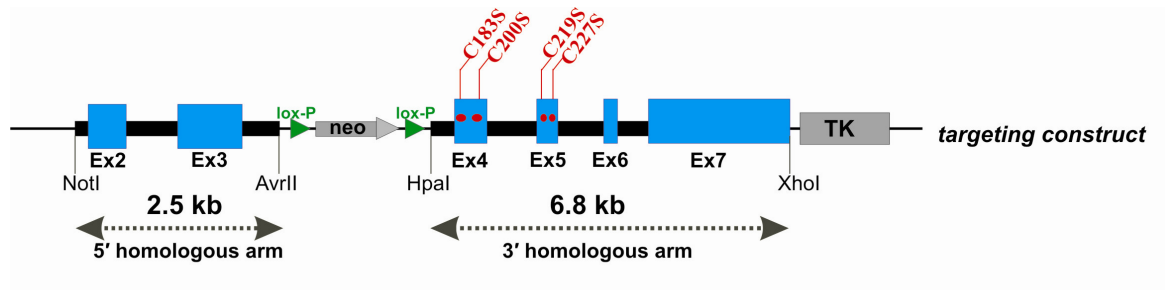


Figure 22: PLP knock-in targeting construct. PEFRTGK12 PLP gene targeting construct with a 2.5 kb left homologous arm and a 6.8 kb right homologous arm. Cys codons involved in formation of disulfide bridges were point mutated to Ser (C183S, C200S, C219S, C227S), depicted as red dots. The neomycin cassette (used for positive selection) flanked by loxP sites is present between the 5' and 3' homologous arms. The HSV-TK (used for negative selection) is located at the 3' end of the construct.

Targeting strategy

The targeting strategy for the PLP gene locus is depicted in figure 23. In the positively homologous recombined clones, the endogenous PLP allele locus containing all four Cys codons in exon IV and V were replaced by serine codons, and a neomycin cassette flanking with loxP sequences is located between exons III and IV.

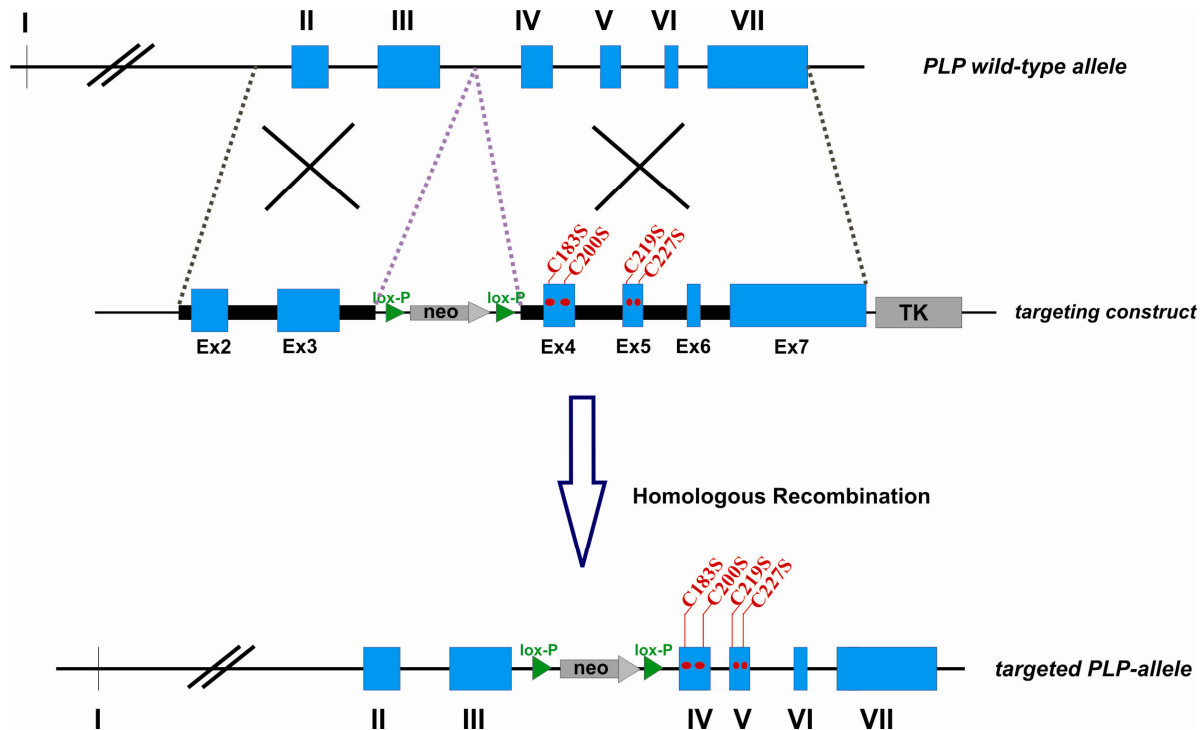


Figure 13: Schematic representation of mouse PLP gene locus targeting strategy. A) WT PLP gene allele B) Final targeted PLP-allele gene locus; Mutated Cys codons (red dots), Neomycin cassette flanked by loxP sites located between exons III and IV.

3.5.2 ES cells electroporation and ES clones screening

ES cells were transfected by electroporation (Biorad). ES cell lines V8.1 (Eggan *et al.*, 2001), 6J (Tanimoto., *et al* 2008) and JM8.F6 (Pettitt., *et al* 2009) (V8.1) previously tested in gene manipulation and germ line transmission were used for electroporations. All ES cell lines were cultured on mitotically inactivated embryonic fibroblast feeders. Leukemia inhibitory factor (LIF) was added to the culture media to prevent differentiation of the ES cells. 2×10^7 ES cells in their exponential growth phase were used for each electroporation with 35-40 μ g of PLP gene targeting construct linearized with NotI or PvuI. Four hours after electroporation, cells were selected in G418 and Ganc selection medium.

Summary of ES cells electroporation and screening

ES cell	PLP targeting constructs	Enzyme used for linearization	No. of clones analyzed	Homologous recombined clones obtained
V8.1	PBS246	PvuI	210	0
6J	PBS246, PEFRTGK12	PvuI and NotI	756 (PvuI), 674 (NotI)	0
JM8.F6	PEFRTGK12	NotI	454	1

Table 5: Summary of electroporation and screening.

3.5.3 Verification of a positive ES clone

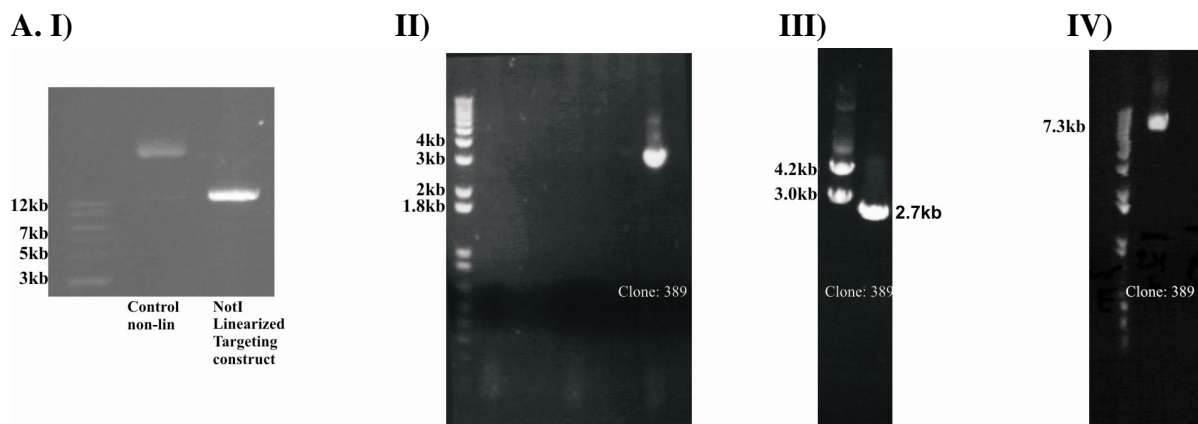
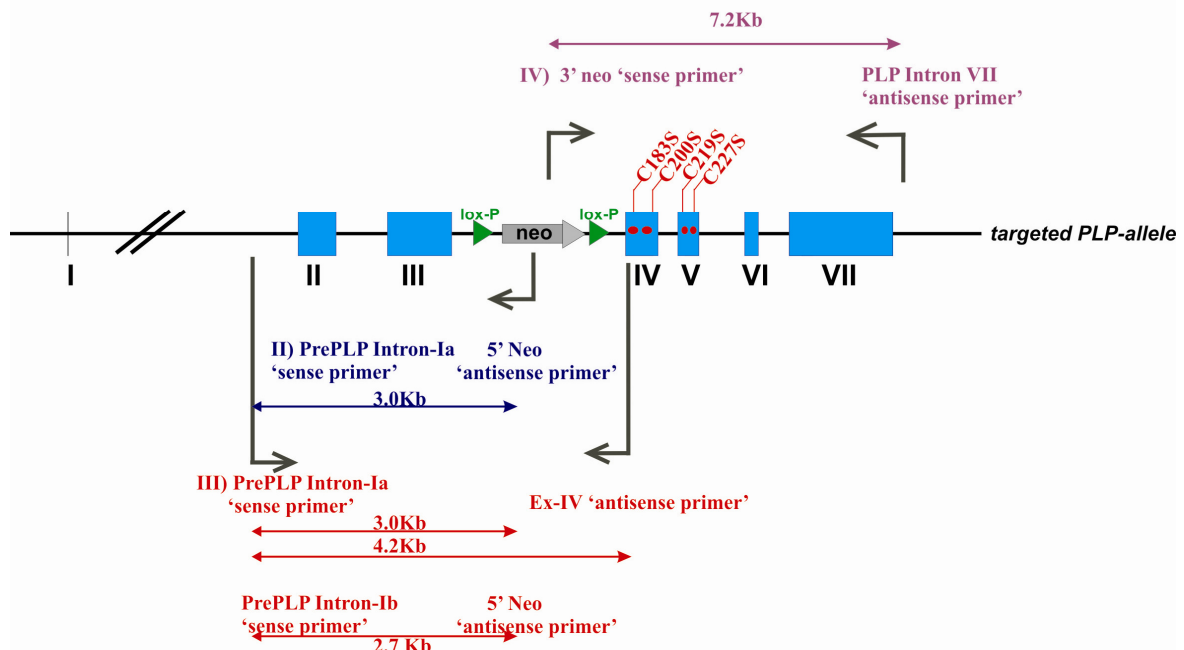


Figure 24: Validation of ES clones for homologous recombination by PCR analysis:

I) Targeting construct linearization: Lane I: DNA marker (NEB), Lane II: control (non-linearized targeting construct), Lane II: NotI linearized targeting construct.

II) Initial screening of ES clones for homologous recombination: a 3kb PCR fragment obtained with Pre PLP Intron-Ia 'sense primer' (primer outside the 5' end of the 5' homology arm) and 5'Neo 'antisense primer' (primer inside the neomycin cassette) confirmed homologous recombination of the 5' fragment. Non-homologous recombination yielded empty lanes.

Further validation of the obtained positive ES clone: Using positive ES clone DNA as a PCR template;

III) Lane-I: targeted PLP allele of 4.2 Kb (homologous fragment of 3.0 kb) + neomycin gene sequence (1.2kb) and WT PLP allele of 3.0 kb (homologously recombined fragment of 3.0 kb); obtained with primers plp intron-Ia ‘sense primer’ (outside the 5’ end of the 5’ homology arm) and PLP Ex-IV ‘antisense primer’ (primer outside the 3’ end of the neo-cassette in exon IV).

Lane-II: 2.7 PCR fragment of targeted allele; obtained by Preplp intron-Ib ‘sense primer’ (Primer outside to the 5’ end of the 5’ targeting arm) and 5’Neo ‘antisense primer’ (primer present in the neomycin cassette). **IV) Validation of 3’ targeting fragment:** A 7.3kb PCR fragment obtained by 3’neo sense primer (present in the neomycin cassette) and PLP Intron VII ‘antisense primer’ (present outside towards the 3’ end of the 3’ homology arm) resulted in a 7.2 kb fragment confirming 3’ homology arm targeting to the endogenous PLP allele in the positive ES cell clone.

3.5.4 Mutated Cys residues validation by DNA sequencing

Homologously targeted ES cell clone with four Cys mutations in PLP gene allele were validated by DNA sequencing; The following DNA sequencing results show the replacement of the four Cys to Ser codons, involved in forming two disulfide bridges (Cys¹⁸³-Cys²²⁷ and Cys²⁰⁰-Cys²¹⁹), located in exon IV and V of PLP gene.

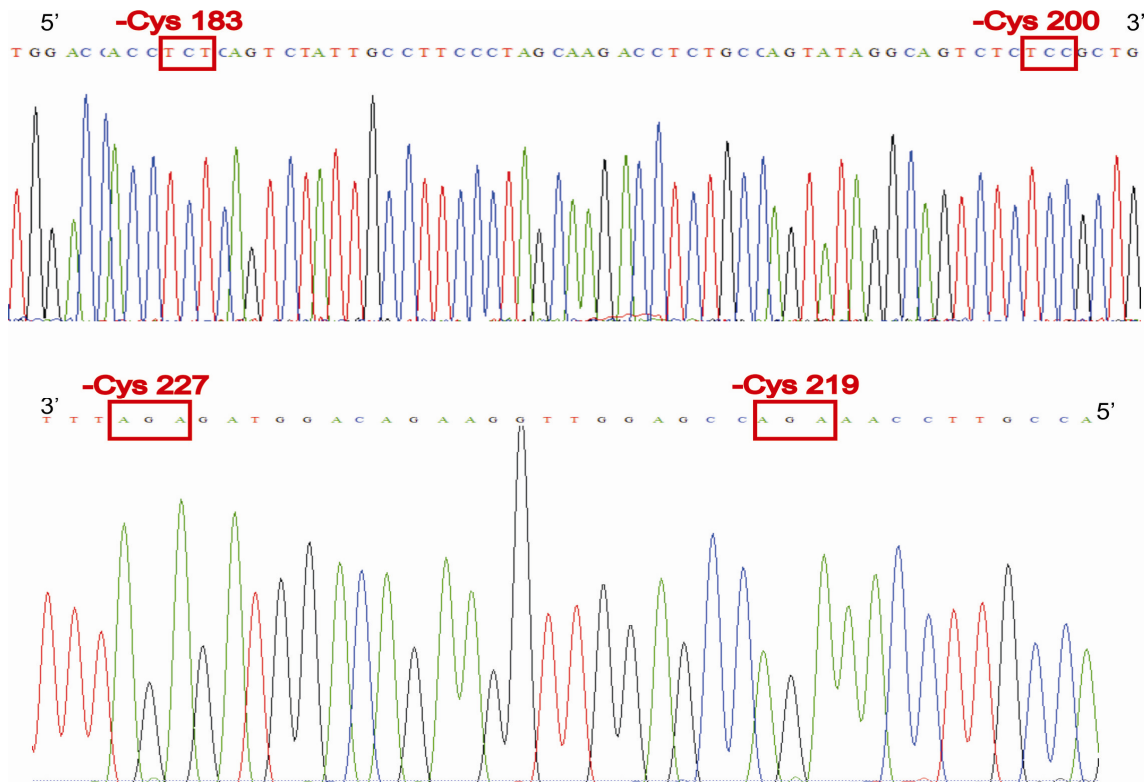


Figure 25: DNA sequencing results of the positive ES clone. Boxes depict the exact location of four Cys codons (183, 200, 219, and 227) that were interchanged with Ser codons.

3.5.5 Karyotyping of positive ES clone

Karyotyping was done to exclude aneuploidy (abnormal chromosomal number). Aneuploidy with monosomic and trisomic conditions in ES cells can impair gene targeting and germ line transmission (Liu *et al.*, 1997; Traut *et al.*, 1984). For karyotyping, ES cells were arrested at metaphase with colcemid and then lysed osmotically. The exposed chromosomes were stained with Giemsa. Chromosomes number was counted using light microscopy. Each ES cell (n=8) has 40 chromosomes and no aneuploidy was detected.

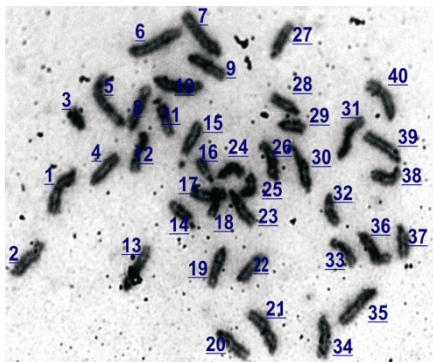


Figure 2: Karyotyping of targeted JM8.F6 ES cell clone. 100x magnification, chromosomes are numbered arbitrarily, image representative of n=8 ES cells.

3.5.6 Embryo manipulation

PLP gene targeted ES clones were injected into the blastocysts to generate PLP knock-in mice. 3.5-day post-coitum (p.c) blastocysts were isolated from super ovulated C57BL/6 pregnant mice. Based on the quality of the blastocysts, 10-25 ES cells were microinjected into the blastocyst inner-cell mass. Successfully injected blastocysts were cultured for 1 hour in the incubator for recovery and 6-10 blastocysts were re-implanted into each uterine horn of pseudo pregnant CD1 mice of day 2.5 p.c.

Targeted ES clone used for blastocyst injections	No. of reimplanted blastocysts	Obtained offsprings	Positively validated offspring derived from PLP gene targeted ES cell clone
JM8.F6	80	18	4 (male), 1(female)

Table 6: Summary of blastocyst injections and offspring obtained.

3.5.7 Chimera validation and breeding

JM8.F6 ES clones of C57BL/6N origin have been shown to have 62% germ line transmission efficiency and produce a black coat color (Pettit *et al.*, 2009). Genotyping of chimeras was done by PCR of tail genomic DNA. Successful chimeras of mice no.1, 4, 9, 12 and 14 were validated as described in figure 27. Thus validated chimeric mice are currently in breeding to test germ line transmission and thus obtain heterozygous PLP knock-in mice.

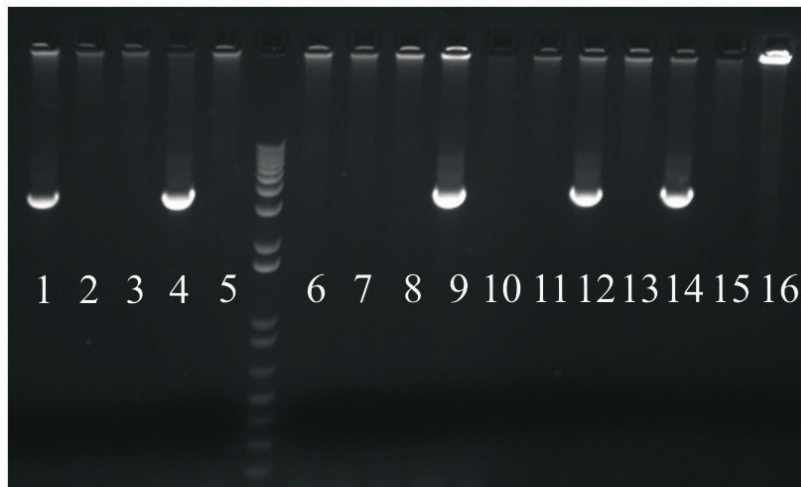


Figure 27: Identification of chimeric mice derived from blastocyst injected targeted ES cells. Tail genomic DNA from 16 pups was used for PCR with the preplp-intron-Ia sense primer (primer outside the 5' end of the 5' homology arm) and 5'Neo antisense primer (primer inside the neomycin cassette in between exon-III and IV). The observed 3kb PCR fragment from mice no.s 1, 4, 9, 12 and 14 are confirmed chimeras.

3.6 PLP and PUFAs pivotal role in the CNS.

The mouse is an excellent mammalian model system to investigate myelination, retinal function, and behavioral physiology. Myelin proteolipid protein (PLP) as well as the nature and ratio of PUFAs in the myelin phospholipids, might be essential in CNS membrane systems. They may also be critical for normal function of the CNS including visual and cognitive functions. To this end, we focused our investigations on the role of PLP in conjunction with PUFAs, by generating and characterizing homozygous *plp*^{-/-}*fads2*^{-/-} double knockout mouse/DM (DM). We describe here the biochemical, cellular, behavioral and myelin ultra-structural properties.

3.6.1 Generation of *plp*^{-/-}*fads2*^{-/-} DM mouse (DM)

Homozygous *plp*^{-/-}*fads2*^{-/-} mice (DM) were obtained by intercrossing PLP null and *fads2* null single mutant mice. Since the homozygous *fads2*^{-/-} mutants were infertile (Stoffel *et al.*, 2008), *fads2* +/- heterozygous male mice were crossed with *plp*^{-/-} homozygous female mice. The thus obtained heterozygous (*plp*^{-/-}*fads2*^{+/-}, *plp*^{+/-}*fads2*^{+/-}) mutants were interbred to obtain DM.

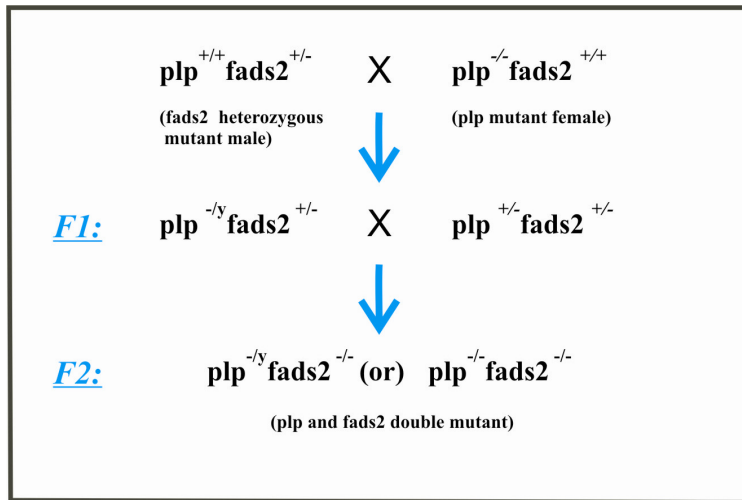


Figure 28: Schematic representation of breeding scheme for generating DM.

3.6.2 Genotyping and validation of DM

The DM mice were confirmed by genotyping with PLP and Fads2 gene specific PCR primers using tail genomic DNA (Figure 29, 30). Furthermore, loss of gene transcripts was validated on RNA level by RT-PCR using PLP and Fads2 cDNA specific primers. Loss of protein expression was validated by Western blots using anti-PLP and anti-Fads2 antibodies, and loss of PLP was also validated by immunohistostainings of brain cryosections (Figure 30).

Genotyping of the PLP allele in the DM was performed with PLP gene specific primers i.e., PLP 5'UTR sense primer (5' UTR 's.p') and neomycin cassette specific antisense primer (Neo 'as.p') which resulted in a 300bp fragment for the knockout PLP allele. The WT PLP allele was verified with the 5'UTR sense primer (5' UTR 's.p') and a gene specific intron-I antisense primer (Intron-I 'as.p') which resulted in a 150bp fragment (Figure 30). The PLP^{-/-} single mutant gene targeting has been described previously in Klugmann *et al.*, 1997.

PCR-genotyping of the fads2 allele of DM were performed with fads2 specific primers i.e., fads2 5' UTR sense primer (5'UTR 's.p') and fads2 exon-I 3'end antisense primer (ex-I 'a.p'), which yielded a 4.2kb fragment whereas the undisrupted WT Fads2 gene yielded a 2.6kb fragment, (Figure 30). Fads2^{-/-} single mutant gene targeting was described previously in Stoffel *et al.*, 2008.

DM gene targeted alleles

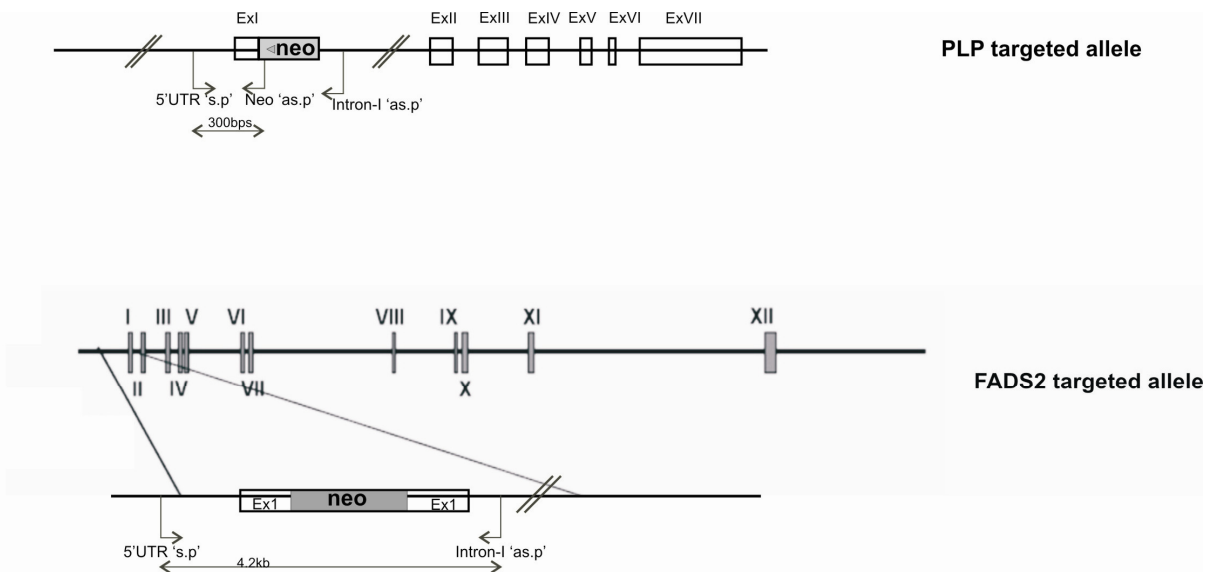


Figure 3: Schematic representation of PLP and Fads2 gene targeted alleles. Neomycin cassette is inserted in antisense direction in both PLP and Fads2 targeted alleles.

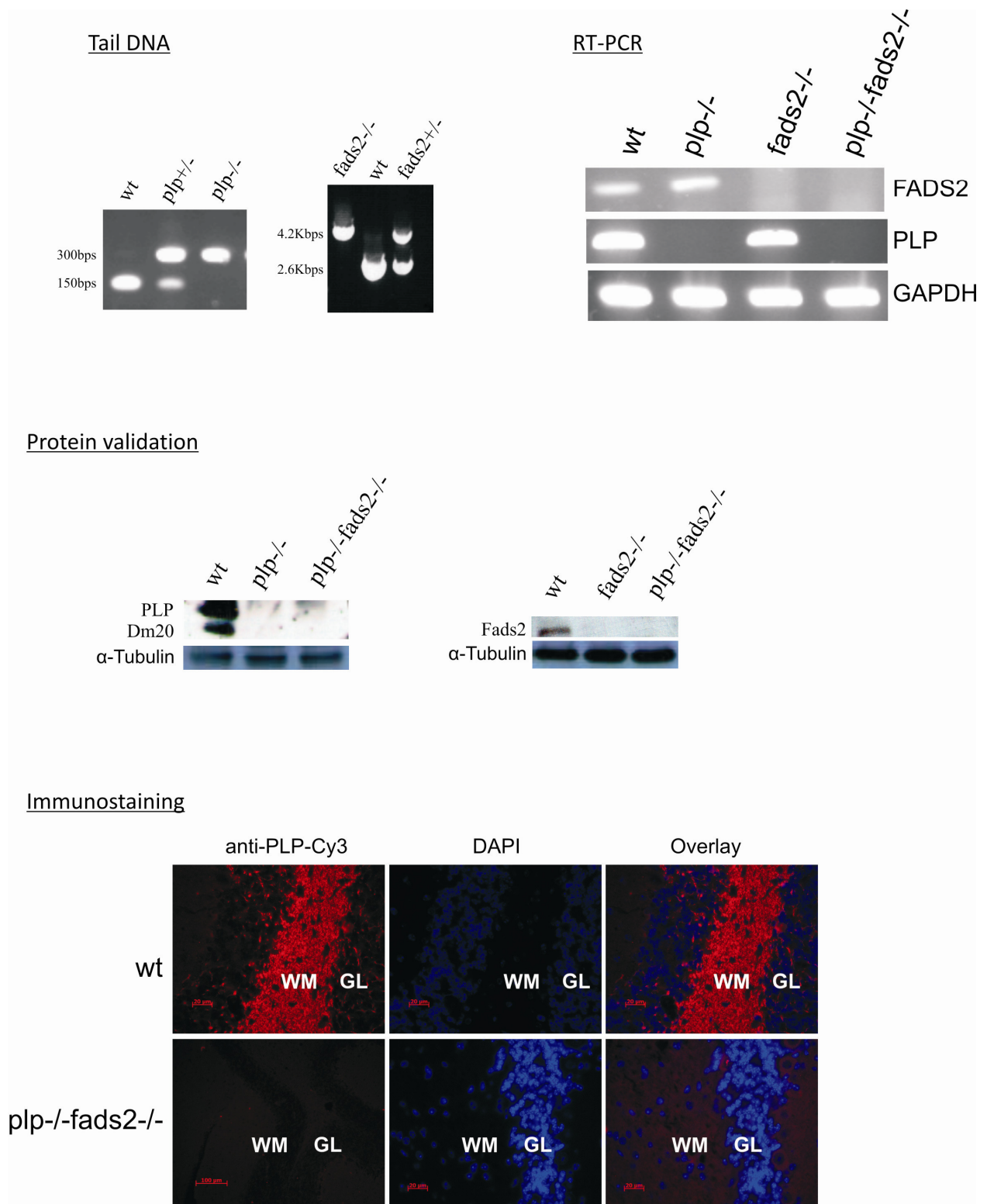


Figure 30: Validation of DM mice: Genotyping was performed using tail DNA with plp and fads2 gene specific primers, loss of PLP and Fads2 proteins were validated using anti-PLP and anti-Fads2 antibodies by Western blotting. Loss of PLP was validated by immunohistochemistry in sagittal brain cerebellar

sections of respective mouse mutants. Immunostaining was done with anti-PLP (Cy3-red), and dapi (blue).

3.6.3 Phenotyping of DM

Homozygous DM mice were viable but infertile, exhibited severe skin lesions and had a decreased lifespan. Mild shivering started from 5 months of age and resulted most often in a cataleptic state. Double heterozygous mutants i.e., *plp^{-/-}fads2^{+/-}* or *plp^{+/-}fads2^{+/-}* showed no significant phenotypic features.

The sterility, dermatitis and decreased life span of homozygous DM are due to the *fads2^{-/-}* allele. Compared to *fads2^{-/-}* single mutants, the DM mice were severely affected. The fertility of the different genotypes of the DM, homozygous and heterozygous mutants, was investigated by interbreeding of heterozygous or homozygous genotypes or with wild-type (C57BL/6) mice for a period of 4-6 months. The homozygous DM mice were infertile whereas the heterozygous *plp^{-/-}fads2^{+/-}*, *plp^{+/-}fads2^{+/-}* mutants were fertile. Fertility status of the different mutants is shown in the table 7. Onset of dermatitis in DMs was observed at age 5-6 months (n=5 animals) and progressed rapidly throughout their lifespan, table 7. Dermatitis was observed around neck or face or back in the form of patches with loss of hair and superficial erosions of the skin layers (Figure 31). No dermatitis was observed in *plp^{+/-}fads2^{+/-}*, *plp^{-/-}fads2^{+/-}*, *plp^{-/-}* or *fads2^{-/-}* heterozygous DMs.

The DM mice life expectancy was less than 10 months (n=6). *Fads2^{-/-}* single mutants had a lifespan of 1 to 1.5 years and all other genotypes showed no considerable change compared with wild-type. A descending order of life expectancy was observed: DM < *fads2^{-/-}* < *plp^{-/-}fads2^{+/-}* < *plp^{+/-}fads2^{+/-}* < *plp^{-/-}* < wild-type (Figure 32 A).

Body weight of all genotypes at p 24-days and 4 months were not significantly different, figure 32b.

Genotype	Sterile/ fertile	Dermatitis	Cataleptic behavior
Wild-type (CJ7BL/6)	Fertile	-	-
PLP null mutant	Fertile	-	-
Fads2 null mutant	Sterile	++	+
PLP+/-/Fads2+/- or PLP-/-/Fads2+/-	Fertile	-	-
DM	Sterile	+++	++

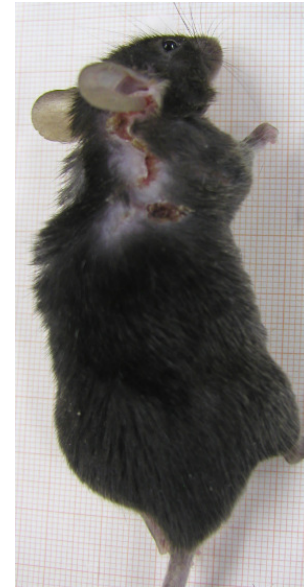


Table 7: Phenotyping of DM (plp-/-fads2-/-), single mutants (plp-/- or fads2-/-) and heterozygous mutants (plp+/-fads2+/- or plp-/-fads2+/-) and their wild-type counterparts. Figure 31: DM mouse (age 6 months / male) effected with dermatitis on neck region. + = estimated extent of severity.

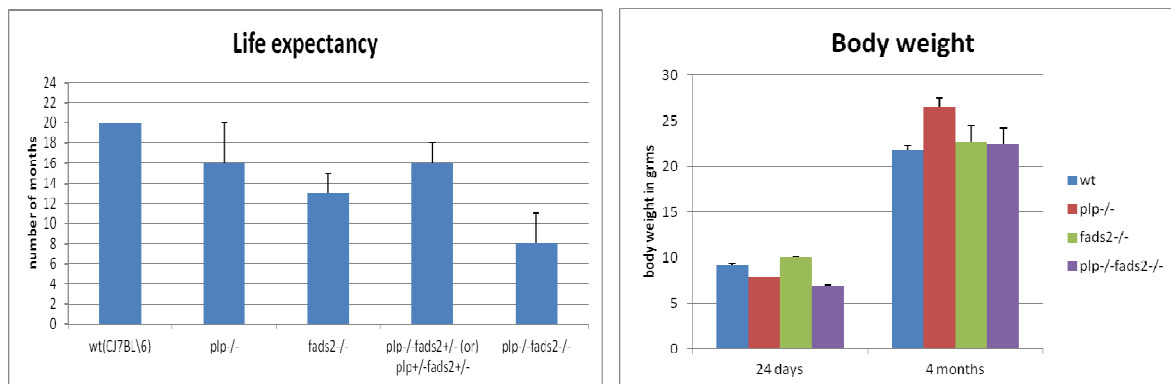


Figure 32: A. Life span of different mutants monitored up to 20 months. B. Body weight measured at p24 and 4-months. Data represented in mean ± SEM.

3.6.4 Gene expression analysis by semi-quantitative RT-PCR

Gene expression at the RNA level and protein expression of myelin/oligodendrocyte-specific proteins and various PUFA biosynthesis regulating desaturases were investigated by Western blot and semi-quantitative RT-PCR. RNA was isolated from whole brains of 22-day-old DM, *plp*^{-/-} single mutant and *fads2*^{-/-} single mutant and compared with wild-type (C57JBL6) mice. Key gene transcripts of myelin membrane and oligodendrocyte proteins in CNS, such as PLP and its isoform Dm20, MBP, MAG, MOG and OMgp, and neural cell adhesion molecules, NCAM-120 and NCAM-140, and tight junction protein connexin-43 were investigated. Gene expression of various major fatty acid desaturases involved in complex series of fatty acid desaturation and elongation steps were analyzed i.e., *Fads1*, *Fads2*, *Fads3*, *SCD1*, *SCD2* and *SCD3* RNA transcripts and likewise CGT (UDP-galactose-ceramide galactosyl transferase), a key enzyme involved in synthesis of galactosphingolipids of the myelin membrane and oligodendrocytes (Schulte and Stoffel, 1993).

The RNA levels of *Fads-3*, *MAG* and *NCAM-140* were partially down-regulated whereas *Fads1* (delta-5 desaturase) is partially up-regulated in DMs in comparison to age matched wild-type control. The GalC sphingolipid synthesizing CGT gene was down regulated in the *fads2*^{-/-} single mutant compared to the *plp*^{-/-} single mutant, DM and wild-type. *SCD3* expression was absent in all genotypes since it is not expressed in brain tissue and used as a control.

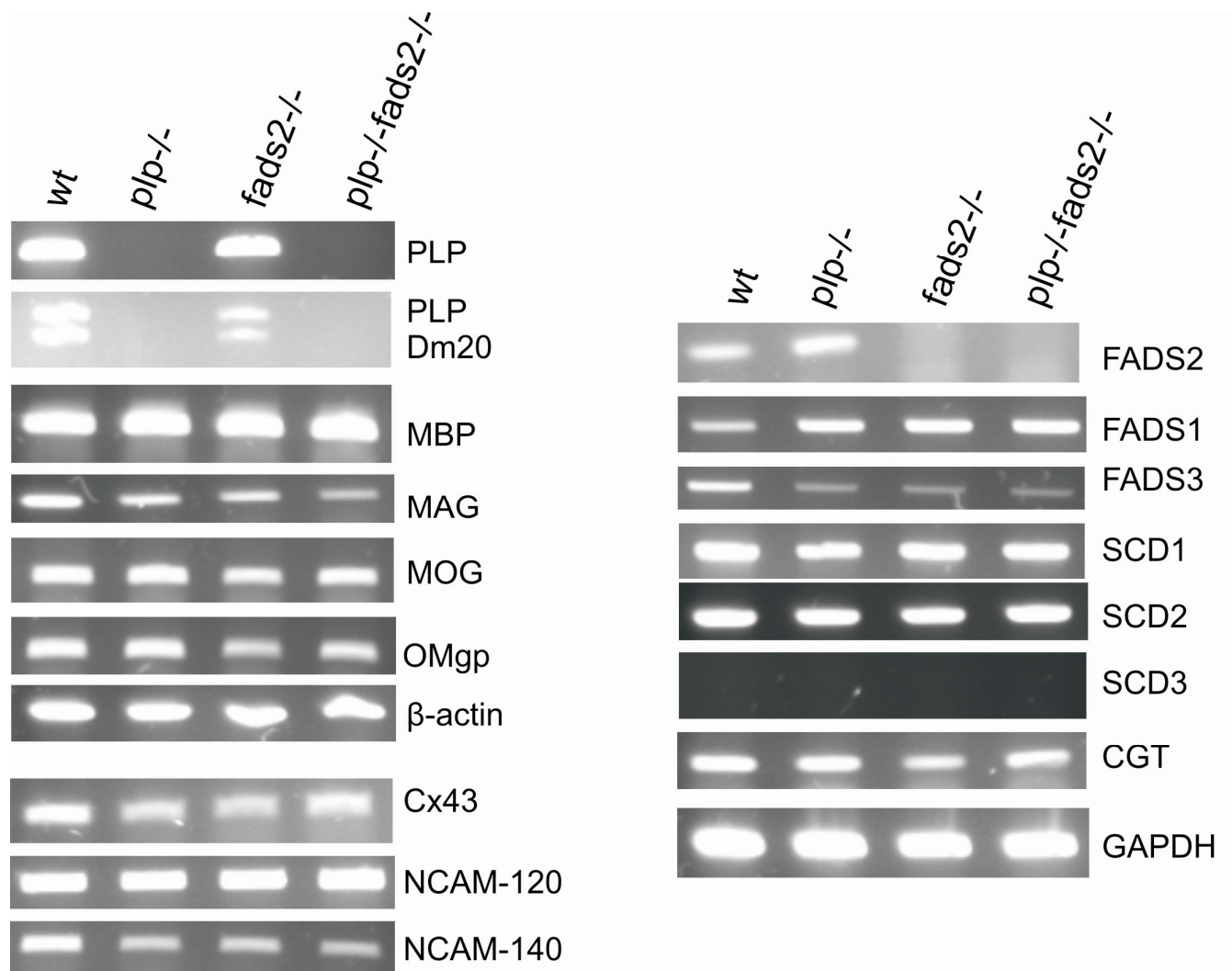


Figure 33: Semi-quantitative RT-PCR analysis. Oligodendrocytes or myelin membrane-specific proteins, neuronal structural adhesive proteins, cell junction proteins as well as key fatty acid desaturases. GAPDH and beta-actin were used as internal loading controls. SCD3 which is not expressed in brain was used as a tissue specific control. Total RNA isolated from brains of *p22*^{-/-} mice of wild-type, *plp*^{-/-}, *fads2*^{-/-} and DM was employed.

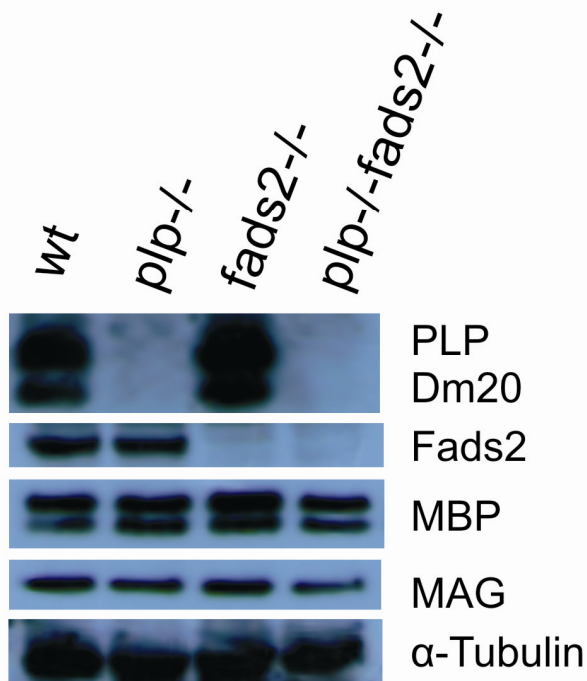
3.6.5 Brain and myelin protein analysis

Whole brain protein lysates of *plp*^{-/-}, *fads2*^{-/-}, DM and wild-type mice, and myelin extract protein lysates of DM and wild-type mice, were used for Western blot analysis. Total brain

lysates were probed with anti-PLP, anti-Fads2, anti-MBP and anti-MAG antibodies. Myelin extracts were probed with anti-PLP, anti-MBP and anti-MAG antibodies.

Protein expression analysis by Western blots revealed that, in contrast to the DM, the wild-type brain protein lysate contained proteolipid protein (PLP) (30 kDa) and its isoform Dm20 (26 kDa), and the Fads2 protein (54 kDa). MBP isoforms (21, 18 and 14kDa) were detected similarly in all genotypes and MAG showed partial down-regulation in total protein and myelin extracts of DM compared to wild-type. The results of MAG gene expression at the RNA level determined by RT-PCR correlated well with the protein analysis data.

A. Total brain protein extract:



B. Myelin extract:

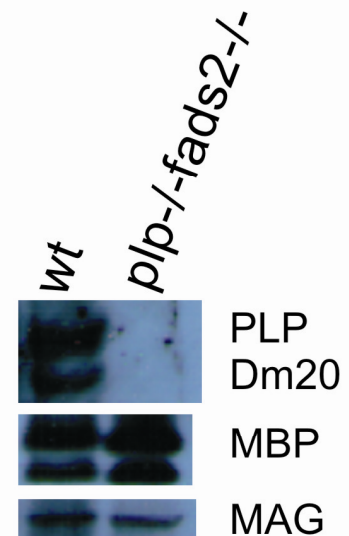


Figure 34: Western blot analysis. Total brain protein extract of wild-type, *plp*^{-/-}, *fads2*^{-/-} and DM mice of p22 were used. Myelin extracts of wild-type and DM mice of 3-month-old were used.

3.6.6 Myelin quantification

Myelin was isolated from whole brains of 5-month-old wild-type and DM mice (n=3) by the discontinuous sucrose gradient centrifugation method (Norton and Poduslo 1973). The isolated

crude myelin extract was lyophilized and weighed. Myelin yield from the DM was significantly lower compared to wild-type.

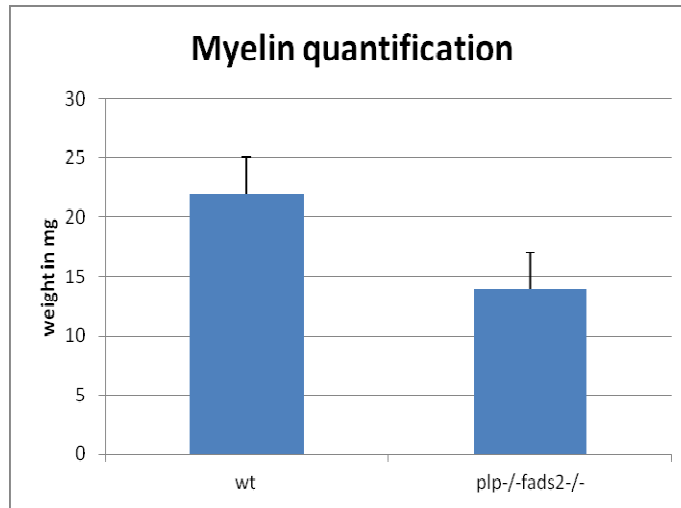


Figure 354: Myelin quantification of DM and wild-type mice. Myelin was isolated by discontinuous sucrose density gradient centrifugation. Data represent mean \pm SEM.

3.6.7 Immunohistochemical stainings

The disturbance of tight junction-associated proteins in Sertoli-cells of testis and gap-junction proteins in granulosa cells of ovarian follicle of *fads2*^{-/-} mutants was reported previously by our laboratory (Stoffel *et al.*, 2008). In the present study, the immunolocalization and expression pattern of tight junction-associated proteins were investigated in cerebellum region of DM brain by IHC. PLP and MBP localization pattern were also investigated.

Sagittal cryosections of brains of p22 *fads2*^{-/-} and DM and wild-type were immunostained for occludin and ZO-1 tight junction-associated proteins using anti-occludin (polyclonal) and anti-ZO-1 (polyclonal) antibodies. The PLP and MBP myelin-specific proteins were probed with anti-PLP (polyclonal) and anti-MBP (monoclonal) antibodies.

In DM, *fads2*^{-/-} and wild-type brain sagittal sections, immunofluorescence staining of anti-occludin and anti-ZO-1 antibodies were irregularly distributed in myelin and granular layers. In DM brain sections, anti-MBP antibody staining was confined to the myelin layer without any mislocalisation. Whereas anti-plp antibody immunostaining was not detected, which, as

expected, confirmed the loss of PLP expression. Thus immunohistochemistry of DM and *fads2*^{-/-} mutant brains revealed that, the tight junction proteins ZO-1 and occludin, localization was inconspicuous whereas the MBP of myelin-specific, localization was not disturbed.

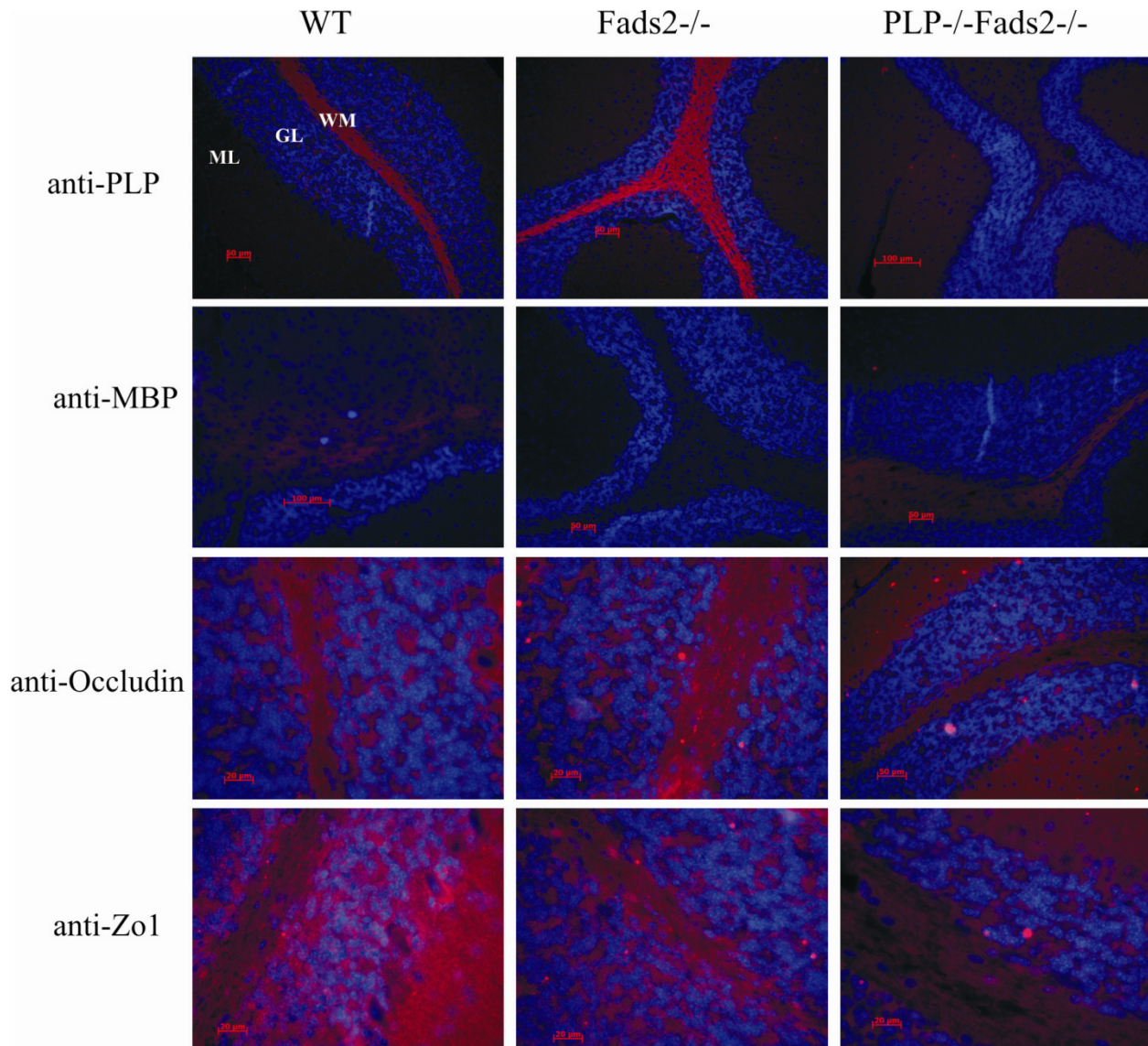


Figure 36: Immunostaining of sagittal sections of mouse cerebellum with anti-PLP, anti-MBP, anti-occludin and anti-ZO-1. Wild-type, *fads2*^{-/-} and DM genotypes were used in the study. Sections stained with anti-occludin and anti-ZO-1 are 63x and sections stained with anti-PLP and anti-MBP antibodies are 40x. ML= molecular layer; GL= granular layer; WM= white matter.

3.6.8 Lipid analysis

3.6.8.1 Brain lipid analysis

The whole brain lipid components and their fatty acid profile of 5-month-old wild-type and DM were analyzed. Whole brain lipids were extracted in chloroform/methanol as described previously. Whole lipid extracts were separated by HTPLC with solvent system chloroform/ethanol/water/triethylamine 35:30:7:35 (V/V/V) (Figure 37 A). Alkali-stable lipids and sphingolipids were extracted from total lipid extracts and separated by HPTLC with a chloroform/methanol/water 65:25:4 (by volume) solvent system (Figure 37 B).

Phosphatidylethanolamine (PE), phosphatidylcholine (PC), phosphatidylserine (PS), phosphatidylinositol (PI), normal fatty acid substituted galactocerebroside (GalC), α -hydroxy GalC (OH-GalC), GalC-derived sulfatides (sGalC) and sphingomyelin (SPM) lipid components (Figure 37 A) and alkali-stable lipid components alone i.e., SPM, GalC, sGalC, and OH-GalC (Figure 37 B), revealed no significant expression differences between wild-type and DM (*plp*^{-/-}/*fads2*^{-/-}). Although the loading concentration may differ between two individual extracts the relative concentrations of lipid components within individual extracts were similar.

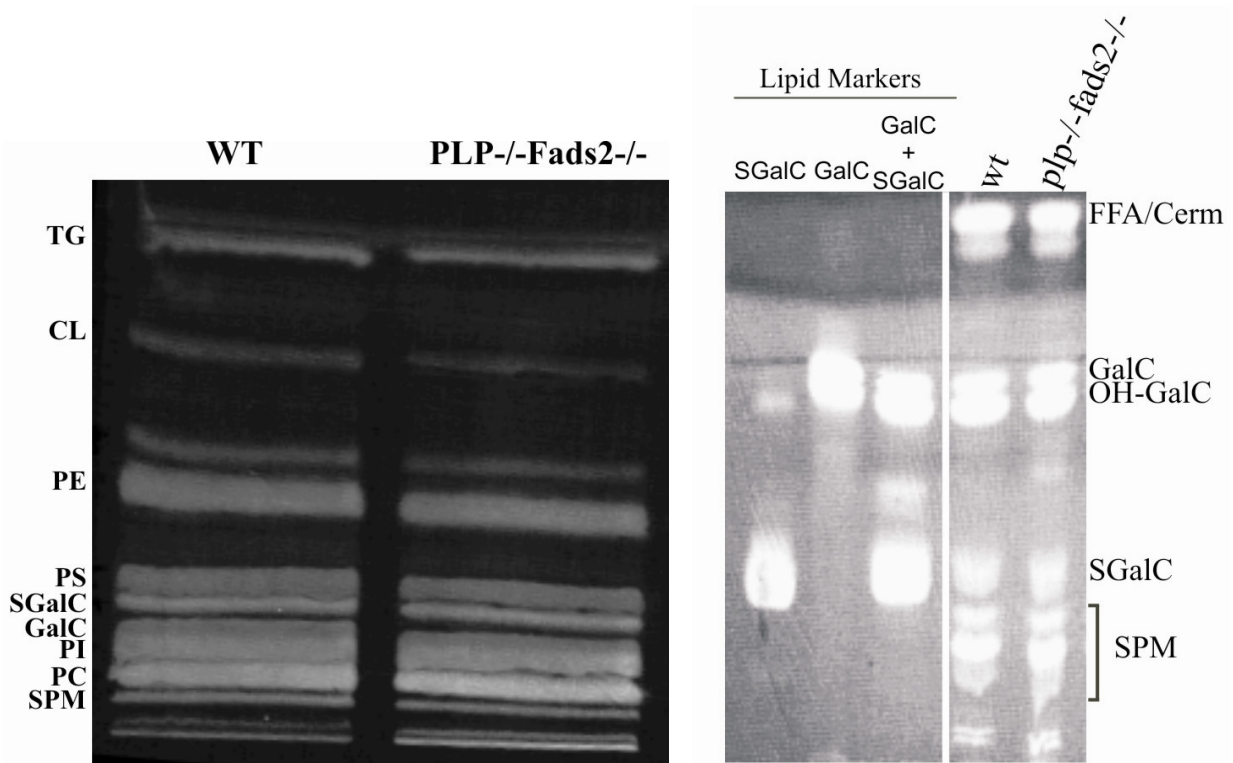


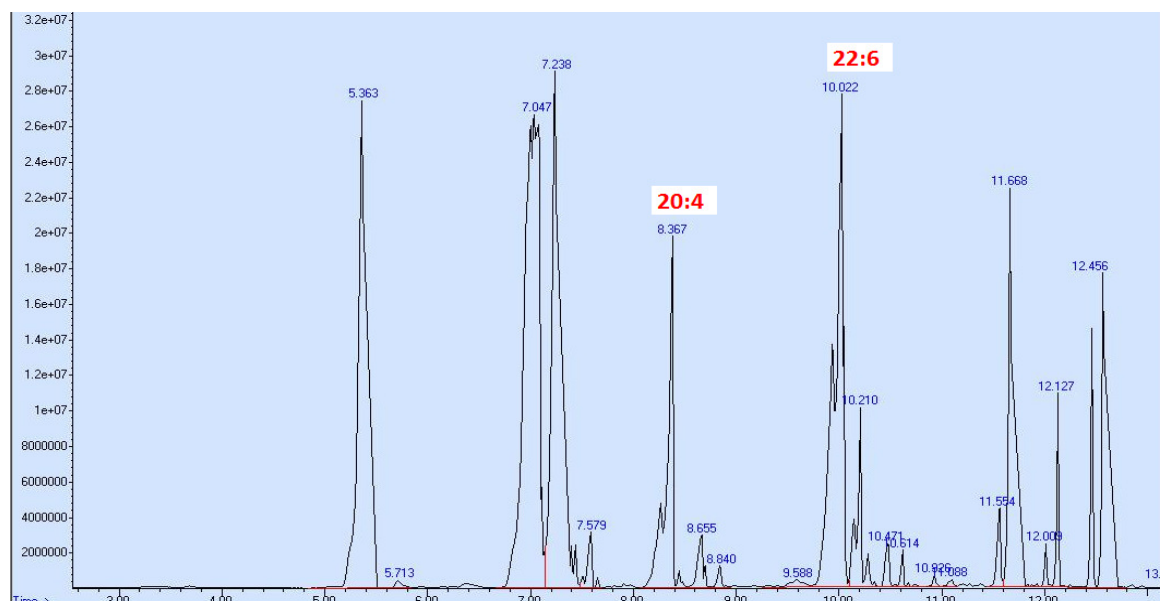
Figure 37: HPTLC of whole lipid extracts (right) and alkali-stable lipids; sphingolipids (left). All lipid bands separated on HPTLC were visualized with primulin staining. TG, triglycerides; CL, cardiolipin; PE, phosphatidylethanolamine; PS, phosphatidylserine; GalC, galactocerebroside; sGalC (GalC-derived sulfatide); PI, phosphatidylinositol; PC, phosphatidylcholine; SPM, sphingomyelin.

3.6.8.2 Brain fatty acid profile

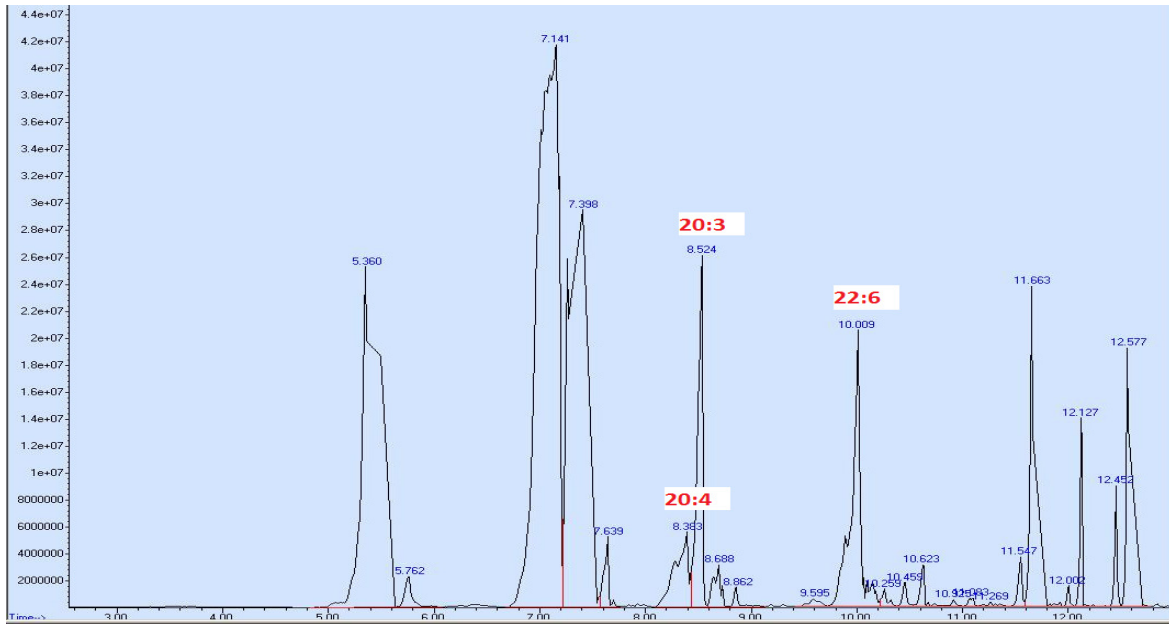
Brain lipid fatty acid profiles i.e., saturated fatty acids, monounsaturated fatty acids and PUFAs, were determined by GC-MS (Gas chromatography-Mass spectroscopy). For GC-MS, total lipid extract was transesterified to fatty-acid methyl esters (FAMES). FAMES were further derivatized to trimethylsilyl-esters by treating with N-methyl-N-trimethylsilyl-trifluoroacetamide (MSTFA) for the detection of long chain-hydroxy fatty acids.

The fatty acid profiles of wild-type and DM mice brains contained similar saturated and mono-unsaturated fatty acids such as palmitic acid (16:0), stearic acid (18:0), docosanoic acid (22:0), oleic acids (18:1), eicosenoic acid (20:1) and tetracosanoic acid (24:1) as well as long carbon chain α -hydroxy-fatty acids such as behenic acid (OH-22:0) and lignoceric acid (OH-24:0), figure 38. The PUFA profile of the DM contained drastically depleted arachidonic acid (20:4) to 2-5% and docosohexanoic acid (22:6) to 40-50%. Moreover the unusual eicosatrienoic acid (20:3) and eicosadienoic acid (20:2) were detected only in the DM fatty acid profile (Figure 38 B, C).

A, Wild-type brain lipid fatty acid methylesters



B. DM brain lipid fatty acid methylesters



C. Wild-type and DM fatty acid profiles

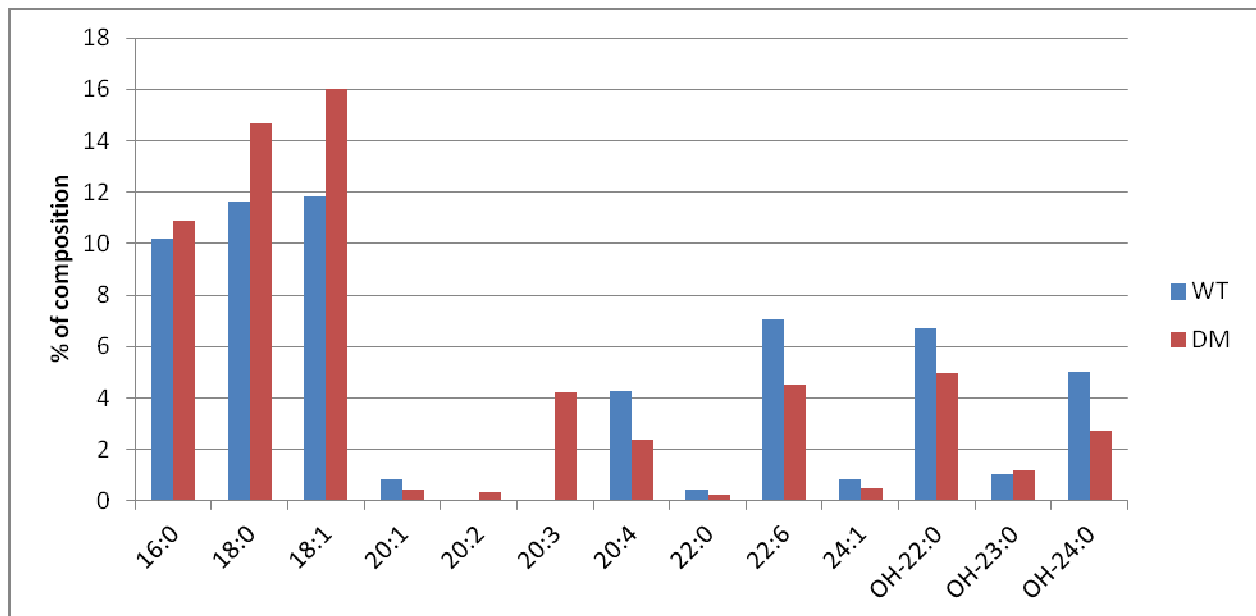


Figure 38: Fatty acid profiles of wild-type and DM. A. GC-MS chromatogram of wild-type brain depicting 20:4 and 22:6 PUFAs among other fatty acids. B. GC-MS chromatogram of DM brain depicting the unusual 20:3 and low concentrations of 20:4 and 22:6 PUFAs among other fatty acids. C. Data obtained from chromatograms of A and B.

3.6.8.3 Brain phospholipids and glycosphingolipids fatty acid profile

Individual phospholipids of brain lipid extracts i.e., SPM, PE, PC, PI, and PS, and galactosphingolipids i.e., GalC, OH-GalC and sGalC were extracted from respective above HPTLC plates. Fatty acid content of individual lipid components was analyzed by GC/MS.

PE of the DM lipid extract showed a 50% decrease in docosahexanoic acid (22:6) level and a large increase in eicosatrienoic acid (20:3) level with no other additional changes. PS of DM exhibited a 50% decrease in 22:6 and complete loss of arachidonic acid (20:4), and the PC exhibited only loss of 20:4, Both PS and PC showed increased levels of linoleic acid (18:2) and no 20:3. DM lipid fatty acids of SPM and PI showed no significant changes.

In DM sphingolipids, GalC fatty acid content indicated decreased lignoceric acid (24:0) and tetracosenoic acid (24:1) and increased linoleic acid (18:2) levels, whereas OH-GalC showed reduced lignoceric acid (OH-24:0) levels. In wild-type and DM the higher carbon fatty acid series of the galactocerebroside sulfate was not altered considerably.

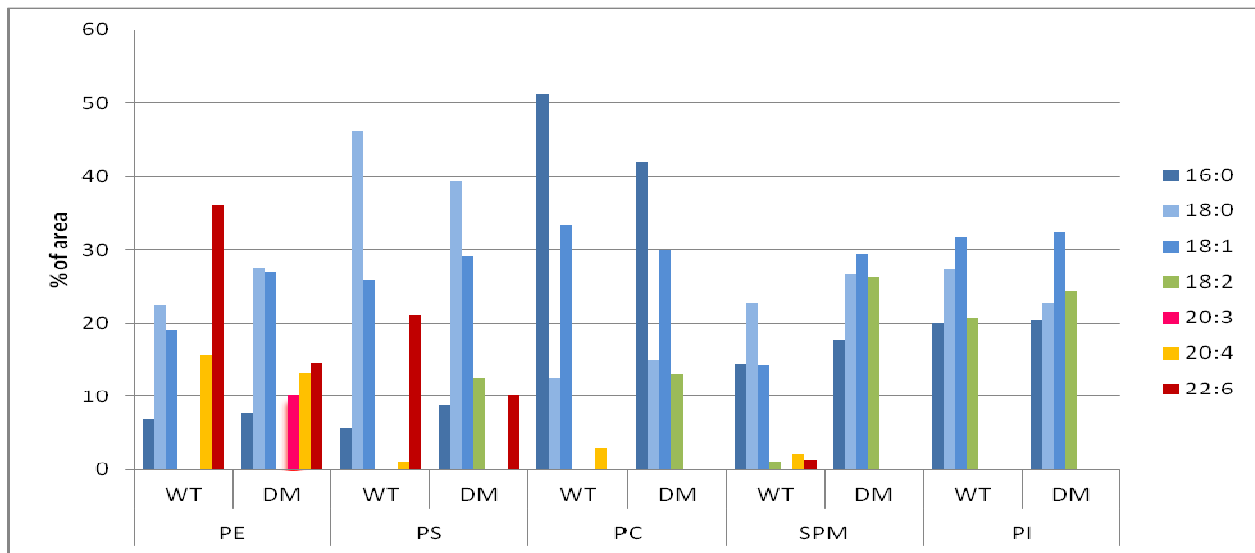


Figure 39: Fatty acid profile of individual phospholipids of wild-type and DM brains. Individual lipid components were analyzed by GC-MS. PE, phosphatidylethanolamine; PS, phosphatidylserine; PC, phosphatidylcholine; SPM, sphingomyelin; PI, phosphatidylinositol.

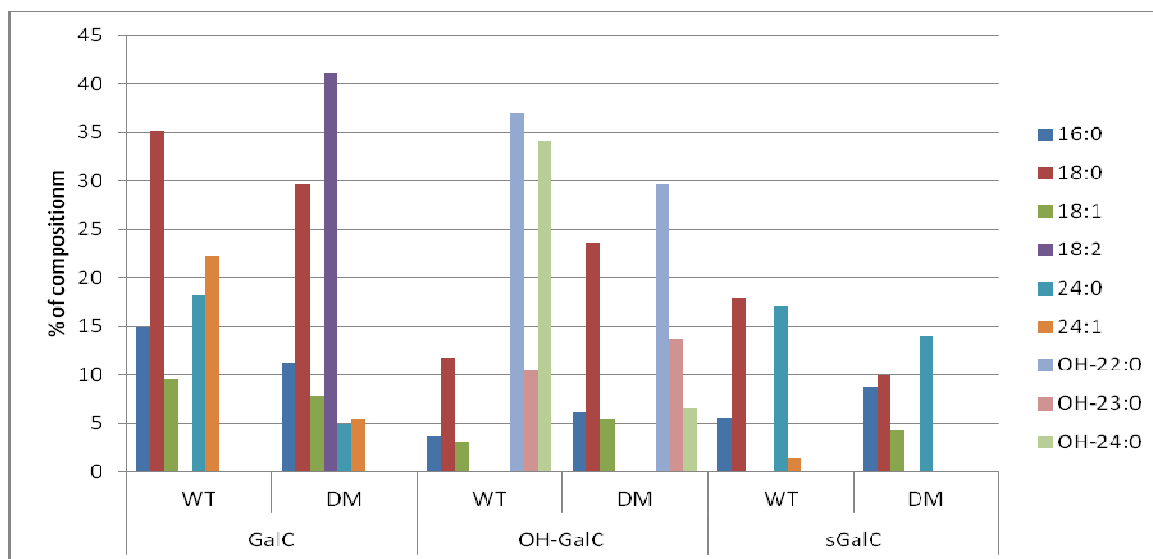


Figure 40: Fatty acid profile of major sphingolipids. Galc (Galactocerebroside), OH-Galc (hydroxy fatty acid galactocerebroside), sGalC (sulfated galactocerebroside) of wild-type and DM mice brain lipid fatty acids were analyzed by GC-MS.

3.6.8.4 Myelin lipid and fatty acid profile analysis

Total myelin was purified from 5-month-old adult mice brain of DM and wild-type by sucrose gradient centrifugation method as described before. Further myelin lipids were extracted with chloroform: methanol, and separated on HPTLC, figure 41. All lipid components in the myelin extract of DM were similar to wild-type myelin lipid components.

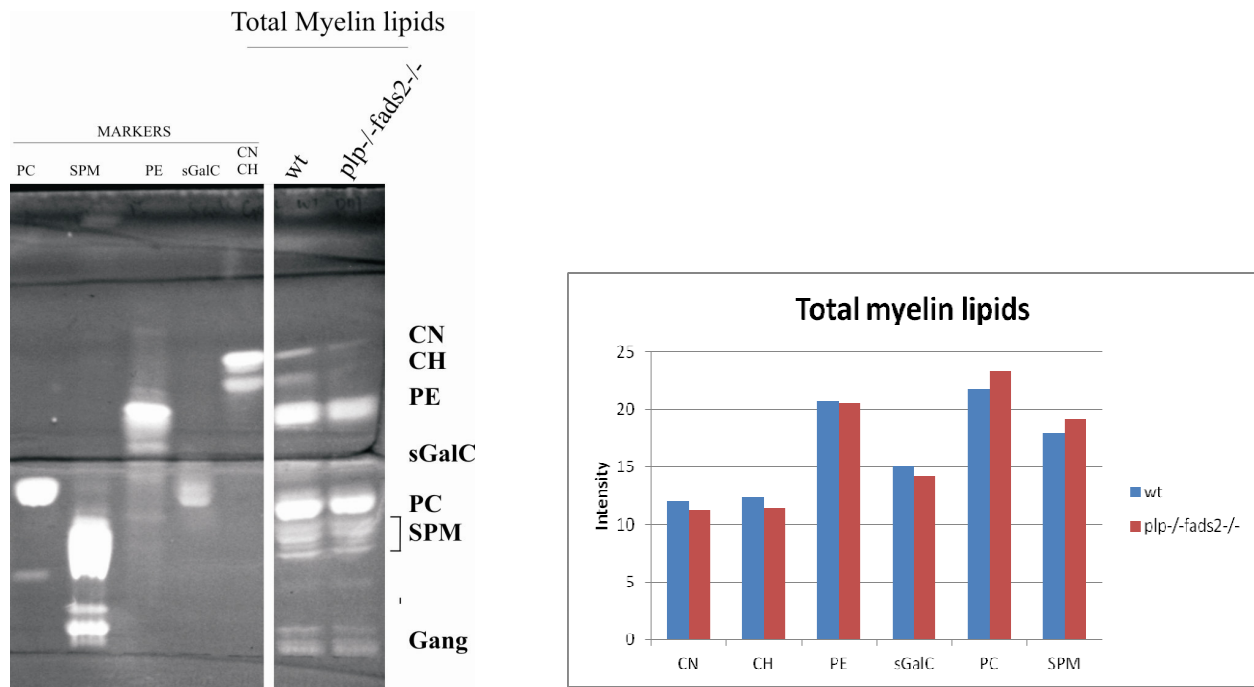


Figure 41: Wild-type and DM brains myelin lipid extracts separated on HPTLC and visualized with primuline reagent, and their band intensities measured with image-J software.

Myelin fatty acid profile analysis

Brain myelin lipid fatty acid profiles were prepared similar to that from brain lipids. In contrast to wild-type, the DM myelin profile showed eicosatrienoic acid (20:3) and eicosadienoic acid (20:2) PUFAs. Myelin PUFAs of the DM were similar to that of brain PUFAs.

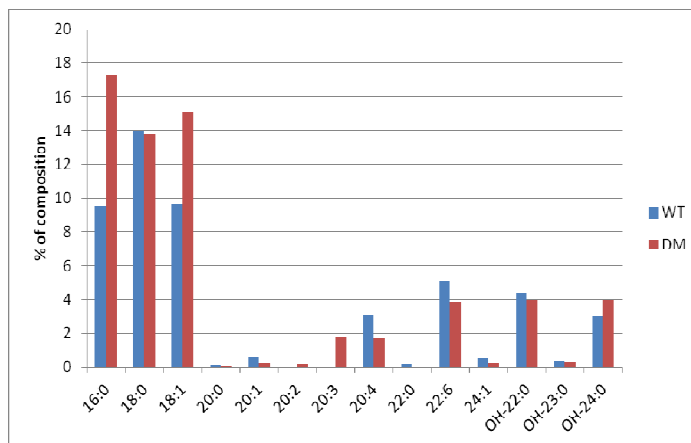


Figure 42: Myelin fatty acid profile of wild-type and DM mice detected by GS-MS method.

3.6.9 Morphology of the myelin sheath

The morphology of the myelin sheath of wild-type and DM optic nerve was investigated by transmission electron microscopy, and p22 mice were used for the study.

In agreement with the previous reports of *plp*^{-/-} single mutant myelin structure (Boison and Stoffel, 1994; Montag *et al.*, 1994; Boison *et al.*, 1995), the electron micrographs of optic nerve cross sections of DM also showed the loss of compact myelin membrane multilayers around axons (Figure 43 B). In addition, DM also exhibited loss of thick myelin sheaths around small and few medium-sized axons, some extent of disordered morphology at the periaxonal collar and periaxonal space (white arrows), and a mild degree of hypomyelination (Figure 43 A, B, and C). The order of major dense lines (MDLs) and double intraperiod dense lines (IDLs) in the myelin membrane appeared to be undisrupted. No axonal degeneration or increase in oligodendrocyte number was detected.

In the longitudinal sections of the optic nerve of the DM, at the node of Ranvier; the paranodal loops, paranodal bridges and juxta-paranodal regions were undisrupted, figure 43 D. The tight junction bridges connecting myelin and axon are also appeared to be normal.

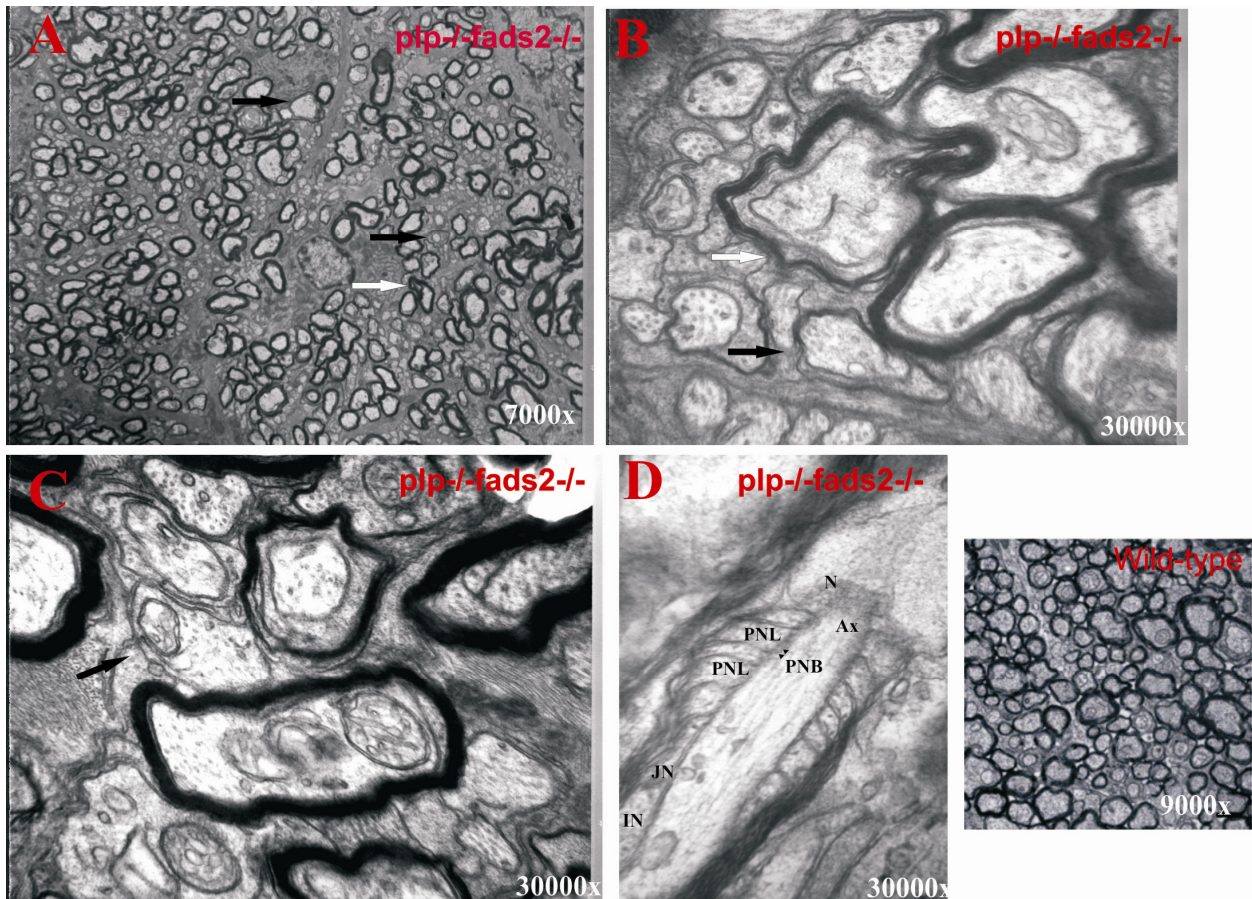


Figure 43: Electron micrographs of *plp*^{-/-}*fads2*^{-/-} and wild-type mice optic nerves. A-C: Transverse sections. A: Depicting mild hypomyelination, 7000x. B-C: 30000x. D: Longitudinal section depicting node of Ranvier and paranodal region, 30000x, PNL= paranodal loop, PNB = paranodal loop bridges, JN = Para Juxtranode, IN= internode, AX = axon. Black arrow = hypomyelination of an axon. White arrow = abnormal myelin structures at periaxonal collar and space. WT: 9000x.

3.6.10 Retinal morphology and function

The retina is a part of CNS comprising of several layers of different types of neurons with synaptic interconnections. Structural morphology of the pigmented layer of retina i.e, retinal pigment epithelium (RPE) was investigated by electron microscopy and the retinal function was investigated using ERG.

Retinal morphology

The retina of wild-type and DM mice of p22 was used for transmission electron microscopy. Structural morphology of the RPE region along with bruch's membrane, and photoreceptor outer segments was investigated.

In contrast to wild-type, the DM retina showed a high content of apical villi like structures embedded with melanine granules towards the apical region of the photoreceptor outer segments (Figure 44, white arrows). In addition, in DM, few melanin granules were present in the RPE and mostly aggregated towards the apical region of photoreceptor outer segments.

There were no other significant morphological differences observed in the RPE region i.e., in the thickness of the Bruch's membrane, and structure of photoreceptor outer segments.

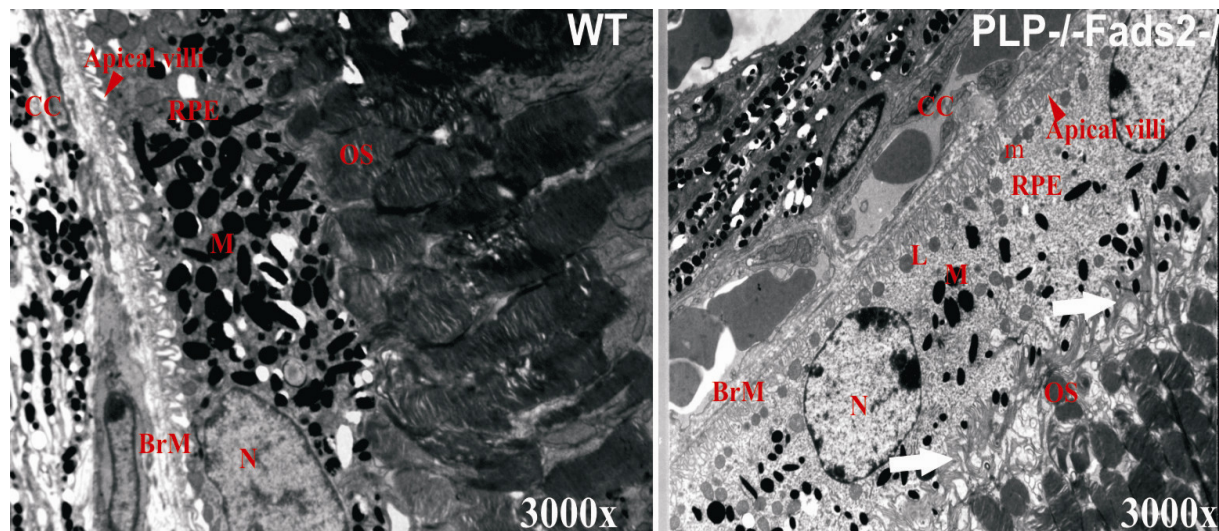


Figure 44: Electron micrographs of wild-type and DM (*plp-/-fads2-/-*) mice retina. Retinal pigment epithelium (RPE) region consisting of Bruch's membrane (BrM), choroid capillaries (CC), thick dense melanin granules (M), phagosomes (P), mitochondria (m), RPE cell nucleus (N), (AV) apical villi projections, and outer segments of photoreceptor cells. White arrow= abnormal apical villi like structures observed in DM retina.

Retinal function analysis

Light induced electrical signals of the eye were measured by electroretinography (ERG). 3-month-old wild-type and DM mice (n=4) were used for ERG. The 'a-wave' amplitude derived from photoreceptors and the 'b-wave' amplitude derived from Mueller cells and bipolar cells, of retina were recorded. Mice that were dark adapted for 24 hours were used for ERG recordings with single flash light of 3 and 10 minutes. In comparison to wild-type recordings, the DM showed a 1.5 to 2 fold decrease in a-wave readings at 3 and 10 minutes of flash light, whereas the b-wave amplitude was not significantly altered. The DM retinal photoreceptor outer segments morphology and function may play vital role in the decrease of a-wave recording and amplitude output.

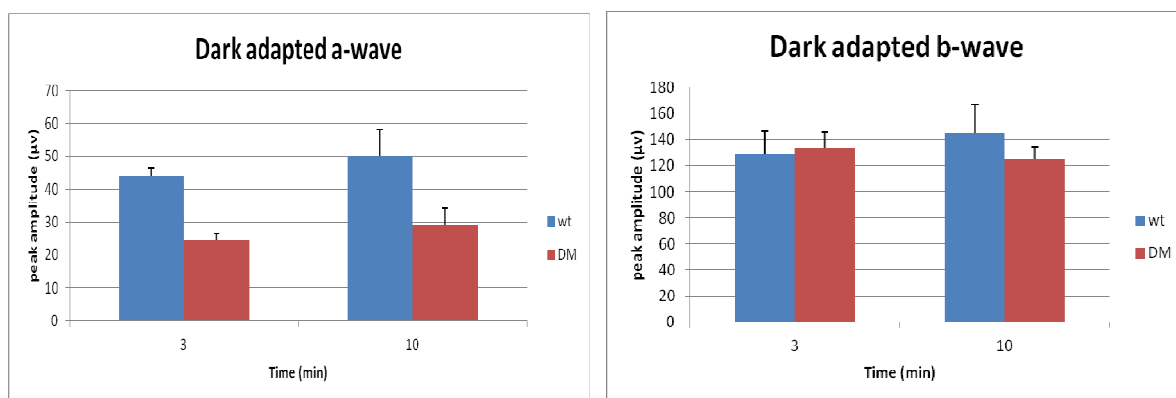


Figure 45: Electrophysiology recordings of wild-type and DM (*plp*^{-/-}*fads2*^{-/-}) mice (n=4). Data represented in mean± SEM.

3.6.11 Behavioral physiology

Behavioral physiology studies with knockout *plp*^{-/-} mutant mice previously showed some extent of defects in neuromotor coordination (Boison and Stoffel., 1994) (Griffith *et al.*, 1998). It is already known from various experiments that the lack of PUFAs may disturb behavioral and cognitive functions (Aid *et al.*, 2003; Luctman and Song, 2012), but till now there are no experiments on mammalian models comparable to our genetic model, in which PUFA synthesis is lacking due to the loss of the key *fads2* desaturase enzyme expression.

We performed various tests to study motor activity, neuromotor coordination and cognitive functions. Physical body movements and neuromotor coordination abilities were assessed by the rotarod test, horizontal rod test, inclined grid test and Morris water maze test. Cognitive functions such as exploratory behavior, anxiety and learning abilities were assessed by T-maze tests, open field test and Morris water maze test. Wild-type (n=8), *plp*^{-/-} (n=8), *fads2*^{-/-} (n=8), and *plp*^{-/-}*fads2*^{-/-} (n=5) mice of 5-month-old were used for the study.

3.6.11.1 Rotarod Task (Wallace *et al.*, 1980)

The rotarod test was employed to assess the motor coordination ability. Tests were performed by placing mice on a rotating rod at constant speed intervals of 16rpm, 24rpm and 36rpm for 2 min

duration. Mice were trained for two days prior to the test, and the test was executed for two days consecutively. Triplicate readings were obtained on each day.

Rotarod test revealed that there was no considerable difference in the latency time of all the genotypes at the low speed point of 16rpm, whereas the single mutants (*plp*^{-/-} and *fads2*^{-/-}) and the DM exhibited less latency time duration at high speed points of 24 and 36rpm compared to their wild-type counterparts. Motor coordination defects among different genotypes was in descending order; wild-type > *plp*^{-/-}*fads2*^{-/-} > *fads2*^{-/-} > *plp*^{-/-}. Results of less severe neuromotor defects in *plp*^{-/-} mutants obtained here were consistent with the previously reported results of Boison and Stoffel, 1994.

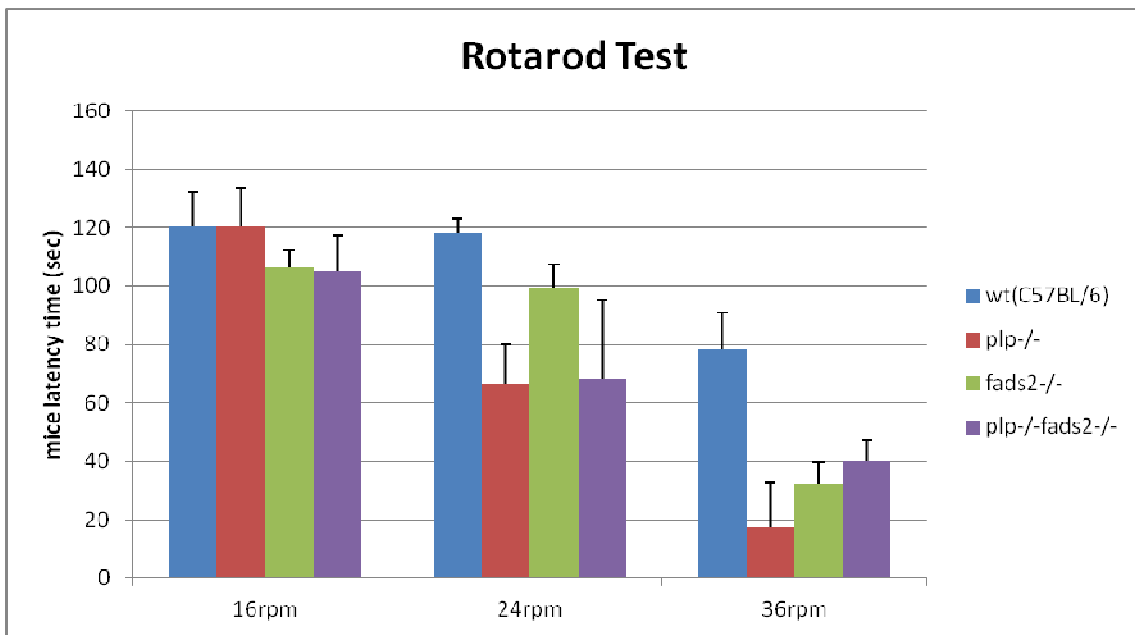


Figure 46: Rotarod task. Latency time of wild-type (C57BL/6), *plp*^{-/-}, *fads2*^{-/-} and DM (*plp*^{-/-}*fads2*^{-/-}) mice on rotarod. Data represented in mean ± SEM. Test performed at 16rpm, 24rpm and 36rpm speed points.

3.6.11.2 Horizontal-Rod Task (Wallace *et al.*, 1980)

The dynamic balancing ability was assessed in this test. The horizontal rod test apparatus consists of two vertical platforms of 80 cm height and a thin metal rod of 60cm long connecting them horizontally. During the test, the mouse was placed on the middle of horizontal metal rod

with its body axis perpendicular such that it holds the metal rod with its front or back paws, and adjusting itself into a tension of 180° rotation. All the animals were subjected to three trials each day for three consecutive days. Mice were carefully observed for their paws co-ordination in holding the metal bar. The balancing latency time duration on the horizontal rod was recorded.

The horizontal rod test revealed there was no considerable difference in dynamic balancing ability among different genotypes, moreover the balancing ability performance of *fads2*^{-/-} mutants were higher compared to that of wild-type was due to their anxious type of behavior.

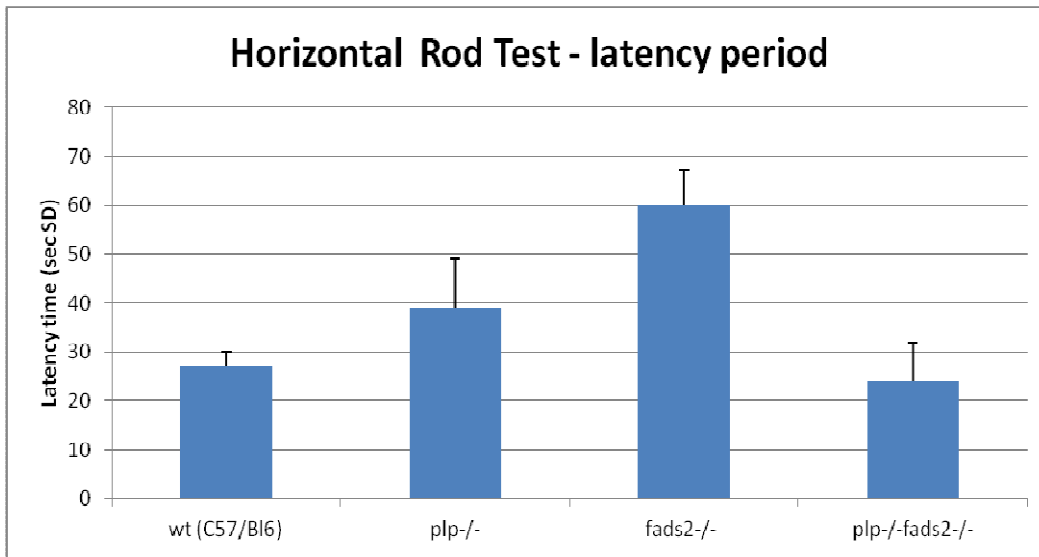


Figure 47: Horizontal rod/bridge task. Mice latency time period on the horizontal rod (with cut off time of 60sec) was recorded. Data represented in mean± SEM.

3.6.11.3 Grid Task

Mice hanging ability and their paws coordination were assessed on the inclined grid. Mice need to balance on the grid by holding with their paws during grid mesh rotation. Mice were placed on the grid and then the grid inclined by 180 degrees so that the mice were hanging upside down holding and balancing with their paws. Mice were observed if they hang with front, back paws or simply falling. All the mice were measured for 120 seconds interval.

All the mutants and WT strains showed similar balancing ability with their paws. Their grid hanging latency time was more than 120 seconds.

3.6.11.4 Open field Task (Barclay *et al.*, 1982)

Anxiety, exploratory behavior and locomotor activity parameters were assessed by open field test. Tests were conducted for 5 minutes duration and animals were tested for five consecutive days. For anxiety determination, mice location at the center or corner of the open field apparatus was measured during each trial. Exploratory or locomotory activity was measured by the number of square crossings, and rearings performed by the animal. Other parameters such as stress were assessed by number of groomings exhibited by the animal during the trial.

From the open field test, based on the duration of the time that the mice spend at the center or towards the corners in the open field apparatus and the number of crossings and rearings exhibited by the mice during the test, it suggests that all genotypes showed no significant differences in anxiety, exploratory and locomotor behavior. The stress level assessed based on number of groomings were also similar among all the genotypes.

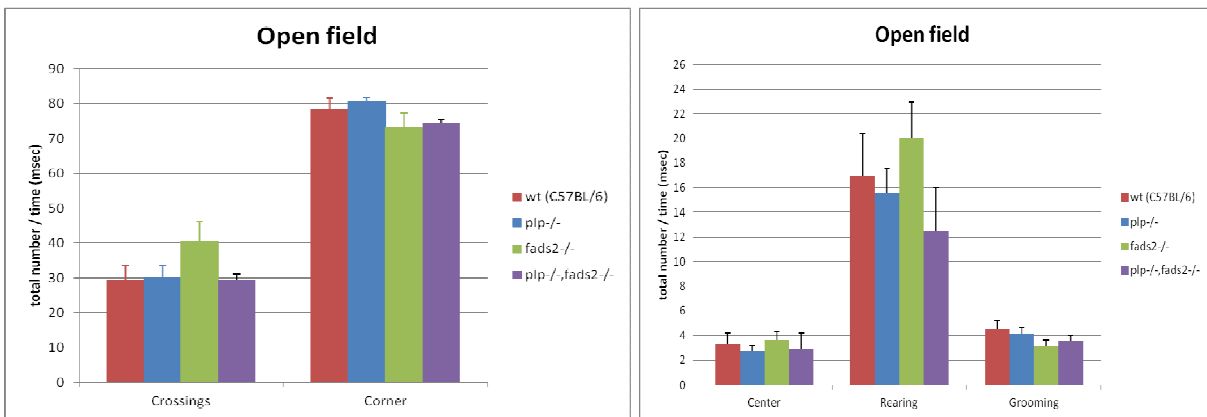


Figure 48: Open field task. Number of square crossings, time spent at the corner and center, number of rearings and grooming behavior exhibited by the mice in the open field apparatus was measured during the trial. Data represented in mean \pm SEM.

3.6.11.5 T-Maze Task

A T-maze test was used to determine cognitive functions such as spontaneous alterations. The hippocampus region of brain plays a major role in spontaneous alterations. T-Maze apparatus is an 'T' shaped apparatus consisting of a starting long arm extended into the perpendicular right

and left exploratory arms, allowing the mouse to start at the long arm and to choose the left or right arm, which reflect the spontaneous alteration capabilities. Each mouse was tested for 30 minutes duration and its choice of entry into the alternate arms was subsequently recorded.

The experimental results showed that wild-type, *plp*^{-/-}, *fads2*^{-/-} and DM mice showed no differences in their spontaneous alteration in choosing subsequently the alternate right and left exploratory arms of the T-maze apparatus.

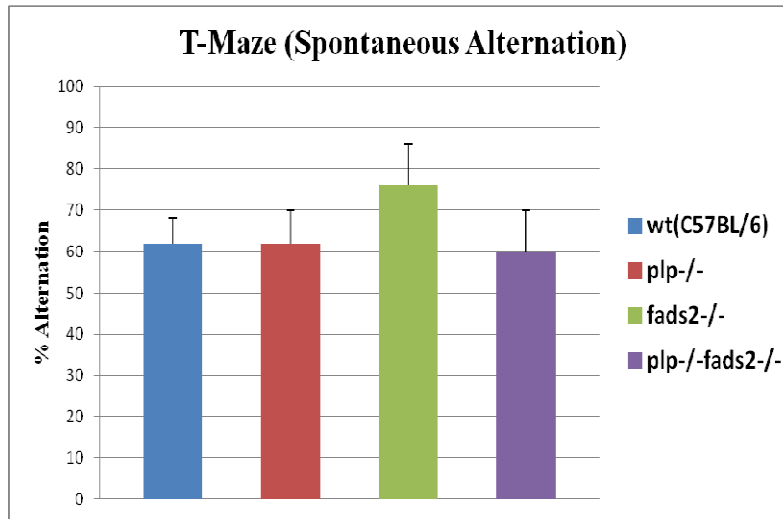


Figure 49: T-Maze task. Order of alternate selection of exploratory arms in T-Maze was recorded, mean ± SEM is represented.

3.6.11.6 Morris Water-Maze Task (Morris *et al.*, 1984)

Morris water maze task (MWT) is extensively used to assess cognitive functions such as spatial acquisition, reference memory and motor coordination defects and animal adaptability to a novel environment. During the test, the spatial acquisition capability and reference memory learned by the mouse in the novel environment were correlated to the animals learning ability and memory. MWT was conducted in two phases, the spatial acquisition phase and the probe trial or reference memory phase as follows.

Spatial acquisition performance

Mice were subjected to a brief spatial acquisition with four trials each day for five consecutive days. The first two days were used for training the mice in the water and directing it to the hidden rescue platform. The escape latency time duration and swimming velocity from day three to five were recorded for determining the spatial acquisition capabilities.

During the spatial acquisition phase trials, all the genotypes showed positive progress in acquiring spatial acquisition/learning capabilities by decreasing their latency time duration in finding the hidden platform. The latency time compared between different genotypes varies in descending order from wild-type (CJ7BL/6) > *plp*^{-/-} > DM (*plp*^{-/-}*fads2*^{-/-}) > *fads2*^{-/-}, suggesting that the extent of adapting spatial acquisition was lowest with *fads2*^{-/-} and DM (*plp*^{-/-}*fads2*^{-/-}) mutants. In order to determine motor coordination capabilities and anxiety levels, the swimming velocity of all the genotypes during the trail was measured, in which the wild-type, *fads2*^{-/-} and DM (*plp*^{-/-}*fads2*^{-/-}) showed similar performance, whereas the *plp*^{-/-} showed lowest swimming velocity.

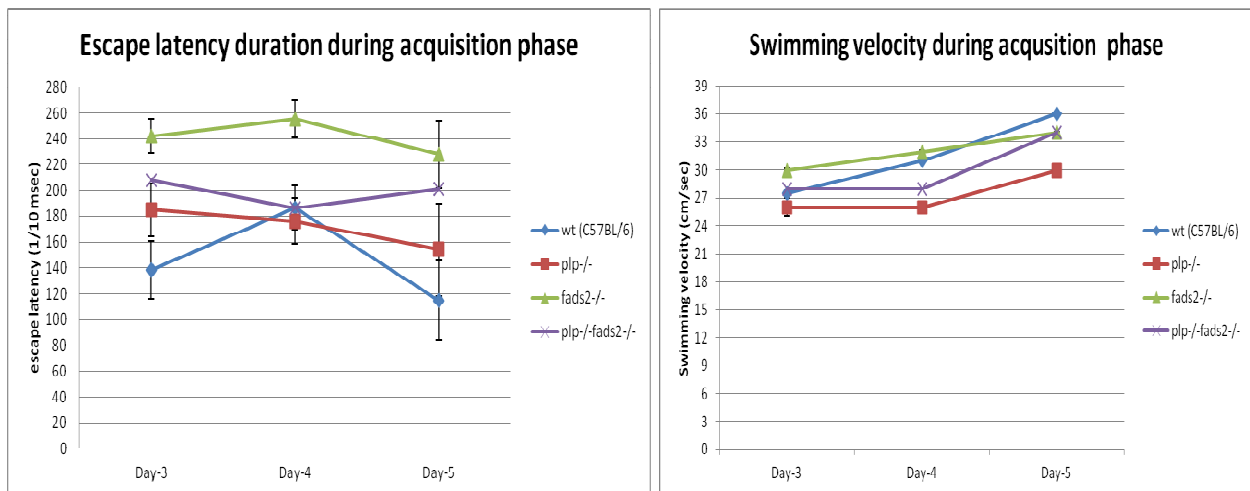


Figure 50: Morris water maze, spatial acquisition phase results: Spatial acquisition phase trials from day 3 to 5 were recorded. A) Time needed to find the hidden rescue platform or escape latency time duration (mean± SEM). B) Swimming velocity of the mice (mean± SEM).

Probe trial performance:

A probe trial was carried out to determine the extent of reference memory obtained from the spatial acquisition phase. The probe trial was done at the end of spatial acquisition day 5 in absence of the hidden platform in the south quadrant. During the probe trial, the total time that

the mouse spent in north, south, west and east quadrants and the number of annulus crossings (crossings made on the platform position that was present in spatial acquisition training phase) were calculated.

In probe trials, all the genotypes spent more time in the south quadrant compared to north, east, and west quadrants. However, in contrast to wild-type, all mutants spent less time in the south quadrant, suggesting that their ability for spatial acquisition was decreased. Regarding annulus crossings, all the mutant types i.e., *plp*^{-/-}, *fads2*^{-/-} and DM (*plp*^{-/-}*fads2*^{-/-}) showed a reduced number of annulus crossings suggesting low levels of reference memory compared to wild-type.

Overall, the MWM test revealed that all mutants showed defects in their cognitive responses of spatial acquisition and reference memory; Among all the mutants, the *fads2*^{-/-} and DM (*plp*^{-/-}*fads2*^{-/-}) showed a higher extent of spatial acquisition defects (i.e., more latency time in finding the hidden rescue platform) and all the mutants showed similar reference memory defects.

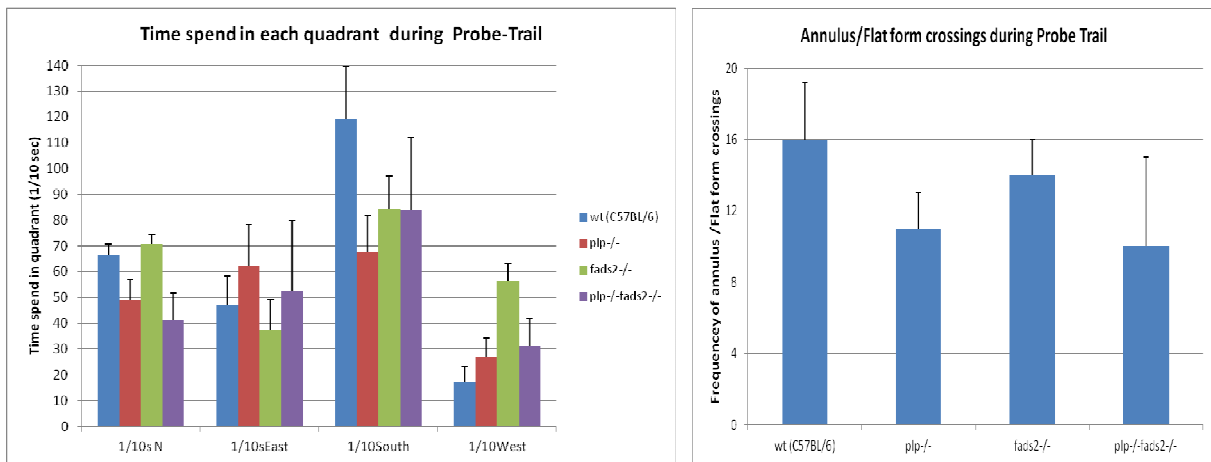


Figure 51: Morris water maze, Probe trial phase results: Probe trial; time interval that the mice spent in north, east, south and west quadrants in search of hidden platform (mean± SEM) average annulus crossings (crossings on the platform position that was present in spatial acquisition phase trails) (mean± SEM).

4 Summary of Results

The results of this thesis can be summarized in two parts.

First part: A. Investigation of Mut-PLP and Mut-Dm20 *in silico* hydrophobic properties, and *in vitro* and *in vivo* cell surface targeting. B. Mut-PLP expression regulated by Nestin enhancer, and transgenic mouse model generation. C. Knock-in mouse model generation lacking PLP/Dm20 two disulfide bridges.

Second part: Plp^{-/-}fads2^{-/-} double-mutant mouse model (DM) generation and characterization, addressing the role of complex structural assembly of CNS myelin proteins and lipids.

First Part:

A. *In silico* structural and hydrophobic properties, and *in vivo* and *in vitro* cell surface targeting were investigated of PLP and its splice variant Dm20, and their mutated forms i.e., Cys-mut PLP (Mut-PLP) and Cys-mut Dm20 (Mut-Dm20). PLP and Dm20 cDNA fragments were initially synthesized from mRNA of WT mouse brain. Site-directed mutagenesis was used to introduce point mutations of Cys with Ser codons at defined locations in PLP and Dm20. A total of 19 PLP and Dm20 cDNA constructs were generated, table 3. From this pool, WT-PLP, WT-Dm20, Mut-PLP (Cys-less PLP) and Mut-Dm20 (Cys-less Dm20) cDNA fragments were used for further investigations.

In silico prediction of protein transmembrane orientation and hydrophobic properties, based on Kyte-Doolittle hydrophobic plots and the amino acid hydrophathy index, were analyzed for WT-PLP, Mut-PLP, WT-Dm20, and Mut-Dm20. Kyte-Doolittle plots revealed a partially disturbed conformation of Mut-PLP, in other word an alteration in the PLP specific domain loop orientation in the lipid membrane in comparison to the WT-PLP. No considerable disturbances were observed among Dm20 mutant and WT forms. Hydropathy index values obtained from SOSUI program resulted in the following descending order of hydrophathy: WT-Dm20>Mut-Dm20>WT-PLP >Mut-PLP, revealing the reduced hydrophathy index values for Mut-Dm20 and Mut-PLP compared to their WT counterparts.

Intracellular trafficking and membrane targeting of WT-PLP, Mut-PLP (Cys-mut PLP), and Mut-Dm20 (Cys-mut Dm20) under *in vitro* and *in vivo* conditions were investigated. WT-PLP-EGFP, Mut-PLP-EGFP and Mut-Dm20-EGFP constructs were generated accordingly and used for transfection of COS-7 cells for *in vitro* studies. WT-PLP-EGFP protein was transported to the plasma membrane, and could be detected in the filopodia or microspikes, endoplasmic reticulum (ER), and Golgi apparatus, but intriguingly, the Mut-PLP-EGFP and Mut-Dm20-EGFP were detected only in ER and the Golgi apparatus and not at the plasma membrane or in filopodia-like structures.

To investigate the intracellular trafficking of WT and Mut-PLP under *in vivo* or native conditions, primary oligodendroglial progenitor cells were isolated from 6-8 day-old neonatal *plp*^{-/-} mice and transfected with WT-PLP-EGFP and Mut-PLP-EGFP constructs. Immunocytochemistry showed that WT-PLP-EGFP was transported and integrated into the plasma membrane but interestingly, the Mut-PLP-EGFP was not transported or integrated at the plasma membrane.

B. In order to investigate the regulation and expression of Mut-PLP under the Nestin enhancer gene element in early stages of CNS development, initially a preliminary NesMut-PLP construct was generated. Its expression was validated by stable transfection into OLN93 oligodendrocyte cells. Semi-quantitative RT-PCR revealed that NesMut-PLP transfected OLN93 oligodendrocyte cells had two folds of higher expression level of mutant PLP compared to the untransfected OLN93 cells. Subsequently, an Nh/MBPMut-PLP transgene construct containing the Nestin enhancer together with a MBP promoter, Mut-PLP, and an IRES separated EGFP was generated. This transgene construct was microinjected into pronuclei of fertilized *plp*^{-/-} mouse eggs. The resultant transgenic mice are currently under investigation.

C. To investigate the structural and functional role of the two disulfide bonds in the PLP's extracellular loop *in vivo*, a knock-in mouse mutant is being generated by a gene targeting approach. A targeting construct containing PLP gene homologous targeting arms, containing four point mutated Cys codons i.e., C183S, C227S, C200S, and C219S (involved in the formation of di-sulfide bonds) in exon IV and V, was generated. The neomycin cassette flanked with Cre-LoxP sequences was present between 5' and 3' homologous targeting arms of the targeting construct. The neomycin-cassette was used as a selection marker and for PCR validation during the process of homologous-recombinant ES cell clones screening. In the obtained positive ES clone, the Cys mutations and correct homologous recombination were confirmed by PCR and DNA sequencing. Karyotyping was also performed and no chromosomal aberrations were detected. The homologously targeted ES clone was injected into blastocysts isolated from CJ7BL/6 mice and re-implanted into foster mothers. Among nineteen (19) offsprings obtained, five (5) were identified as positive chimeras, which are currently in breeding to obtain PLP knock-in heterozygous mice.

Second part:

DM (plp^{-/-}-fads2^{-/-} double mutant) mice were generated by crossing plp^{-/-} with fads2^{+/-} single mutants. Validation of the DM mice was done by PCR-genotyping with PLP and Fads2 gene specific primers. Furthermore, absence of PLP and Fads2 in the DM was confirmed on RNA and protein level. Absence of PLP was also confirmed by immunostaining of DM brain cryosections with anti-PLP antibody. Phenotypes exhibited by the DM included reduced lifespan, severe dermatitis and sterility: DM mice had a reduced life span of less than 10 months compared to the plp^{-/-} (20 months) and fads2^{-/-} mice (>16 months). DM also showed extensive dermatitis compared to age matched fads2^{-/-} single mutant mice. Likely due to infertility in the fads2^{-/-} mice, the DM were also infertile. Moreover, partial tremors and seizures were observed in the adult DM starting from five months of age.

The expression of various myelin/oligodendrocyte specific protein gene transcripts such as PLP, MBP, MAG, MOG and OMgp, and gene transcripts of fatty acid desaturases such as Fads1, Fads2, Fads3, SCD1, SCD2, SCD3, and cell adhesion molecules such as NCAM-120, NCAM-140, along with tight junction protein CX-43 were investigated in the brain tissue of wild-type, plp^{-/-}, fads2^{-/-}, and DM mice by semi-quantitative RT-PCR. Gene transcription levels were found to be similar between all the genotypes except the MAG gene transcript which was partially down-regulated in DM compared to wild-type (BL6CJ/7), whereas single mutants of plp^{-/-} and fad2^{-/-} showed normal expression of MAG. The level of myelin protein expression was investigated by Western blotting using anti-PLP, anti-MBP, and anti-MAG. MAG expression was partially down-regulated in DM, compared to wild-type. To determine potential disturbances in the localization of myelin specific proteins and tight junction proteins in the brain cryo-sections of wild-type, fads2^{-/-} and DM, were immunostained with myelin specific anti-PLP and anti-MBP, and tight junction specific anti-occludin and anti-ZO-1 antibodies. Inconspicuous differences were observed in the localizations of occludin, ZO-1, whereas the PLP and MBP are confined to the myelin region of the cerebellum.

Whole brain and myelin lipid components were extracted from adult wild-type and DM and analyzed by HPTLC. All the major lipid components i.e., phosphatidylethanolamine (PE), phosphatidylcholine (PC), phosphatidylserine (PS), phosphatidylinositol (PI), sphingomyelin (SPM), galactocerebroside (GalC) and sulfated Galc (sGalC) were detected at similar expression levels with no significant differences between wild-type and DM lipids. Furthermore, the fatty acid profile of the whole brain and myelin lipid extracts of wild-type and DM were analyzed by GC-MS. In contrast to wild-type, in the DM, arachidonic acid (20:4) and docosahexanoic acid (22:6) levels were depleted drastically, and the unusual PUFAs i.e., eicosatrienoic acid (20:3) and eicosadienoic acid (20:2) were detected instead. Fatty acid species of individual phospholipid and sphingolipid components of wild-type and DM brain tissues were also analyzed by GC-MS. In contrast to wild-type, in DM the PE contains higher 20:3 levels, whereas

PC and PS contains high 18:2 levels, compensating for the decreased levels of 20:4 and 20:6 PUFAs in PE, PC and PS.

Myelin morphology of the optic nerve of p22 wild-type and DM mice was investigated by electron microscopy. The DM differed from WT, and showed perturbation of myelin sheath morphology including the periaxonal space and periaxonal collar around few axons. Furthermore, a certain degree of hypomyelination was also detected, whereas the paranodal region at the node of Ranvier was not disturbed.

Retinal morphology and function in p22 wild-type and DM mice was investigated by electron microscopy and electroretinography (ERG), respectively. In contrast to wild-type retinal morphology, the DM mice showed apical villi like structures with embedded melanin granules towards the apical region of the outer segments. The electroretinography (ERG) recordings of DM showed two fold decrease of a-wave amplitude at 3 and 10 minutes flash light in contrast to wild-type.

Behavioral physiology, such as neuromotor coordination and cognitive abilities, of wild-type, *plp*^{-/-}, *fads2*^{-/-}, and DM mice was investigated with rotarod, inclined grid, horizontal rod, T-Maze, open field and Morris water-maze tasks. Rotarod and Morris water-maze tasks revealed significant defects in motor coordination of all mutants compared to wild-type. Inclined grid and horizontal rod tasks used in assessing the balancing ability showed no significant differences among all the genotypes including wild-type. T-Maze task also showed no significant differences in spontaneous alterations among different genotypes. The open field task used in assessing the anxiety type of behavior showed similar pattern of anxiety among different genotypes. The Morris water-maze task revealed that all mutant genotypes compared to the wild-type, showed considerable defects in their cognitive ability i.e., spatial acquisition and reference memory.

5 Discussion

5.1 Cys residues are critical for PLP and Dm20 targeting to the cell surface

PLP and its isoform Dm20 are strictly conserved regarding their intracellular trafficking and plasma membrane targeting, and have specific structural and functional roles in myelin morphology. Along with the structural role of PLP and Dm20 in myelin compaction, their cell surface targeting in oligodendrocytes is critically important since defects in their targeting to the cell surface may result in a broad spectrum of X-linked dysmyelinating disorders such as PMD and SPG2. The PLP/Dm20 Cys residues are involved in posttranslational modifications such as thio-acylation and in the formation of two disulphide bridges present in the extra cellular loop-II. Post-translational modifications such as thio-acylation play a critical role in protein transportation and sorting. Similarly, the post-translational modifications of PLP/Dm20, i.e., thio-acylation and the formation of two disulfide bridges might be essential for proper protein folding and targeting to the plasma membrane. Previously it was reported that truncated fragments of PLP, i.e. a peptide containing the N-terminal 13 amino acids of PLP, containing only three fatty acyl chains, fused to LacZ (Wight *et al.*, 1993) or to EYFP (Schneider *et al.*, 2005), is sufficient for PLP trafficking to the plasma membrane. There are also reports regarding some PLP/Dm20 Cys point mutations that could correlate with the PMD phenotype. Here, we investigated the significance of Cys residues of PLP and Dm20 in cell surface trafficking.

The influence of PLP Cys residues in intracellular targeting was studied by generating mutant forms of PLP and Dm20, Cys-mut PLP (Mut-PLP) and Cys-mut Dm20 (Mut-Dm20) constructs, in which all Cys residues were substituted by Ser residues and fused with an EGFP tag for intracellular localization. Furthermore, using transfection studies of Mut-PLP and Mut-Dm20, we could determine that the lack of Cys residues impaired normal trafficking of both isoforms. Interestingly, Mut-PLP and Mut-Dm20 were retained in the ER or Golgi and neither isoforms were detectable at the plasma membrane under *in vivo* or native and *in vitro* conditions. This implies that PLP and Dm20 Cys residues, their S-acylation and disulfide bridge formation are crucial for exit from the ER or Golgi and targeting to the plasma membrane. Moreover, the disulphide bridges in the extra-cellular outer loop region of PLP and Dm20 may have a prominent role in stabilizing the extra-cellular loop and thus overall PLP conformation, which may in turn be critical in proper cell surface targeting. On the other hand, WT-PLP and WT-Dm20 are integral transmembrane proteins and are strongly hydrophobic. By using an *in silico* protein structural prediction i.e., based on kyte-doolittle hydrophathy plots, we could determine that Mut-PLP and Mut-Dm20 are likely to exhibit an impaired intracellular loop structural conformation along with decreased hydrophobicity, which may affect their integration into the

lipid bilayer during trafficking to the cell surface. Impaired hydrophobic properties of PLP/Dm20 might also affect their proper vesicular membrane internalization for trafficking from the Golgi apparatus to the cell surface.

5.1.1 Similar trafficking of Mut-PLP and Mut-Dm20 in COS-7 cells and PMD

The underlying intracellular trafficking defects of PLP and Dm20 under *in vitro* conditions may shed light on the *in vivo* PMD phenotype. Moreover, the differential trafficking between PLP and Dm20 under *in vitro* conditions in COS-7 cells might correlate with the extent of PMD severity, i.e. impaired sorting of both PLP and Dm20 isoforms to the cell surface could result in severe or congenital PMD, whereas only Dm20 targeting to the plasma membrane could result in the less severe or classical PMD (Gow and Lazzarini, 1996). Similarly, in our *in vitro* COS-7 cells assay we could show that the intracellular trafficking of Mut-PLP and Mut-Dm20 was similar. Both mutant isoforms could not be detected at the cell surface, which might be a prominent feature of the severe or congenital PMD phenotype under *in vivo* conditions.

5.1.2 Differential trafficking *in vitro* and *in vivo*

The present study has been conducted in heterologous system *in vitro* i.e., COS-7 cells and in homologous or native system *in vivo* i.e., in primary oligodendrocytes that were isolated from neonatal PLP-null mice. Both cell lines were of a PLP null background and are perfect models. Although COS-7 cells are heterologous and immortalized cells compared to primary cultures of oligodendrocytes of glial lineage used in this study, the intracellular trafficking of wild-type and Mut-PLP in COS-7 cells is similar to primary cultures of oligodendrocytes, revealing that the targeting strategy may not be restricted to native cell types.

The importance of palmitoylation in protein sorting has also been well demonstrated with several other proteins such as PSD-95. PSD-95 is a neuronal transmembrane protein regulated by its N-terminal palmitoylation for trafficking from the neuronal cell body to destined postsynaptic densities (E1-Husseini *et al.*, 2000a).

5.1.3 Cys-mut PLP (Mut-PLP) expression in early CNS developmental stages

In contrast to PLP expression in oligodendrocytes and its critical role in myelination, Mut-PLP expression in the early glial lineage and subsequent precursors reveals its specific functional role in myelinogenesis and myelin morphology under *in vivo* conditions. From various transgenic mouse models it has been shown that the Nestin second intron enhancer is highly specific towards early brain development and in early and late precursors of the oligodendroglial lineage. In the present work, we validated Nestin enhancer regulation on Mut-PLP and a transgenic mouse is being generated, as discussed below.

5.1.3.1 Validation of Nestin enhancer regulation of Mut-PLP

To validate the Nestin enhancer gene element on Mut-PLP *in vitro*, Mut-PLP was over-expressed under the control of the Nestin enhancer gene element together with the TK-promoter in immortalized oligodendrocytes or OLN93 cells. Investigation of the levels of over-expression indicated a two fold increase in Mut-PLP expression. This suggested that the Nestin enhancer is an active gene regulatory element capable of regulating Mut-PLP. Previously, it was reported that Nestin is down-regulated in differentiating oligodendrocytes (Almazan G *et al.*, 2001), here we have demonstrated that the Nestin enhancer may facilitate over-expression of Mut-PLP in OLN-93 cells which are capable of expressing myelin specific genes and are of glial lineage.

5.1.3.2 Generation of a transgenic mouse expressing Mut-PLP regulated by the Nestin enhancer region.

The Nestin enhancer was used with the MBP promoter as a gene regulatory element enabling expression of Mut-PLP in early CNS development specifically in the oligodendrocyte lineage. Previously, the MBP promoter was well characterized as a strong promoter, active in early embryonic CNS development and in the glial lineage. The transgene construct used in generating transgenic mouse mutant also contains an IRES sequence and an EGFP marker. The IRES sequence present in between Mut-PLP and EGFP sequences was predicted to facilitate independent translational initiation of Mut-PLP and EGFP under the same cis-regulatory element and enables us to investigate the functional role of Mut-PLP independent to that of EFGE. The EGFP marker could be used in tracking the Mut-PLP expression pattern in different stages of

CNS brain development and in subsequent oligodendroglial lineage. The transgenic mutant is being generated by injecting the transgene into the pronuclei of oocytes. To eliminate background of endogenous wild-type PLP/Dm20 expression in the transgenic mutant, we injected the transgene into the pronuclei of PLP-null mouse oocytes. Thus, the transgenic mouse mutant is still being produced is currently under obtaining founder mice.

5.2 Knock-in mouse mutant of PLP/Dm20-lacking disulfide bridges

PLP and Dm20 have two disulfide bridges, i.e., Cys183-Cys227 (proximal disulfide bridge) and Cy200-Cys219 (outer disulfide bridge), in their extra cellular loop-II. Recently, it was reported that a patient with a point mutation in PLP Cys codon (C183R) which is involved in proximal disulfide bridge formation, exhibited the classical PMD phenotype (Fukumura *et al.*, 2011). It is speculated that this lack of disulfide bridges in the extra cellular loop of PLP may influence PLP structural conformation, which results in its misfolding and ER retention due to prolonged binding with the ER calnexin chaperone. Prolonged binding with calnexin may accumulate PLP in the cytoplasm, which is possibly toxic and further resulting in apoptosis of oligodendrocytes leading to PMD. Recently, it was also shown *in vitro* in COS-7 cells, that PLP retention in the ER is due to the PLP extra cellular loop free Cys residue cross linkages in the ER. It has been suggested that of two disulfide bridges in the extra cellular loop of PLP/Dm20, only the proximal disulphide bridge is important for ER quality control and exit (Dhaunchak and Nave, 2007). For investigating the role of Cys bridges of PLP/Dm20 in CNS and specifically on the myelin phenotype, a knock-in mouse mutant is being generated.

A gene targeting approach is being used to generate a knock-in mouse mutant in which the two disulfide bridges (proximal and outer bridges) of PLP/Dm20 are deleted. Thus the knock-in mutant mouse is still being produced, which is currently at chimera breeding step. Since the PLP knock-in mouse mutant is being generated by altering the endogenous PLP gene locus at confined Cys codon positions, instead of wild-type PLP expression, only PLP and Dm20-lacking two disulfide bridges in their extra cellular loop should be expressed. Moreover, in the PLP knock-in mutant, expression of the PLP/Dm20-lacking disulfide bridges would be obtained under endogenous wild-type PLP gene regulatory elements.

5.3 The role of PLP and PUFA in the CNS

The CNS myelin membrane is composed of unique proteins such as PLP, and has a high lipid content including phospholipids which account for 40-45% of total lipid content. PUFAs such as docosahexaenoic acid (DHA) and arachidonic acid (AA) are the major components of the phospholipids in the myelin membrane and in the brain (Youdim *et al.*, 2000). In the CNS myelin, PLP and major PUFAs play critical structural and functional roles. Lack of PLP and PUFA in phospholipids, in CNS myelin membrane could reveal their direct impact in the CNS; that is on myelin membrane morphology, biochemical and cellular functions and in relation to behavioral physiology. Therefore a *plp*^{-/-}*fads2*^{-/-} double knock-out mouse mutant has been generated and characterized in the present work.

The genetically defined *plp*^{-/-}*fads2*^{-/-} double knock-out mouse (DM) was validated on the genomic, mRNA and protein level. The DM brain fatty acid profile showed drastically depleted major PUFAs. Intriguingly, the DHA quantity levels were depleted only to 50-60%. Despite lack of *Fads2* and thus the *in vivo* PUFA synthesizing function in the DM, the maintenance of high DHA content in the brain was possibly due to accumulation of DHA from the diet or through cross reactive pathways, which require further investigation. The maintenance of high DHA levels in the brain of the DM should be considered in light of previously reported DHA conservation in the brains across several vertebrate species (Anderson *et al.*, 1990; Tinoco *et al.*, 1982), this supports the importance of DHA as structural entities in the membrane phospholipids, or as precursors of docosanoids, etc.

The DM fatty acid profile showed elevated levels of unusual eicosatrienoic acid (20:3), and a high level of eicosadienoic acid (20:2), which is in agreement with the *fads2*^{-/-} single mutant fatty acid profile reported by Stroud *et al.*, 2008. Stroud *et al.*, 2008 speculated that 20:3 could be catalyzed from the fatty acid derivative of linoleic acid by delta-5 desaturase/*fads1* in the absence of delta-6 desaturase/*fads2*, which is also possible in our DM. Based on the PUFA profile of DM brain tissue, we propose that the elongase and delta-5 desaturase catalyze an unusually high level of 20:3 and 20:2 PUFAs from 18:2 (linoleic acid/n-6) and the lack of major PUFAs synthesis, as depicted in Figure 52. The exact sequence of delta-5 desaturase and elongase catalysis in the pathway could be verified based on 20:3 and 20:2 structures, which is still under investigation. The elevated level of 20:3 in the DM brain might be essential for compensating the depleted level of 20:4 (n-6) and 22:6 (n-3) in the membrane phospholipids and in eicosanoid synthesis.

Of the fatty acid profile of individual major phospholipids in DM brain lipids, major PUFAs including 20:4 (eicosatetraenoic acid) and 22:6 (docosahexaenoic acid) are depleted in phosphatidylethanolamine (PE), phosphatidylserine (PS), and phosphatidylcholine (PC). Interestingly, the depleted major PUFAs 20:4 and 22:6 were substituted with the unusual 20:3 in PE, whereas they were substituted with 18:2 in PS and PC. Substitution of the critical 20:4 and 22:6 with unusual 20:3 primarily in PE, might be due to the higher PE content among the myelin membrane phospholipids and its involvement in various pathways. Thus, overall depletion of

PUFAs in major phospholipids such as PE, PS, and PC, may in turn reduce unsaturation levels and increase the saturation index, decreasing myelin membrane fluidity and thus perturbing its functional role.

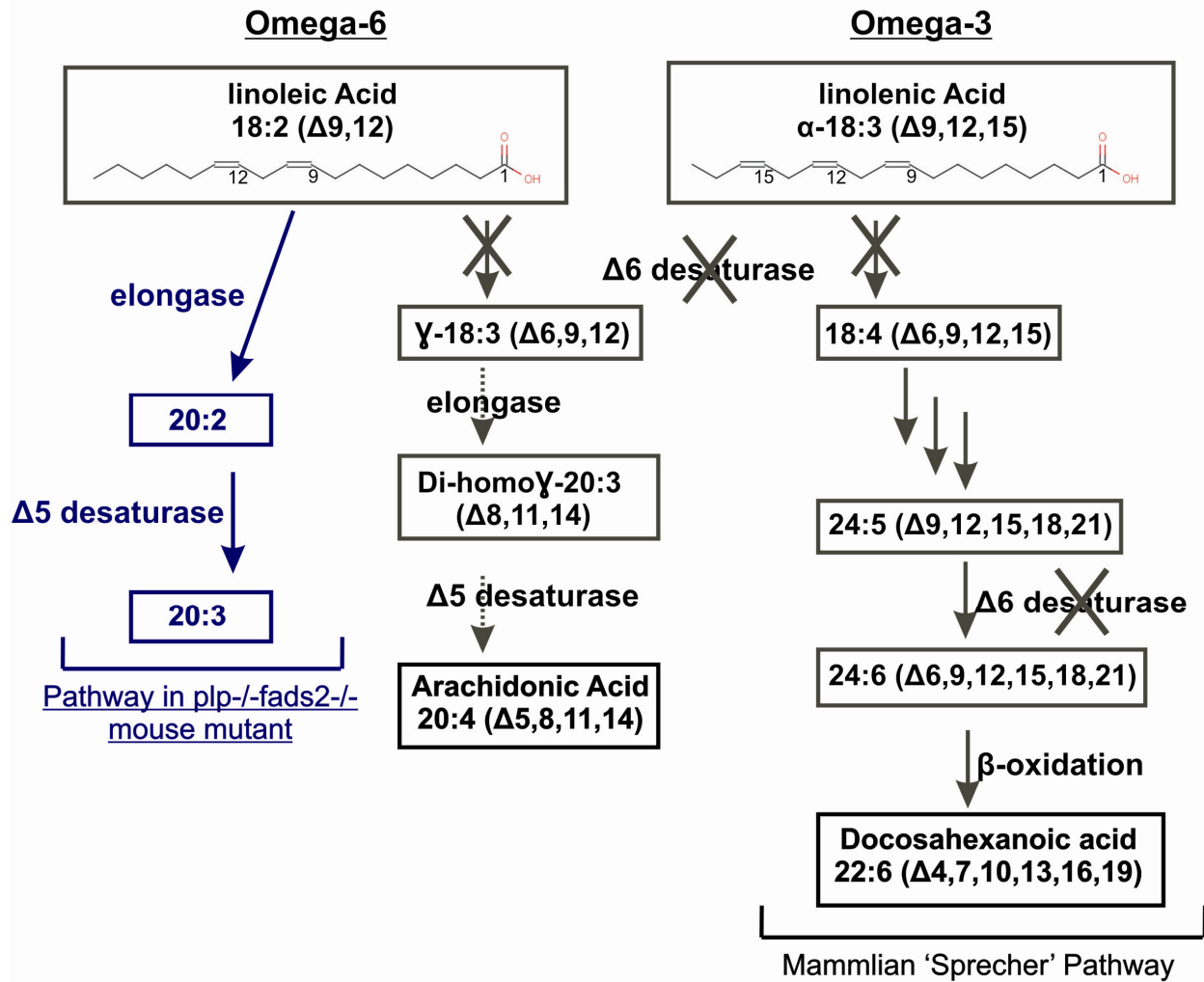


Figure 52: Proposed desaturation and elongation of the PUFA synthesizing cascade in the DM brain, based on its PUFAs profile.

The DM exhibited profound defects in its CNS myelin morphology. DM showed myelin morphological defects such as hypomyelination with reduced myelin thickness, loss of myelin compaction, architecture and reduced overall myelin production in the CNS. The significant

reduction in the total CNS myelin quantity in the DM brain is also a prominent feature for hypomyelination condition. Since PLP together with the PUFA are the major structural constituents of the myelin membrane, their absence might had profound effect on myelin membrane biosynthesis, myelin membrane fluidity or saturation index and on its biophysical properties. Furthermore, as observed in the electron micrographs of DM CNS myelin, the myelin paranodal junctions were not disturbed. In contrast to previous report (Stoffel *et al.*, 2008) of disturbance of tight-junction association proteins in the Sertoli cells of testis and gap junction proteins in ovarian follicles due to the lack of PUFA, here the undisrupted paranaodal junction observed in the myelin of DM might be due to the conserved levels of DHA in the CNS myelin membrane phospholipids compared to testis.

Based on *in vitro* experiments in oligodendrocytes it was shown that PUFA supplements could alter the myelin protein expression level, and could impact oligodendrocytes plasma membrane filopodia-like structures. In contrast, in our present *in vivo* study, the myelin proteins (MBP, MOG and MOBP) mRNA expression levels were not significantly altered in the DM brain. Although MAG was only 0.5 fold down-regulated at the mRNA and protein level in DM in contrast to the single mutants and wild-type counterparts, apart from its partial role towards axon-glia contact, its major role in the myelin membrane is unknown. Fatty acid synthesizing desaturase isoforms of FADs and SCDs were also investigated in the DM. In the PUFA synthesizing pathway, there is competition between n-3 and n-6 FAs for the same elongases and desaturases, and there are multiple desaturase isoforms which are expressed in a tissue specific manner. It has also recently been shown that one of the isoforms of fads, fads3, is up-regulated during LC-PUFA supplementation *in vivo* (Reardon *et al.*, 2012). However, in the present study we did not observe any changes in the mRNA expression levels of various desaturase isoforms, i.e., Fads1, Fads2, Fads3, and Scd1 and Scd2, in the DM brain tissue. Regarding critical myelin specific proteins such as NCAM (both isoforms i.e., NCAM-120 or NCAM-140), major myelin lipid GalC synthesizing enzyme CGT, and tight junction protein connexin-43, no major or significant expression differences were observed. This may suggest that the myelin proteins, desaturases and their isoform expression are highly regulated. Moreover, the PLP and delta-6/fads2 functions may not be substituted by other myelin specific proteins or desaturases in the DM.

It was also previously reported that various mouse mutants, such as *plp*^{-/-}, *fads2*^{-/-}, *mag*^{-/-}, and *plp*^{-/-}*mbp*^{-/-}, also have no major significant changes in their critical myelin protein gene expression profile nor compensate their functions (Stoffel *et al.*, 1997, Uschkureit *et al.*, 2000; Stroud *et al.*, 2009). This is in agreement with our observed results with the DM brain gene expression profile.

Photoreceptor outer segments in the retina contain high DHA and AA content in membrane phospholipids. In the DM, the photoreceptor outer segment and RPE region morphology were not significantly perturbed but mild distortions in the arrangement of apical villi in apical RPE region were observed. Functional assessment of retina function by ERG revealed a two-fold

decrease in ERG a-wave amplitude in the DM in contrast to the wild-type. Thus, the partial level of apical villi disturbance or its undetected structural morphological alterations might have shown an effect in decreasing ERG a-wave output. We can also speculate that the lack of PUFA content, especially DHA and AA, might have shown defects in the underlying molecular electrochemical signaling cascades. Moreover, although the photoreceptor outer segments were composed majorly of DHA and PUFAs in their membrane phospholipids, they appeared to be normal in the DM, which awaits further molecular level investigation.

Among the phenotypic features of the DM, the sterility and skin-dermatitis were also observed in *fads2*^{-/-} single mutants and therefore are likely contributed from the *fads2*^{-/-} single mutants. The DM also exhibited additional phenotypic features in contrast to their single mutants, such as apathetic behavior, partial but significant tremors and seizures, starting from 5 months. The DM mice also had a profound reduction in life span. These features of DMs may be correlated to its membrane systems morphological phenotypic defects i.e., hypomyelination disorder observed in the CNS. These observed phenotypic features are also in close agreement with the PMD or SPG2 disease condition where CNS hypomyelination or dysmyelination are the prominent features.

The motor coordination assessed by rota-rod and the Morris water maze-based swimming velocity parameter revealed partial but statistically significant defects in DM (*plp*^{-/-}*fads2*^{-/-}) and in *plp*^{-/-} and *fads2*^{-/-} mouse mutants compared to wild-type. Previously, it was reported that *plp*^{-/-} mouse mutants with CNS myelin compaction defects have partial neuromotor coordination defects (Boison and Stoffel, 1994; Gutierrez *et al.*, 1995). It was also reported that the CGT-null mutant with dysmyelination exhibited profound hind limb paralysis and motor coordination defects. Similarly, the CNS myelin defects in the DM, specifically the loss of myelin compaction phenotype derived from *plp*^{-/-} mutant might have contributed to the DM mice neuromotor coordination defects. The cognitive abilities, specifically the acquisition ability and the reference memory, were partially decreased in all the mutants including the DM mice in contrast to wild-type counterparts. It has been shown that the deficiency of myelin i.e., in the case of shiverer mutant or MBP null mutant, could decrease learning ability (Inagawa *et al.*, 1988). Moreover, it has been also well documented that the cognitive abilities could also be correlated to CNS myelin disorders such as dysmyelination, hypomyelination, neurodegenerative disorders such as MS, and ageing. Hence we can speculate that the DM containing CNS myelin morphology defects such as hypomyelination, and depleted major PUFA conditions have contributed towards its cognitive impairment.

6 Materials and methods

6.1 Cell culture methods

6.1.1 Oligodendrocytes preparation and transfection

Primary oligodendrocytes preparation: 6 to 8 day-old 3-4 plp^{-/-} mice were scarified, and appropriate quantity of brains were dissected and used according to the oligodendrocyte preparation kit (MACS, Miltenyi); Initially brain cells were dissociated with gentle Macs Dissociator (Miltenyi) and further immature or mature oligodendrocytes were purified with anti-O4 micro beads (Miltenyi) using MACS separator (Miltenyi). Thus separated and purified cultures containing pre or mature oligodendrocytes (Cizkova *et al.*, 2009; Jungblut *et al.*, 2012) were supplemented with Macs neuro-supplement media (Miltenyi) accordingly for further use.

Culturing conditions and transfection: Pre-oligodendrocytes were incubated (at 37°C and 5% CO₂) in 24-well plates with MACS-neuro medium (Miltenyi Biotech) containing 10µg/ml penicillin/streptomycin. Transient transfection was carried out with NanoJuice liposome transfection reagent (Novagen) according to the manufacturer protocol.

6.1.2 ES cell culture

ES-cells were incubated (at 37°C and 5%CO₂) in DMEM medium; containing 15%FCS, 100mg/ml penicillin/streptomycin, 0.03%glutamine, 1250ULIF, and 1mM 2-mercapthoethanol. ES-cells were cultured on embryonic fibroblasts.

6.1.3 Electroporation and Selection of ES cells

ES-cells in active growth phase and in culture for at least two days were used for electroporation. Four hours before electroporation, the medium was changed. 30-40 μ g of the linearized targeting vector was used for ES cells electroporation; Approximately 2×10^7 ES cells were washed twice with PBS (Ca^{2+} and Mg^{2+} -free), and trypsinized as follows: Cell were incubated with 3 ml trypsin/EDTA (0.05%) for 3-5 min at 37°C. After incubation, trypsin reaction was stopped by adding 7ml of ES medium and resuspended until a single cell suspension is formed and sedimented at 1000rpm for 4 minutes. The supernatant was carefully removed and the pellet was diluted with appropriate volume.

ES cells were counted, and 1.2-1.5 $\times 10^7$ cells were resuspended in 800 μ l of PBS with 30-40 μ g of linearized DNA and transferred into a 0.4cm electroporation cuvette (BIORAD), and the rest of the cells were used as control. Electroporation was carried out with a pulse of 500V and 230 μ f at RT. After five minutes of incubation at room temperature or on ice, the electroporated cells were transferred into 10ml of ES wild-type medium, resuspended, and the medium was distributed equally to five 90mm cell culture petri dishes seeded with fibroblast cells (2x10⁶ cells / plate).

Selection of ES cell clones

24 hours after electroporation, the ES cell medium was replaced with the G418-containing ES medium for 5 days. After 5 days, the G418 containing medium is replaced by ganciclovir-containing medium and cultured for 5 days. The selection resistant ES clones were manually picked.

Isolation of the ES cell clones

Plates containing ES cell clones were washed with PBS and picked manually under microscope, and transferred to the 96-cell culture plates. 96-cell culture plates containing clones were immediately trypsinized for detachment, and transferred to 96-well plate seeded with embryonic fibroblasts. After 3-4 days of culture, cells were trypsinized. 50% of cells were transferred to gelatin coated 96-well plates which were used for the isolation of genomic DNA and the remaining 50% were cryo-preserved.

6.1.4 Karyotyping of ES cells

ES cells cultured on gelatinized 90mm round petri-dishes were used in karyotyping as follows:

1. Cell cycle arrest by colchicine treatment

- a. To 5ml of medium in a 90mm petri dish containing ES cells, 33 μ l of colchicine solution (Demecolcine solution, Sigma) was added
- b. Allowed incubation for 50 min at 37°C.

2. Cells were washed 3 times with PBS, and detached with trypsin

3. Osmolysis with hypotonic KCL solution (0.56%)

- a. Cells were centrifuged for 8 min at 500g, and the supernatant was discarded
- b. 1ml of KCl was added drop wise to the precipitate for osmolysis
- c. 3ml KCl was added and cells were resuspended carefully
- d. Cell were incubated for 8-10min at room temperature, and centrifuged for 5min at 500g and the supernatant was discarded.

4. Fixation

- a. In the residual liquid cells were gently re-suspend
- b. 2 ml of ice-cold fresh fixative [methanol / acetic acid (3:1)] was added drop wise
- c. Incubated for 5 min at RT and centrifuged at 500g for 5min, and supernatant was aspirated
- d. Steps a to c were repeated for 1 to 2 times, the final precipitate was dissolved in 0.5-1 ml fixative solution
- e. Cells were dropped from a Pasteur pipette from at least 30cm height on a clean microscopic slides and allowed to dry

5. Staining

- a. Slides were immersed in giemsa staining solution (Giemsa stain, GS-500, Sigma)
- b. Washed with water, air dried, and mounted with mounting media (Merck).

Chromosomes of individual cells were examined at 63X magnification.

6.1.5 Cryopreservation of ES cells and COS-7 cells

Freshly prepared ice cold freezing medium (Wild type-cell culture medium with additional 20% FCS, and 10% DMSO, or as prescribed) was used for cryopreserving the cells. To the 96-well plate containing ES-cells in 50µl of wild-type medium, freshly prepared ice cold freezing medium of 50µl was added and the plate immediately wrapped in an aluminum foil and transferred initially to -20°C for 24 hrs and finally to -80°C.

6.1.6 Thawing and expansion of ES-cells and COS-cells

For thawing and expanding, the frozen 96-well plates or 1 ml tubes from -80°C were transferred and incubated at 37°C or at RT for 3-6 min. According to the frozen medium used initially in cryo-preserving, two volumes of wild-type medium was added gently by suspending cells up and down and transferred to a new 96-well plate or to 90mm plates already seeded with fibroblasts in case of ES-cells, or to a gelatin plate in case of COS-7 cells.

6.1.7 COS-7 cell culture and transfection

Culturing conditions: COS-7 cells were incubated (37°C and 5%CO₂) in DMEM with 10% FCS, 10µg/ml penicillin/streptomycin and 1mM sodium pyruvate.

6.1.8 Embryonic fibroblasts culture

Culturing conditions: Mouse embryonic fibroblasts were cultured at 37°C and 5%CO₂ in DMEM with 10% FCS and 10µg/ml penicillin/streptomycin and 0.03% glutamine.

6.1.9 Lipofection (DNA-Lipofectamine 2000), Electroporation of COS-7 and OLN93 cells

DNA transfection into COS-7 and OLN93 cells was carried out by lipofection (DNA-lipofectamine 2000, Invitrogen) or by electroporation accordingly. For lipofection the manufacturer's protocol was followed. 5×10^6 OLN93 cells were electroporated with 0.8 μ g of linearized plasmid DNA in 0.8 ml of culture medium at 450 V and 250 μ F (0.4cm cuvette). Thereafter, cells were suspended in 10ml of medium and distributed at various concentrations (500-2000 μ l) to 90mm-cell culture round petri dishes seeded with fibroblasts.

6.1.10 Stable selection of COS-7 or OLN93 cells

After 24 hours of transfection (lipofectamine or electroporation), the wild-type medium was replaced with G418 containing wild-type medium for two weeks, for selection. The resistant COS-7 or OLN93 clones were picked under the microscope and transferred to a 24-well plate for further analysis.

6.2 Molecular biology methods

6.2.1 Plasmid-DNA preparation

Plasmid mini-preparations of 3ml of overnight culture were performed according to the method of Birnboim (Birnboim, 1979). Plasmid maxi-preparations were carried out using Qiagen tip-500 columns (Qiagen) according to the manufacturer's instructions.

6.2.2 Extraction of DNA from agarose gels

DNA fragments were eluted from TBE (Tris-borate-EDTA) gels using NucleoSpin columns (Macherey & Nagel) as described in the manufacturer's protocol.

6.2.3 DNA isolation from ES cells or COS-7 cells

Following protocol was employed for 96-well plate, 24-well plate, and as well as 90mm-petri dishes containing confluent ES cells, accordingly. The following procedure is described for 24-well plate; ES cells were cultured until confluent on gelatin-coated 24-well plates. The medium was removed and cells were washed with 500 μ l of PBS and incubated overnight in 500 μ l of lysis buffer (100mM Tris/HCl [pH 8.5], 5mM EDTA [pH 8], and 200mM NaCl, 0.2%SDS) and 5 μ l of proteinase K (10mg/ml) at 37°C. Thereafter, the lysate was transferred to Eppendorf tubes and 450 μ l of isopropanol was added. Incubated for 10 minutes at RT and centrifuged at 13,000rpm at 4°C for 15 minutes. The DNA pellet obtained was washed with 70% ethanol of 500 μ l. After briefly drying, DNA was dissolved in 200 μ l of TE or 10mM Tris/HCl (pH 8) for 3 hours at 55°C. Confluent grown ES cells on 90mm plates were trypsinized prior to the lysis for DNA preparation.

6.2.4 Genomic DNA isolation from mouse tail

For preparation of genomic DNA from mouse tails, about 0.5cm of tail tip biopsy was incubated overnight for digestion at 55°C at 1100rpm in 700 μ l of lysis buffer (50mM Tris-HCl pH 8.0, 100mM EDTA, 100mM NaCl and 1%SDS) and 30 μ l of proteinase K (10mg/ml). DNA was precipitated with isopropanol, washed with 70% alcohol, and dissolved in 200 μ l TE.

6.2.5 Restriction analysis/digestion

Plasmid DNA of 0.7-0.8µg was digested with 1U of the appropriate restriction endonuclease for 1-2 hours at 37°C, according to the manufacturer's protocol.

6.2.6 Ligation

Ligation was performed at 14°C in 20µl of volume overnight with 1U T4-DNA-ligase. PCR fragments ligation and cloning were performed with the TA Cloning Kit (Invitrogen) according to the manufacturer's instructions.

Before ligation, 5'-end dephosphorylation was done by treating alkaline phosphatase (Roche) in order to prevent self ligation, according to the manufacturer's protocol

6.2.7 Preparation of Competent Cells and transformation of plasmid DNA

Competent *E. coli* cells (DH5α) were prepared as previously described in Hanahan, 1983.

Transformation of plasmid DNA into competent cells

Frozen competent cells of 100µl were thawed on ice. Plasmid DNA of 3 to 5µl or ligation mixture of 20µl was gently mixed with the freshly thawed ice cold competent cells and incubated for 30 minutes on ice. A heat shock was given for 90 seconds at 42°C, 1000µl of ice cold LB medium was added and incubated for an hour at 37°C in a water bath. Cells were plated on LB plates containing appropriate antibiotics for selection.

6.2.8 Polymerase chain reaction (PCR)

Reactions were performed in 20 or 50µl accordingly in a Peltier Thermal Cycler (Biozym).

Template-concentration used in the range of: 5ng-50ng plasmid DNA, 1-5µg cDNA, 3ng-20ng PCR-fragments, 300ng genomic DNA. dNTP concentration: 100 nmol. Primer concentration: 200 nmol. Taq polymerase (Expand High Fidelity PCR kit and the Long Template PCR kit, Roche): 1U/100µl. Reaction Buffer: 100mM Tris-Cl, pH 8.3, 500mM KCl, 15mM MgCl₂, 0.01%gelatin.

Standard conditions of the PCR cycle were:

Denaturation: 94°C, 1-3min

Amplification: 94°C, 1-3min (denaturation), 50-70°C, 1-3 min (Annealing), 72 ° C, 1 min/kb (elongation)

Elongation: 72 ° C, 10 min.

Some of the standard PCR programs used in the present study:

Desatgen-PCR program

1= 94°C 2min
2=94°C 15min
3=60°C 30min
4=68°C 7min
5=go to 2 (for 9x)
6=94°C 15min
7=60°C 30min
8=68°C 7min (+ 5sec/cycle)
9=go to 6 (for 19x)
10=68°C 7min
11=4°C end

(Total of 4hours 51min)

Used for genomic DNA

Desatura-PCR program

1=94°C 2min
2=93°C 1min
3=60°C 1min
4=72°C 2:30min
5=go to 2 (for 30x)
6=72°C 10min
7=4°C end

(Total of 3hours)
(used for SDM and for cDNA)

RT-PCR program

1=94°C 2min
2=93°C 1min
3=60°C 1min
4=72°C 2:30min
5=go to 2 (for 30x)
6=72°C 10min
7=4°C end

The annealing temperature was chosen about 3-5°C below the estimated melting temperature of the primers. The elongation time focused on the length of the expected amplicon is approximately 1 min/kb. PCR products were analyzed by gel electrophoresis on TBE agarose gels.

For site directed mutagenesis, appropriate mutated primers were used in the normal PCR mixture with appropriate PCR temperature conditions based on primers point mutations.

6.2.9 DNA sequencing and Synthesis of oligonucleotide

DNA Sequence analysis was done by the analytical department of the Center for Molecular Medicine Cologne (CMMC) using an ALF Express (Pharmacia) or an ABI-377 (Applied Biosystems).

Synthesis of oligonucleotides

Oligonucleotides were synthesized by Metabion, Germany.

6.2.10 RNA preparation

RNA preparations were carried out using the TRIzol® LS Reagent (Life Technologies) according to the manufacturer's specifications.

6.2.11 RT-PCR (Reverse transcription-PCR)

For the preparation of cDNA, 5 or 10µg of RNA was used. 2µl of p (DN6) (50µM, Boehringer) was added and filled up with water to a volume of 31.5µl. The mixture was incubated for 10 minutes at 70°C, and cooled for 2min on ice. 10µl of 5x RT buffer (Gibco/BRL), 4µl DTT (0.1M), 0.5µl RNAsin (Boehringer) and 2µl of dNTPs mix (10mM) were added and incubated for 10 minutes at 25°C, incubated at 42°C for two min, and 2µl of SuperScript-II (Gibco/BRL) was added. Total reaction time was 50 minutes at 42°C. Enzyme was denaturated by heating at 70°C for 15 minutes.

Semi-quantitative PCR

2µl of above reverse transcription derived cDNA was used for PCR and semi-quantified as follow:

Semi-quantification (non-radioactive/cold): PCR product was separated on agarose gels and quantified with Image Quant software version 5.1 (Molecular Dynamics).

Semi-quantification (radioactive/hot): Radioactive DNA labeled PCR were separated on a polyacrylamide gel dried and further analyzed by means of the gel phosphoimager SI 445 and semi-quantified by Image Quant software Version5.1 (Molecular Dynamics).

6.2.12 Radioactive DNA labeling

Radiolabeling of DNA fragments with [32P] dATP and [32P] dCTP (Amersham) was performed by means of the random primed DNA labeling kit (Boehringer) according to the manufacturer instructions. The removal of unincorporated nucleotides was performed by Probe Quant G-50 Micro Columns (Amersham).

6.3 Biochemical methods

6.3.1 Protein quantification

The protein was quantified by photometric determination using the BCA assay (Smith, 1985) (Pierce; Cu⁺ BCA protein complex) according to the manufacturer's instructions.

6.3.2 SDS-polyacrylamide gel electrophoresis (SDS-PAGE)

For protein expression analysis Bis-Tris gels (Invitrogen) of 4-12% concentration were used. After electrophoresis, gels were stained with Coomassie R-250 (0.3% in 10% acetic acid, 40% methanol), or silver (Blum *et al.*, 1987).

Myelin samples were separated under non-reducing conditions (sample buffer: 10% glycerol, 125 mM Tris-Cl, pH 6.8, 4% SDS, and 0.02% bromophenol blue). For reducing the sample preparation, 4% β -mercaptoethanol was added. Samples were boiled for 3 min before application.

6.3.3 Myelin preparation (Based on sucrose gradient separation)

Myelin from freshly extracted mouse brains was prepared according to the Norton and Podulso (sucrose gradient) myelin extraction protocol (Norton and Podulso, 1973); Mouse brains were homogenized (Elvehjem Potter) in 12ml of 0.3M sucrose and gently overlaid on top of 0.85M sucrose in 30ml glass tube with a Pasteur pipette. After centrifugation at 10,000g at 4°C for 20min, the white myelin interphase formed, was carefully collected into 30ml test tube and washed three times with double volume of water at 10,000 g, at 4°C for 20min. Thus obtained white precipitate (myelin) was dissolved in 500 μ l SDS buffer (non-reducing). 10-50 μ l aliquots were used for SDS-PAGE.

6.3.4 Lipid analysis

Total brain or myelin lipids extraction: Freshly obtained brains or isolated myelin from the brain, were subjected to ultra-turrax in CHCl₃/methanol (2:1) and then incubated at 55°C in a water bath for lipid extraction. Extracts were centrifuged at 3000g for 4min. The precipitate was collected and again extracted with CHCl₃/Methanol (1:1) and subsequently repeated with CHCl₃/methanol (1:2). Thus obtained three supernatants in previous subsequent steps were collected, mixed and dried under N₂ and further dissolved in 2-4 ml of CHCl₃/Methanol (1:1).

For thin-layer chromatography analysis HPTLC silica gel 60 plates (Merck) were used. Lipid samples were applied and separated in different mobile phases: development of total lipids; CHCl₃/methanol/H₂O (65:25:4), and separation of gangliosides; CHCl₃/methanol/NH₄OH [2N] (60:35:4).

For detecting or verifying the separated lipids, HPTLC plates were stained in different ways: for total lipid detection; ashing with 50% H₂SO₄ and incubation for 3-5min at 120°C, for phospholipids detection; Zinzadze staining (Dittmer and Lester, 1964), for glycolipids detection; Anthrone staining (Ledeen and Yu, 1982), for sialic acid containing lipids; orcinol staining (Ledeen, 1966), and for amine containing lipids; ninhydrin staining.

Transesterification: Total lipids or separated individual phospholipids or sphingolipids were used for transesterification. First, the lipid extract was dried with N₂. To the dried lipid extract in an air tight flask or test tube, 2ml of Methonal.HCl was added and incubated at 80°C for 2 hours. An equal amount of water was added. Further, methyl esterified fatty acids were extracted in Hexane-Ether (1:1) of 2-4 ml.

Fatty acid Silylation: MSTFA (N-methyl-trimethylsilyltrifluoroacetamide) of 30µl was added to 150-200µl of fatty acid methyl esters (FAME) for obtaining fatty acid silyl derivatives which were further characterized by GC-MS to identify long chain hydroxy-fatty acids.

6.3.5 Gas Chromatography–Mass Spectrometry (GC-MS)

Silylated transesterified lipids in CH₂Cl₂ solvent were used for GC-MS. The GC gradient ran from 160°C to 240°C, the temperature rise per minute was 4°C. GC separated individual compounds were detected by the mass spectrometer detector was based on individual fragments mass to charge ratio (M/Z). Obtained mass spectra with retention times of several individual fatty acids were analyzed manually by employing NEST database and Data analysis package (HP-MSD).

6.4 Immunological methods

6.4.1 Western blotting

Western Blot NuPage system (Invitrogen) was used according to the instructions of the manufacturer. After gel electrophoresis separation of the proteins they were transferred (3h, 1mA/cm², Sartoblot S II; Sartorius) onto a nitrocellulose membrane (Schleicher & Schuell) by semi-dry electroblotting method (Harlow and Lane, 1988).

For blotting, the blot was constructed as follows:

Cathode;

Two Whatman filter paper soaked with 25 mM Tris pH 9.8, 20% methanol (40mM ϵ -aminocaproic acid, optional);

Gel, nitrocellulose membrane;

Two Whatman filter paper soaked in 25 mM Tris, pH 10.4, and 20% methanol;

Two Whatman filter paper soaked in 25 mM Tris, pH 10.4, 20% methanol.

After transfer, the nitrocellulose membrane (Schleicher Schuell) was hybridized and blocked in TBS and 5% milk powder for 2 hours at RT or overnights in order to saturate free binding sites, then incubated with the first antibody in TBS and 5% milk powder for 1 hour at RT or over night at 4 ° C. Subsequently, the blot was washed three times for 10 minutes with TBS-T (TBS, 0.1% Tween 20) and incubated with the second antibody conjugated with peroxidase in TBS 5% milk powder for 1 hour. After three washings for 10 minutes each with TBS-T, the blot was developed. For peroxidase staining luminol detection reagent (100mM Tris/HCl [pH 8, 5], 2.5mM luminol, 0.35mM coumaric, 0.01% H₂O₂) was used. The chemiluminescence was detected by X-ray films (Kodak, Fuji).

Optimized concentrations of primary antibodies were used: anti-PLP serum: 1:400; anti-MBP antibody (monoclonal anti-mouse MBP Boehringer) 1:5000; anti-mouse serum MOG 1:1000, anti-rabbit serum MOG 1:10000). After washings, the secondary incubation with anti-rabbit or anti-mouse IgG peroxidase conjugate of FITC of CY3 (Sigma) for 1 h at room temperature in TBS and 5% milk powder was performed accordingly.

6.4.2 Immunostaining of cells

Cells were plated on poly-L-lysine coated cover-slips. Fixation was done with 4% paraformaldehyde in PBS for 10 minutes, and washed one time and permeabilized with PBS/0.5% Triton X-100 for 15 minutes. Blocking of the cells was carried out for 1 hour at RT with 3% BSA in PBS. Washed with PBS for three times with 5 min incubation, and incubated for one hour with the primary antibody or anti-serum in the predetermined dilution in PBS and 1% BSA. After washing four times with PBS, the second antibody was added and incubated for 1 hour at RT. Double staining was performed accordingly with two types of fluorescent Cy3 (red) or FITC (green) conjugated antibodies. Dapi counterstaining; Dapi was combined with the secondary antibody. Secondary antibody incubation was done in the dark. Preparations were washed three times with PBS/0.2% Triton X-100 and twice with PBS and then mounted on the microscopic slide.

EGFP fluorescence analysis

Cells were plated onto poly-L-lysine coated 96-well culture plate (Nunc) or on to cover slips present inside the 24 well plates. . Thus prepared plates were observed under a Zeiss Axioscop fluorescence microscope (with a filter for enhanced GFP; Chroma Analytical) and thus observed images were documented by using the Zeiss Axiovision documentation method.

6.4.3 Mouse brain fixation for cryo-sectioning

Mice were anesthetized with Nembutal and perfused through the left ventricle with 4% paraformaldehyde/2%glutaraldehyde in PBS. The brain was dissected, post-fixed for three hours in the perfusion solution and stored in 10ml of 0.5M sucrose overnight at 4°C. Further, tissue was embedded in OCT (Tissue Tek, Miles Scientific, Naperville), and sections of 8-10µm thick were obtained on microscopic slides (Superfrost Plus) at -20°C using a Cryotom (Bird, AS650). Sections were stored at -20°C.

6.4.3.1 Cryo-sections immunohistochemical staining

Brain paraffin sections were fixed for 10 minutes with 4% paraformaldehyde in PBS. Non-specific binding sites were blocked with 3% BSA in PBS for 1 hour at room temperature. Incubation was performed with the primary antibody or anti-serum in 1% BSA/PBS for 2 hours at room temperature, washed three times with PBS (1% BSA/0.2% Triton X-100), incubated with the fluorescent conjugated secondary antibody for 1 hour at RT in the dark. After three washes with PBS/1% BSA, 0.2% Triton X-100, and slide was mounted with glycerol gelatin (2.5% DABCO, Merck) under a cover slip.

6.4.4 Mouse brain fixation for paraffin sectioning

Mice were anesthetized with Nembutal and perfused through the left ventricle with 4% paraformaldehyde/2% glutaraldehyde in PBS. Brains were dissected and post-fixed overnight in 4% paraformaldehyde/2% glutaraldehyde at 4°C. Subsequently brains were embedded in an automated paraffin embedding machine according to the following program:

- 1h 70% ethanol
- 2h 70% ethanol
- 2h 96% ethanol
- 2h 96% ethanol
- 3h 100% ethanol
- 3h isopropanol
- 3h xylene
- 3h xylene
- 3h xylene
- 3h paraffin
- 3h paraffin (with vacuum)

Then the specimens were casted in a paraffin block and sliced appropriately on a microtome.

6.4.4.1 Paraffin sections immunohistochemical and hematoxylin-eosin staining

Paraffin sections were de-waxed for 20 minutes in xylol and another 20 minutes in a fresh solution of xylol, then rehydrated prior to staining in a descending alcohol series (100% ethanol, 90% ethanol, 70% and 50% ethanol) for 5 min each, washed with PBS and the procedure for immunohistochemical staining of cryosections followed. For hematoxylin/eosin staining, sections were placed in eosin for 5min and then rinsed in distilled water. They were then placed in hematoxylin for 5min, rinsed with distilled water and placed under tap water for 5minutes. Thereafter, the specimens were dehydrated in an ascending ethanol series (20%, 40%, 60%, 80% ethanol and 100% isopropanol) and mounted in mounting media (Merck).

6.5 Electron microscopy

Freshly dissected mouse optic nerve was post-fixed in 2%paraformaldehyde, 2%glutaraldehyde, 0.15Mcacodylate buffer. Further embedding, sectioning, and visualization of electron micrographs were performed at the Institute of Anatomy, University of Cologne.

6.6 Methods for generating mice mutants (Transgenic and Knock-in mutants)

6.6.1 Mice maintenance

Mice strains such as CD1 (outbred), and C57/Bl6 (with various genotypes such as *plp*^{-/-}, *fads2*^{-/-}, *plp*^{-/-}*fads2*^{-/-}, PLP knock-in chimera; inbred), were maintained throughout the study in an artificial day-night cycle (lighting: 5:00 to 19:00 o'clock, darkness: 19:00 to 5:00 o'clock) with free access to food and water.

6.6.2 Microinjection

DNA microinjection into the pronuclei was performed according to the protocol described in Hogan, 1986 as follows: Oocytes spending females (plp^{-/-} mice) were super-ovulated two days prior to the microinjection with 5U gonadotropin, and after 46-48 hours stimulated with 5U human chorio gonadotropin and mated immediately with plp^{-/-} male mice. After 24 hours of matting, females were selected by plug check. Then eggs were collected from the ampoule of the oviduct, and stored in M16 medium (16x Earle, 0.1 M pyruvate; 100x P/S, 37.5 x NaHCO₃, 100 mg of BSA) in an incubator (37°C and 5%CO₂). Further, injections into the oocytes were done in M2 medium (Sigma) with a microinjector (Eppendorf type 5242, Jun-Air compressor model 6) on micromanipulator stand (Leitz TypM), under the microscope (Wild/army castle). Successfully injected eggs were not disturbed for two to three hours and were re-implanted into the infundibulum of uterine tubes of a pseudo-pregnant mouse (one day pc; s mated with vasectomized males).

6.6.3 Vasectomized males

Vasectomized male mice at least two months old were used for obtaining pseudopregnant female mice for re-implantation of eggs (Hogan, 1986).

6.6.4 Blastocyst injection

Blastocysts were released into the DFH medium (DMEM; 10%FCS containing 20mM Hepes) from the uteri (3.5 days pc) dissected from at least four weeks old super-ovulated wild-type mice (C57/B16). After isolation of blastocysts in DF medium (DMEM, 10%FCS) further incubated at 37°C and 4.8%CO₂. The blastocysts injection was carried out in DFH-medium; Approximately 20 ES cells were deposited on to the inner cell mass of blastocysts. The blastocyst injections were carried under the microscope (Leitz Axiovert 10) with a micromanipulator (Leitz TypM).

Successfully injected blastocysts were cultured for one to two hours in M16 medium and re-implanted into the uterine horn or uterus of 5-10 pseudopregnant mice (2.5 day pc; mated with vasectomized male)

6.7 Behavioral physiology

Behavioral physiology tasks were modified from Wallace *et al.*, 1980 and Morris, 1984. The open field and Morris water maze trail data were recorded in a software program (i.e., OFAKS and MWAKS), obtained from Neuroscience physiology department, Anatomy Institute, University of Cologne. Various genotypes i.e., wild-type (n=8), *plp*^{-/-} (n=8), *fads2*^{-/-} (n=8), and *plp*^{-/-}*fads2*^{-/-} (n=5) mice, of 5-months-old were used in the present study.

6.7.1 Rotarod

Animals were placed on a resting rod of diameter 3cm, and at a height of 30cm above the ground. Rod was rotated constantly at different speed intervals i.e., 16rpm, 24rpm, and 36rpm for 2 min. Initially mice were trained for 2 days at 12 rpm. On day-3 and 4 the test was performed with three trails per day. The latency time of the mouse on the rotating rod in all trails were recorded and statistically analyzed.

6.7.2 Horizontal rod and Grid task

Three trails were performed on each day for three consecutive days. The first two days trails were used as a training period, whereas the third day performance was recorded and analyzed further.

In horizontal rod task, mice were placed in the middle of a horizontal metal rod bridging two platforms (2X2, 80cm length), and the latency time of mice on the horizontal rod was recorded. Similarly in the grid task, mice were placed on the grid and rotated in 180°. Mice latency time on the grid was recorded with cutoff of 2 min and further readings were statistically analyzed.

6.7.3 T-maze

Mouse was kept at the starting position in the T-Maze apparatus and after 5 seconds the start door was opened free to enter the left or right arm. Thus a series of 15 free-choice trails were carried out. The choice of the left or right arm chosen by the mouse was noted for further calculations.

6.7.4 Open field

The mouse was placed in the center of the open field apparatus (60 X 60 cm), the bottom platform being subdivided into 10 x 10 cm squares. During the test various behavioral patterns such as square crossings, time at corners and middle, number of groomings and rearings were recorded by the open field software (OFAKS). Each trail was recorded for 5 minutes. Animals were tested one time per day for five consecutive days.

6.7.5 Morris water maze (Morris *et al.*, 1984)

Morris water maze experiments were performed in a circular polyethylene water tub (69 cm diameter and 22 cm height); with appropriate water levels, and a mouse resting platform of 7.5cm diameter that was submerged approximately 0.5cm of water level and was placed in south quadrant at a constant place. The tub was virtually divided into four quadrants i.e., north, south, east, and west. The entire tub was monitored with a video cam and behavioral scoring exhibited by the mice was entered into Morris water maze software (MWAKS). Water temperature was maintained at 21 to 22°C.

In all trails; mice were released into the Morris water maze tub from north quadrant, and platform location was in the south quadrant (in probe trail platform was removed). Mice swimming latency time, number of crossings along four quadrants (north, south, east, and west), mice location and total time duration in each quadrant was recorded.

Procedure: After releasing the mouse into the water pool along the walls of the tub in north quadrant, the Morris water maze program was started immediately. When animals found the platform, they are allowed to rest for 10 sec, or if the animal cannot find the platform after 90 sec

of the trail they are directed towards the platform and allowed to sit on the platform for 20 sec. After each trail mice were dried with a towel and set back in the cage for 15-20 sec before the new trial begins. Thus, four trails were performed per day for 5 consecutive days. During the trail; escape latency, square crossings and swimming speed, and the time spend in each quadrant, were recorded by the Morris water maze program. On day 5; a probe trail was performed with no platform in the south quadrant, and the number of crossings on the position of the absent platform and the time spent in each quadrant was recorded and analyzed statistically.

6.8 Bioinformatic programs and servers

Lipid structural analysis/drawing	Lipidomic Gateway (http://www.lipidmaps.org/tools/index.html) (http://www.emolecules.com/)
Kyte-Doolittle hydrophathy plots	DNA star – Laser gene (http://www.dnastar.com/t-products-lasergene.aspx)
Hyrdophobic properties prediction	SOSUI (http://bp.nuap.nagoya-u.ac.jp/sosui/sosui_submit.html)
Signal peptide prediction	SignalP v3.1 (http://www.cbs.dtu.dk/services/SignalP)
Protein parameters	Expasy ProtParam (http://www.expasy.ch/tools/protparam.html)
Domain prediction servers	SMART (http://smart.embl-heidelberg.de/)
DNA editing tools	Sequence manipulation suite (http://www.bioinformatics.org/sms/index.html)
Alignment programs	Mult Alin (http://multalin.toulouse.inra.fr/multalin/multalin.html) ClustalX v1.81 Boxshade v3.21 (http://www.ch.embnet.org/software/BOX_form.html)
Phylogenetic program	Phylip v3.66
Graphical software Vector	NTI (Invitrogen)

7 Appendix

7.1 Plasmids used in the present study

pBS 246	Gibco
pBluescriptII SK(+)	Stratagene
pcDNA3.1	Invitrogen
PCR 2.1	Invitrogen
pEGFPN-2	Clontech
pIRES-EGFP	Clontech

7.2 Oligonucleotides

Primer	Sequence	Purpose
PLPCDNA se	GAC ATG GGC TTG TTG GTC GTC GGC TAG ATC TCT	PLP/Dm20 Cys Site- directed mutagenesis (SDM)
PLPmut C24 s	GCC ACT GGA TTG TCG TTC TTT GGA GTG GCA	
PLPmut C24 as	TGC CAC TCC AAA GAA CGA CAA TCC AGT GGC	
PLPmut C32/34 s	GCA CTG TTC TCG GGA TCG GGA CAT GAA GCT	
PLPmut C32/34 as	AGC TTC ATG TCC CGA TCC CGA GAA CAG TGC	
PLPmut C108 s	TAC AAG ACC ACC ATC TGC GGC AAG GGC CTG	
PLPmut C108 as	CAG GCC CTT GCC GCA GAT GGT GGT CTT GTA	
PLPmut C138/140 s	GAG CGG GTG TCG CAT TCG TTG GGA AAA TGG	
PLPmut C138/140 as	CCA TTT TCC CAA CGA ATG CGA CAC CCG CTC	
PLPmut C168 s	GTG TTT GCC TCT TCG GCT GTA CCT GTG TAC	
PLPmut C168 as	GTA CAC AGG TAC AGC CGA AGA GGC AAA CAC	
PLPmut C183 s	TGG ACC ACC TCT CAG TCT ATT GCC TTC CCT	
PLPmut C183 as	AGG GAA GGC AAT AGA CTG AGA GGT GGT CCA	
PLPmut C200 s	GGC AGT CTC TCT GCT GAT GCC AGA ATG TAT	
PLPmut C200 as	ATA CAT TCT GGC ATC AGC AGA GAG ACT GCC	
PLPmut C219 s	GGC AGG GTT TCT GGC TCC AAC CTT CTG TCC	
PLPmut C219 as	GGA CAG AAG GTT GGA GCC AGA AAC CTT GCC	
PLPmut C227 s	CTT CTG TCC ATC TCT AAA ACA GCT GAG TTC	

PLPmut C227 as	GAA CTC AGC TGT TTT AGA GAT GGA CAG AAG	
PLPmut as	GAG CTC AGA ACT TGG TGC CTC GGC CCG TGA	
Fusion PLPXhoI se	CTG GAA TTC GGC TCG AGA TGG GCT TGT TAG	Transfection constructs
Fusion PLPPstI as	GAA TTC GGC TTG ACT GCA GAA CTT GTT GCC	
Human Nestin se	GAC TTC CAA GGC CTC TTC TAG CCT GGA	
Hum.Nestin Ex II se	TCG GCA GCA GCT GGC GCA CCT CAA GAT	
MBP Prom43-20 se	ACC AGA TCT TAT CGA TCA CCG TGG CTT	
MBP Prom1286-1309 a.se	GGA CTC TGA GAT CGA TTC TTT GAA GGT	
MBP No RS a.se	GTC TGC TGT GTG CTT GGA GTC TGT CAC	
MBP No RS se	ACT GCG GCT TAC AGA GGA GCC AGA TCC	
Ires2-egfp 1980 se	GTA CAA GTA AAG TGG ACG GGA CTC TAG ATC	
Ires2-egfp 1980 a.se	GAT CTA GAG TCC CGT CCA CTT TAC TTG TAC	
pIRES-EGFP 2k a.se	ACG CCT TAA GAT ACA TTG ATG AGT TTG GAC A	
Pre PLP Int-Ia sense primer	CCC TCT GTA GCC AAT TAC TCT ATT TCC TGC	
Pre PLP intron-Ib sense	CTA TAG TTA GAA ATA GTG TGA CTA TTT ACA	
PLP EX-IV antisense primer	AGG GAA GGC AAT AGA CTG AGA GGT GGT CCA	
PLP Intron-VII as	ATC GAT CTT TCA CTC CTC CTC GAG TTG CAG	
GPLP start EX VII se	GAGAGTCTTGCAGTGATTAATCTCTCTCTG	
3' neo 'sense primer'	GCG CAT CGC CTT CTC TCG CCT TCT TGA	
Infusion GPLP ExVII XhoIStuI (43 bs)	CCA GCT GCA ACT CGA GTC GCA GAG GAG TGA AAG GCC TAA TTG A	
Infusion GPLP IntVII XhoI a.se (43bs)	CAT TAA TTA ACT CGA GTA TGC ACA GAA TGA ATG CAT GTC TCT TTG	
5' Neo 'antisense primer'	TGC GAA TCG GGA GCG GCG ATA CCG TA	
Intron-I 'as.p'	TCT GTT TTG CGG CTG ACT TTG	plp ^{-/-} fads2 ^{-/-} mice genotyping
5' UTR 's.p'	GGA GAG GAG GAG GGA AAC GAG	
Neo 'as.p'	TTG GCG GCG AAT GGG CTG AC	
5'UTR 's.p' (Fads2)	CCT TCC TTG TTC CAG ACA CGG TCT CAA GAG	
ex-I 'a.p' (Fads2)	CGT AGC ATC TTC TCC CGA ATA GTG TCC GAT	
NCAM 140 s	CCA TCA GAC ACT ATC TGG TC	RT-PCR
NCAM 140 as	TCAGGAAGTAGCAGGTGATG	
NCAM 120 s	CCT GAA GAG CAT CCA GTA CA	
NCAM 120 as	ATG AAT TCC AAG GAC TCC TG	
RT-MAG s	TGC TCA CCA GCA TCC TCA CG	
RT-MAG as	AGC AGC CTC CTC TCA GAT CC	
RT-MOG s	CCA AGA GGA GGC AGC AAT GG	
RT-MOG as	GTT GTA GCA GAT GAT CAA GG	

MBP s	TAC CTG GCC ACA GCA AGT AC
MBP as	GTC ACA ATG TTC TTG AAG
OMgp s	GCA GCA GCT GCA ACT CTA AC
OMgp as	GAA GCA TTT ACT TTC CAA GCA
m vimentin s	ACT ATT GGC CGC CTG CAG GAT GAG ATC CAA
m vimentin as	CAA GGT CAT CGT GAT GCT GAG AAG TCT CAT
FADS2 se	ATG GGG AAG GGA GGT AAC CAG GGA GAG GG
FADS2 as	TCA TTT ATG GAG GTA AGC ATC CAG CCA CAG
FADS1 s	GGT ATA TTT TCT ATT ATTG TGG TTC AGC GGA
FADS1 as	TAA ACA ATG TCC GCG AAG GCT GTG AGC AGG
FADS3 s	TGA AGT TGA AAA TCT GGC GTA CAT GCT GGT
FADS3 as	ATG TCG CCA GAC TTC TTC AGG GAC CCG ATG
SCD1 s	CAT GCT CCA AGA GAT CTC CA
SCD1 as	CGG CTG TGA TGC CCA GAG CG
SCD2 s	TTG AAA AGA GTT CTC ACC ACT GGG GAG CAG
SCD3 s	TAT TGA GGG CAT TGG AGC CGG AGT CCA TCG
SCDx as	CTT GTA GTA CCT CCT CTG GAA CAT CAC CAG
CGT s	GAA ATT CAC AAG GAT CAA CC
CGT as	GTC CAT TAA CTG TGC TAT GC
CNX43 1021 s	ACC AAC GGC CCC ACT CTC ACC TAT GTC TCC
CNX43 1350 as	TAA ATC TCC AGG TCA TCA GGC CGA GGT CTG
GAPDH s	GAC CAC CCT GTT GCT GTA GC
GAPDH as	GAG CTG AAC GGG AAG CTC AC
Beta-actin s	TAT GGA ATC CTG TGG CAT CCA TGA AAC TAC
Beta-actin as	GGT GTA AAA CGC AGC TCA GTA ACA GTC CGC

7.3 Abbreviations

AA	Arachidonic acid
cDNA	complementary DNA
CMV	Cytomegalovirus
CoA	Coenzym A
CGT	UDP-galactose:ceramide galactosyltransferase
DM	Double mutant (plp ^{-/-} fads2 ^{-/-} knock out mouse mutant)
DMSO	Dimethyl sulfoxide
DNA	Deoxyribonucleic acid
DMEM	Dulbecco's modified eagle medium
DHA	Docosahexaenoic acid
dNTP	Deoxynucleoside Triphosphate

<i>E. coli</i>	Escherichia coli
EDTA	Ethylene diamine tetra-acetic acid
EGFP	enhanced green fluorescent protein
ER	endoplasmic reticulum
EPA	Eicosapentaenoic acid
ES-cell	Embryonic stem cell
FAD	Fatty acid desaturase
Ganc	Ganciclovir sodium
GAPDH	Glyceraldehyde 3-phosphate dehydrogenase
HGPRT	Hypoxanthin-Guaninphosphoribosyltransferase
HRP	Horseradish peroxidase
IDL	Inter dense line (Myelin membrane)
IgG	Immunoglobulin G
Kb	Kilobase
kDa	Kilodalton
LIF	leukemia inhibitory factor
loxP	locus of X-over P1
M	Molar
mM	millimolar
mg	milligram
min	minute
ml	milliliter
MBP	Myelin basic protein
MDL	Major dense layer (Myelin membrane)
MOG	Myelin oligodendrocyte protein
MAG	Myelin-associated glycoprotein
MSTFA	N-Methyl-N-trimethylsilyl-trifluoroacetamide
MWM	Morris water maze
ng	nanogram
nM	nanomolar
Neo	neomycin phosphotransferase
NCAM	Neural Cell Adhesion Molecule
O.D	optical density
OMgP	Oligodendrocyte-myelin glycoprotein
PCR	polymerase chain reaction
PLP	proteolipid protein
PBS	phosphate-buffered saline
RNA	Ribonucleic acid
SCD	Stearoyl-CoA desaturase
SDS	Sodium dodecyl sulphate
SDS-PAGE	SDS-polyacrylamide gel electrophoresis
Sec	Second
TK	Thymidine kinase
TBE	Tris buffer EDTA
TBS	Tris buffer saline
TBS-T	TBS-Tween

Tris	tris(hydroxymethyl)aminomethane
U	Unit
UDP	Uridine diphosphate
WT	Wild-type
μg	microgram
μl	micro liter
μm	micromolar

8 References

- Aid, S., S. Vancassel, C. Poumes-Ballihaut, S. Chalon, P. Guesnet and M. Laviolle (2003). "Effect of a diet-induced n-3 PUFA depletion on cholinergic parameters in the rat hippocampus." *J Lipid Res* 44(8): 1545-1551.
- Almazan, G., J. M. Vela, E. Molina-Holgado and C. Guaza (2001). "Re-evaluation of nestin as a marker of oligodendrocyte lineage cells." *Microsc Res Tech* 52(6): 753-765.
- Anderson, G. J., W. E. Connor and J. D. Corliss (1990). "Docosahexaenoic acid is the preferred dietary n-3 fatty acid for the development of the brain and retina." *Pediatr Res* 27(1): 89-97.
- Babinet, C. (2000). "Transgenic mice: an irreplaceable tool for the study of mammalian development and biology." *J Am Soc Nephrol* 11 Suppl 16: S88-94.
- Barbarese, E., D. E. Koppel, M. P. Deutscher, C. L. Smith, K. Ainger, F. Morgan and J. H. Carson (1995). "Protein translation components are colocalized in granules in oligodendrocytes." *J Cell Sci* 108 (Pt 8)(Pt 8): 2781-2790.
- Barclay, L. L., G. E. Gibson and J. P. Blass (1982). "Cholinergic therapy of abnormal open-field behavior in thiamin-deficient rats." *J Nutr* 112(10): 1906-1913.
- Bazan, N. G., E. B. Rodriguez de Turco and W. C. Gordon (1993). "Pathways for the uptake and conservation of docosahexaenoic acid in photoreceptors and synapses: biochemical and autoradiographic studies." *Can J Physiol Pharmacol* 71(9): 690-698.
- Bird, T. D., D. F. Farrell and S. M. Sumi (1978). "Brain lipid composition of the shiverer mouse: (genetic defect in myelin development)." *J Neurochem* 31(1): 387-391.
- Blum, M., H. Beier and H. J. Gross (1987). Improved silverstaining of plant proteins, RNA and DNA in polyacrylamid gels. *Electrophoresis* 8: 93-99.
- Birnboim, H. C. and J. Doly (1979). "A rapid alkaline extraction procedure for screening recombinant plasmid DNA." *Nucleic Acids Res* 7(6): 1513-1523.
- Boison, D., H. Bussow, D. D'Urso, H. W. Muller and W. Stoffel (1995). "Adhesive properties of proteolipid protein are responsible for the compaction of CNS myelin sheaths." *J Neurosci* 15(8): 5502-5513.
- Boison, D. and W. Stoffel (1994). "Disruption of the compacted myelin sheath of axons of the central nervous system in proteolipid protein-deficient mice." *Proc Natl Acad Sci U S A* 91(24): 11709-11713.

- Bongarzone, E. R., C. W. Campagnoni, K. Kampf, E. C. Jacobs, V. W. Handley, V. Schonmann and A. T. Campagnoni (1999). "Identification of a new exon in the myelin proteolipid protein gene encoding novel protein isoforms that are restricted to the somata of oligodendrocytes and neurons." *J Neurosci* 19(19): 8349-8357.
- Bosio, A., E. Binczek and W. Stoffel (1996). "Functional breakdown of the lipid bilayer of the myelin membrane in central and peripheral nervous system by disrupted galactocerebroside synthesis." *Proc Natl Acad Sci U S A* 93(23): 13280-13285.
- Bradley, A., M. Evans, M. H. Kaufman and E. Robertson (1984). "Formation of germ-line chimaeras from embryo-derived teratocarcinoma cell lines." *Nature* 309(5965): 255-256.
- Campagnoni, A. T., T. M. Pribyl, C. W. Campagnoni, K. Kampf, S. Amur-Umarjee, C. F. Landry, V. W. Handley, S. L. Newman, B. Garbay and K. Kitamura (1993). "Structure and developmental regulation of Golli-mbp, a 105-kilobase gene that encompasses the myelin basic protein gene and is expressed in cells in the oligodendrocyte lineage in the brain." *J Biol Chem* 268(7): 4930-4938.
- Capecchi, M. R. (1994). Targeted gene replacement. *Sci Am* 270: 52-9.
- Carrie, I., M. Clement, D. de Javel, H. Frances and J. M. Bourre (2000). "Phospholipid supplementation reverses behavioral and biochemical alterations induced by n-3 polyunsaturated fatty acid deficiency in mice." *J Lipid Res* 41(3): 473-480.
- Cizkova, D., M. Cizek, M. Nagyova, L. Slovinska, I. Novotna, S. Jergova, J. Radonak, J. Hlucilova and I. Vanicky (2009). "Enrichment of rat oligodendrocyte progenitor cells by magnetic cell sorting." *J Neurosci Methods* 184(1): 88-94.
- Clarke, S. D. (2001). "Polyunsaturated fatty acid regulation of gene transcription: a molecular mechanism to improve the metabolic syndrome." *J Nutr* 131(4): 1129-1132.
- Compston, A., J. Zajicek, J. Sussman, A. Webb, G. Hall, D. Muir, C. Shaw, A. Wood and N. Scolding (1997). "Glial lineages and myelination in the central nervous system." *J Anat* 190 (Pt 2)(Pt 2): 161-200.
- Dhaunchak, A. S., D. R. Colman and K. A. Nave (2011). "Misalignment of PLP/DM20 transmembrane domains determines protein misfolding in Pelizaeus-Merzbacher disease." *J Neurosci* 31(42): 14961-14971.
- Dhaunchak, A. S. and K. A. Nave (2007). "A common mechanism of PLP/DM20 misfolding causes cysteine-mediated endoplasmic reticulum retention in oligodendrocytes and Pelizaeus-Merzbacher disease." *Proc Natl Acad Sci U S A* 104(45): 17813-17818.

Diehl, H. J., M. Schaich, R. M. Budzinski and W. Stoffel (1986). "Individual exons encode the integral membrane domains of human myelin proteolipid protein." *Proc Natl Acad Sci U S A* 83(24): 9807-9811.

Dittmer, J. C. and R. L. Lester (1964). "A SIMPLE, SPECIFIC SPRAY FOR THE DETECTION OF PHOSPHOLIPIDS ON THIN-LAYER CHROMATOGRAMS." *J Lipid Res* 15: 126-127.

Edgar, J. M., M. McLaughlin, H. B. Werner, M. C. McCulloch, J. A. Barrie, A. Brown, A. B. Faichney, N. Snaidero, K. A. Nave and I. R. Griffiths (2009). "Early ultrastructural defects of axons and axon-glia junctions in mice lacking expression of Cnp1." *Glia* 57(16): 1815-1824.

Eggan, K., H. Akutsu, J. Loring, L. Jackson-Grusby, M. Klemm, W. M. Rideout, 3rd, R. Yanagimachi and R. Jaenisch (2001). "Hybrid vigor, fetal overgrowth, and viability of mice derived by nuclear cloning and tetraploid embryo complementation." *Proc Natl Acad Sci U S A* 98(11): 6209-6214.

Einheber, S., G. Zanazzi, W. Ching, S. Scherer, T. A. Milner, E. Peles and J. L. Salzer (1997). "The axonal membrane protein Caspr, a homologue of neurexin IV, is a component of the septate-like paranodal junctions that assemble during myelination." *J Cell Biol* 139(6): 1495-1506.

El-Husseini, A. E., E. Schnell, D. M. Chetkovich, R. A. Nicoll and D. S. Bredt (2000). "PSD-95 involvement in maturation of excitatory synapses." *Science* 290(5495): 1364-1368.

Fukumura, S., N. Adachi, M. Nagao and H. Tsutsumi (2011). "A novel proteolipid protein 1 gene mutation causing classical type Pelizaeus-Merzbacher disease." *Brain Dev* 33(8): 697-699.

Gallo, V. and R. C. Armstrong (1995). "Developmental and growth factor-induced regulation of nestin in oligodendrocyte lineage cells." *J Neurosci* 15(1 Pt 1): 394-406.

Gordon, J. W. and F. H. Ruddle (1983). "Gene transfer into mouse embryos: production of transgenic mice by pronuclear injection." *Methods Enzymol* 101: 411-433.

Gow, A., V. L. Friedrich, Jr. and R. A. Lazzarini (1994). "Many naturally occurring mutations of myelin proteolipid protein impair its intracellular transport." *J Neurosci Res* 37(5): 574-583.

Gow, A. and R. A. Lazzarini (1996). "A cellular mechanism governing the severity of Pelizaeus-Merzbacher disease." *Nat Genet* 13(4): 422-428.

Gow, A., C. M. Southwood, J. S. Li, M. Pariali, G. P. Riordan, S. E. Brodie, J. Danias, J. M. Bronstein, B. Kachar and R. A. Lazzarini (1999). "CNS myelin and sertoli cell tight junction strands are absent in *Osp/claudin-11* null mice." *Cell* 99(6): 649-659.

Greer, J. M., C. A. Dyer, M. Pakaski, C. Symonowicz and M. B. Lees (1996). "Orientation of myelin proteolipid protein in the oligodendrocyte cell membrane." *Neurochem Res* 21(4): 431-440.

Griffiths, I., M. Klugmann, T. Anderson, D. Yool, C. Thomson, M. H. Schwab, A. Schneider, F. Zimmermann, M. McCulloch, N. Nadon and K. A. Nave (1998). "Axonal swellings and degeneration in mice lacking the major proteolipid of myelin." *Science* 280(5369): 1610-1613.

Grossi, S., S. Regis, R. Biancheri, M. Mort, S. Lualdi, E. Bertini, G. Uziel, O. Boespflug-Tanguy, A. Simonati, F. Corsolini, E. Demir, V. Marchiani, A. Percesepe, F. Stanzial, A. Rossi, C. Vaurs-Barriere, D. N. Cooper and M. Filocamo (2011). "Molecular genetic analysis of the PLP1 gene in 38 families with PLP1-related disorders: identification and functional characterization of 11 novel PLP1 mutations." *Orphanet J Rare Dis* 6: 40.

Gutierrez, R., D. Boison, U. Heinemann and W. Stoffel (1995). "Decompaction of CNS myelin leads to a reduction of the conduction velocity of action potentials in optic nerve." *Neurosci Lett* 195(2): 93-96.

Hanahan, D. (1983). "Studies on transformation of *Escherichia coli* with plasmids." *J Mol Biol* 166(4): 557-580.

Hansen, H. S. and B. Jensen (1985). "Essential function of linoleic acid esterified in acylglucosylceramide and acylceramide in maintaining the epidermal water permeability barrier. Evidence from feeding studies with oleate, linoleate, arachidonate, columbinic acid and alpha-linolenate." *Biochim Biophys Acta* 834(3): 357-363.

Hartman, B. K., H. C. Agrawal, D. Agrawal and S. Kalmbach (1982). "Development and maturation of central nervous system myelin: comparison of immunohistochemical localization of proteolipid protein and basic protein in myelin and oligodendrocytes." *Proc Natl Acad Sci U S A* 79(13): 4217-4220.

Hasty, P., J. Rivera-Perez, C. Chang and A. Bradley (1991). "Target frequency and integration pattern for insertion and replacement vectors in embryonic stem cells." *Mol Cell Biol* 11(9): 4509-4517.

Harlow, E. and D. Lane (1988). *Antibodies, a laboratory manual*, C.S.H. Press.

Hogan, E. L., F. Constantini and E. Lacy (1986). *Manipulating the mouse embryo*. New York, Cold Spring Harbour Laboratory.

He, C., X. Qu, L. Cui, J. Wang and J. X. Kang (2009). "Improved spatial learning performance of fat-1 mice is associated with enhanced neurogenesis and neuritegenesis by docosahexaenoic acid." *Proc Natl Acad Sci U S A* 106(27): 11370-11375.

- Honke, K., Y. Hirahara, J. Dupree, K. Suzuki, B. Popko, K. Fukushima, J. Fukushima, T. Nagasawa, N. Yoshida, Y. Wada and N. Taniguchi (2002). "Paranodal junction formation and spermatogenesis require sulfoglycolipids." *Proc Natl Acad Sci U S A* 99(7): 4227-4232.
- Imgrund, S., D. Hartmann, H. Farwanah, M. Eckhardt, R. Sandhoff, J. Degen, V. Gieselmann, K. Sandhoff and K. Willecke (2009). "Adult ceramide synthase 2 (CERS2)-deficient mice exhibit myelin sheath defects, cerebellar degeneration, and hepatocarcinomas." *J Biol Chem* 284(48): 33549-33560.
- Inagawa, K., S. Watanabe, Y. Tsukada and K. Mikoshiba (1988). "The role of myelination in learning performance observed in two strains of myelin-deficient mutant mice (shiverer and mld)." *Behav Neural Biol* 50(2): 184-192.
- Itakura, K., J. J. Rossi and R. B. Wallace (1984). "Synthesis and use of synthetic oligonucleotides." *Annu Rev Biochem* 53: 323-356.
- Jang, Y. K., J. J. Park, M. C. Lee, B. H. Yoon, Y. S. Yang, S. E. Yang and S. U. Kim (2004). "Retinoic acid-mediated induction of neurons and glial cells from human umbilical cord-derived hematopoietic stem cells." *J Neurosci Res* 75(4): 573-584.
- Jeffrey, B. G., H. S. Weisinger, M. Neuringer and D. C. Mitchell (2001). "The role of docosahexaenoic acid in retinal function." *Lipids* 36(9): 859-871.
- Johansson, C. B., C. Lothian, M. Molin, H. Okano and U. Lendahl (2002). "Nestin enhancer requirements for expression in normal and injured adult CNS." *J Neurosci Res* 69(6): 784-794.
- Jungblut, M., M. C. Tiveron, S. Barral, B. Abrahamsen, S. Knobel, S. Pennartz, J. Schmitz, M. Perraut, F. W. Pfrieder, W. Stoffel, H. Cremer and A. Bosio (2012). "Isolation and characterization of living primary astroglial cells using the new GLAST-specific monoclonal antibody ACSA-1." *Glia* 60(6): 894-907.
- Kalwy, S. A. and R. Smith (1994). "Mechanisms of myelin basic protein and proteolipid protein targeting in oligodendrocytes (review)." *Mol Membr Biol* 11(2): 67-78.
- Karim, S. A., J. A. Barrie, M. C. McCulloch, P. Montague, J. M. Edgar, D. Kirkham, T. J. Anderson, K. A. Nave, I. R. Griffiths and M. McLaughlin (2007). "PLP overexpression perturbs myelin protein composition and myelination in a mouse model of Pelizaeus-Merzbacher disease." *Glia* 55(4): 341-351.
- Kim, T. and S. E. Pfeiffer (1999). "Myelin glycosphingolipid/cholesterol-enriched microdomains selectively sequester the non-compact myelin proteins CNP and MOG." *J Neurocytol* 28(4-5): 281-293.

Kimura, M., M. Sato, A. Akatsuka, S. Nozawa-Kimura, R. Takahashi, M. Yokoyama, T. Nomura and M. Katsuki (1989). "Restoration of myelin formation by a single type of myelin basic protein in transgenic shiverer mice." *Proc Natl Acad Sci U S A* 86(14): 5661-5665.

Klugmann, M., M. H. Schwab, A. Puhlhofer, A. Schneider, F. Zimmermann, I. R. Griffiths and K. A. Nave (1997). "Assembly of CNS myelin in the absence of proteolipid protein." *Neuron* 18(1): 59-70.

Koeppen, A. H. and Y. Robitaille (2002). "Pelizaeus-Merzbacher disease." *J Neuropathol Exp Neurol* 61(9): 747-759.

Koizume, S., S. Takizawa, K. Fujita, N. Aida, S. Yamashita, Y. Miyagi and H. Osaka (2006). "Aberrant trafficking of a proteolipid protein in a mild Pelizaeus-Merzbacher disease." *Neuroscience* 141(4): 1861-1869.

Kondo, T. and M. Raff (2000). "Oligodendrocyte precursor cells reprogrammed to become multipotential CNS stem cells." *Science* 289(5485): 1754-1757.

Kramer, E. M., A. Schardt and K. A. Nave (2001). "Membrane traffic in myelinating oligodendrocytes." *Microsc Res Tech* 52(6): 656-671.

Kramer-Albers, E. M., K. Gehrig-Burger, C. Thiele, J. Trotter and K. A. Nave (2006). "Perturbed interactions of mutant proteolipid protein/DM20 with cholesterol and lipid rafts in oligodendroglia: implications for dysmyelination in spastic paraplegia." *J Neurosci* 26(45): 11743-11752.

Kroepfl, J. F. and M. V. Gardinier (2001). "Mutually exclusive apicobasolateral sorting of two oligodendroglial membrane proteins, proteolipid protein and myelin/oligodendrocyte glycoprotein, in Madin-Darby canine kidney cells." *J Neurosci Res* 66(6): 1140-1148.

Kyte, J. and R. F. Doolittle (1982). "A simple method for displaying the hydropathic character of a protein." *J Mol Biol* 157(1): 105-132.

Laezza, C., J. Wolff and M. Bifulco (1997). "Identification of a 48-kDa prenylated protein that associates with microtubules as 2',3'-cyclic nucleotide 3'-phosphodiesterase in FRTL-5 cells." *FEBS Lett* 413(2): 260-264.

Ledeen, R. (1966). "The chemistry of gangliosides: a review." *J Am Oil Chem Soc* 43(2): 57-66.

Ledeen, R. W. and R. K. Yu (1982). "Gangliosides: structure, isolation, and analysis." *Methods Enzymol* 83: 139-191.

Lee, J., M. Gravel, R. Zhang, P. Thibault and P. E. Braun (2005). "Process outgrowth in oligodendrocytes is mediated by CNP, a novel microtubule assembly myelin protein." *J Cell Biol* 170(4): 661-673.

Lendahl, U., L. B. Zimmerman and R. D. McKay (1990). "CNS stem cells express a new class of intermediate filament protein." *Cell* 60(4): 585-595.

LeVine, S. M. and J. E. Goldman (1988). "Spatial and temporal patterns of oligodendrocyte differentiation in rat cerebrum and cerebellum." *J Comp Neurol* 277(3): 441-455.

Li, C., M. B. Tropak, R. Gerlai, S. Clapoff, W. Abramow-Newerly, B. Trapp, A. Peterson and J. Roder (1994). "Myelination in the absence of myelin-associated glycoprotein." *Nature* 369(6483): 747-750.

Liu, Y., R. Jandacek, T. Rider, P. Tso and R. K. McNamara (2009). "Elevated delta-6 desaturase (FADS2) expression in the postmortem prefrontal cortex of schizophrenic patients: relationship with fatty acid composition." *Schizophr Res* 109(1-3): 113-120.

Lothian, C. and U. Lendahl (1997). "An evolutionarily conserved region in the second intron of the human nestin gene directs gene expression to CNS progenitor cells and to early neural crest cells." *Eur J Neurosci* 9(3): 452-462.

Lothian, C., N. Prakash, U. Lendahl and G. M. Wahlstrom (1999). "Identification of both general and region-specific embryonic CNS enhancer elements in the nestin promoter." *Exp Cell Res* 248(2): 509-519.

Luchtman, D. W. and C. Song (2013). "Cognitive enhancement by omega-3 fatty acids from childhood to old age: Findings from animal and clinical studies." *Neuropharmacology* 64(1): 550-565.

Mansour, S. L., K. R. Thomas and M. R. Capecchi (1988). "Disruption of the proto-oncogene int-2 in mouse embryo-derived stem cells: a general strategy for targeting mutations to non-selectable genes." *Nature* 336(6197): 348-352.

Mathisen, P. M., S. Pease, J. Garvey, L. Hood and C. Readhead (1993). "Identification of an embryonic isoform of myelin basic protein that is expressed widely in the mouse embryo." *Proc Natl Acad Sci U S A* 90(21): 10125-10129.

Meinzinger, S. (2004) *Biochemische und molekularbiologische Studien zur Funktionsanalyse der UDP-Galaktose: Ceramid Galaktosyltransferase*, Universität zu Köln.

Minuk, J. and P. E. Braun (1996). "Differential intracellular sorting of the myelin-associated glycoprotein isoforms." *J Neurosci Res* 44(5): 411-420.

Mitaku, S., T. Hirokawa and T. Tsuji (2002). "Amphiphilicity index of polar amino acids as an aid in the characterization of amino acid preference at membrane-water interfaces." *Bioinformatics* 18(4): 608-616.

- Miura, M., T. Tamura, A. Aoyama and K. Mikoshiba (1989). "The promoter elements of the mouse myelin basic protein gene function efficiently in NG108-15 neuronal/glia cells." *Gene* 75(1): 31-38.
- Miyao, Y., K. Shimizu, M. Tamura, H. Akita, K. Ikeda, E. Mabuchi, H. Kishima, T. Hayakawa and K. Ikenaka (1997). "Usefulness of a mouse myelin basic protein promoter for gene therapy of malignant glioma: myelin basic protein promoter is strongly active in human malignant glioma cells." *Jpn J Cancer Res* 88(7): 678-686.
- Montag, D., K. P. Giese, U. Bartsch, R. Martini, Y. Lang, H. Bluthmann, J. Karthigasan, D. A. Kirschner, E. S. Wintergerst, K. A. Nave and *et al.* (1994). "Mice deficient for the myelin-associated glycoprotein show subtle abnormalities in myelin." *Neuron* 13(1): 229-246.
- Montgomery, D. L. (1994). "Astrocytes: form, functions, and roles in disease." *Vet Pathol* 31(2): 145-167.
- Morris, R. (1984). "Developments of a water-maze procedure for studying spatial learning in the rat." *J Neurosci Methods* 11(1): 47-60.
- Mutschler, E. (1991). *Arzneimittelwirkung. Lehrbuch der Pharmakologie und Toxikologie.* Stuttgart, Wissenschaftliche Verlagsgesellschaft mbH.
- Nagara, H., K. Suzuki and J. Tateishi (1983). "Radial component of central myelin in shiverer mouse." *Brain Res* 263(2): 336-339.
- Nakajima, K., K. Ikenaka, T. Kagawa, J. Aruga, J. Nakao, K. Nakahira, C. Shiota, S. U. Kim and K. Mikoshiba (1993). "Novel isoforms of mouse myelin basic protein predominantly expressed in embryonic stage." *J Neurochem* 60(4): 1554-1563.
- Nakamura, M. T. and T. Y. Nara (2004). "Structure, function, and dietary regulation of delta6, delta5, and delta9 desaturases." *Annu Rev Nutr* 24: 345-376.
- Nave, K. A., C. Lai, F. E. Bloom and R. J. Milner (1987). "Splice site selection in the proteolipid protein (PLP) gene transcript and primary structure of the DM-20 protein of central nervous system myelin." *Proc Natl Acad Sci U S A* 84(16): 5665-5669.
- Newman, S., K. Kitamura and A. T. Campagnoni (1987). "Identification of a cDNA coding for a fifth form of myelin basic protein in mouse." *Proc Natl Acad Sci U S A* 84(3): 886-890.
- Norton, W. T. and S. E. Poduslo (1973). "Myelination in rat brain: method of myelin isolation." *J Neurochem* 21(4): 749-757.
- Norton W, Cammer W (1984) Isolation and characterization of myelin. In: *Myelin* (Morell P, ed), pp 147-180. New York: Plenum.

Osada, J. and N. Maeda (1998). "Preparation of knockout mice." *Methods Mol Biol* 110: 79-92.

Ozias, M. K., S. E. Carlson and B. Levant (2007). "Maternal parity and diet (n-3) polyunsaturated fatty acid concentration influence accretion of brain phospholipid docosahexaenoic acid in developing rats." *J Nutr* 137(1): 125-129.

Paul Carter (1986). Site-directed mutagenesis *Biochem. J.* (1986) 237, 1-7

Pettitt, S. J., Q. Liang, X. Y. Rairdan, J. L. Moran, H. M. Prosser, D. R. Beier, K. C. Lloyd, A. Bradley and W. C. Skarnes (2009). "Agouti C57BL/6N embryonic stem cells for mouse genetic resources." *Nat Methods* 6(7): 493-495.

Poggel, C. (2000) Genexpressions-Profil einer dysmyelinisierenden Doppel *knockout*-Mausmutante (*mbp*^{-/-} *plp*^{-/-}) und *Rescue*-Versuch des normalen Phänotyps, Universität zu Köln.

Pfeiffer, S. E., A. E. Warrington and R. Bansal (1993). "The oligodendrocyte and its many cellular processes." *Trends Cell Biol* 3(6): 191-197.

Pfrieger, F. W. and B. A. Barres (1995). "What the fly's glia tell the fly's brain." *Cell* 83(5): 671-674.

Poltorak, M., R. Sadoul, G. Keilhauer, C. Landa, T. Fahrig and M. Schachner (1987). "Myelin-associated glycoprotein, a member of the L2/HNK-1 family of neural cell adhesion molecules, is involved in neuron-oligodendrocyte and oligodendrocyte-oligodendrocyte interaction." *J Cell Biol* 105(4): 1893-1899.

Rasband, M. N., J. Tayler, Y. Kaga, Y. Yang, C. Lappe-Siefke, K. A. Nave and R. Bansal (2005). "CNP is required for maintenance of axon-glia interactions at nodes of Ranvier in the CNS." *Glia* 50(1): 86-90.

Readhead, C., A. Schneider, I. Griffiths and K. A. Nave (1994). "Premature arrest of myelin formation in transgenic mice with increased proteolipid protein gene dosage." *Neuron* 12(3): 583-595.

Reardon, H. T., A. T. Hsieh, W. Jung Park, K. S. Kothapalli, J. C. Anthony, P. W. Nathanielsz and J. Thomas Brenna (2012). "Dietary long-chain polyunsaturated fatty acids upregulate expression of FADS3 transcripts." *Prostaglandins Leukot Essent Fatty Acids*.

Reynolds, R. and G. P. Wilkin (1988). "Development of macroglial cells in rat cerebellum. II. An in situ immunohistochemical study of oligodendroglial lineage from precursor to mature myelinating cell." *Development* 102(2): 409-425.

Roqueta-Rivera, M., C. K. Stroud, W. M. Haschek, S. J. Akare, M. Segre, R. S. Brush, M. P. Agbaga, R. E. Anderson, R. A. Hess and M. T. Nakamura (2010). "Docosahexaenoic acid

supplementation fully restores fertility and spermatogenesis in male delta-6 desaturase-null mice." *J Lipid Res* 51(2): 360-367.

Saher, G., B. Brugger, C. Lappe-Siefke, W. Mobius, R. Tozawa, M. C. Wehr, F. Wieland, S. Ishibashi and K. A. Nave (2005). "High cholesterol level is essential for myelin membrane growth." *Nat Neurosci* 8(4): 468-475.

Saher, G., S. Quintes and K. A. Nave (2011). "Cholesterol: a novel regulatory role in myelin formation." *Neuroscientist* 17(1): 79-93.

Salvati, S., F. Natali, L. Attorri, R. Di Benedetto, F. Leonardi, A. Di Biase, F. Ferri, S. Fortuna, P. Lorenzini, M. Sanchez, L. Ricceri and L. Vitelli (2008). "Eicosapentaenoic acid stimulates the expression of myelin proteins in rat brain." *J Neurosci Res* 86(4): 776-784.

Salvati, S., F. Natali, L. Attorri, C. Raggi, A. Di Biase and M. Sanchez (2004). "Stimulation of myelin proteolipid protein gene expression by eicosapentaenoic acid in C6 glioma cells." *Neurochem Int* 44(5): 331-338.

Schafer, D. P., R. Bansal, K. L. Hedstrom, S. E. Pfeiffer and M. N. Rasband (2004). "Does paranode formation and maintenance require partitioning of neurofascin 155 into lipid rafts?" *J Neurosci* 24(13): 3176-3185.

Schaich, M., R. M. Budzinski and W. Stoffel (1986). "Cloned proteolipid protein and myelin basic protein cDNA. Transcription of the two genes during myelination." *Biol Chem Hoppe Seyler* 367(8): 825-834.

Schliess, F. and W. Stoffel (1991). "Evolution of the myelin integral membrane proteins of the central nervous system." *Biol Chem Hoppe Seyler* 372(9): 865-874.

Schneider, A., H. Lander, G. Schulz, H. Wolburg, K. A. Nave, J. B. Schulz and M. Simons (2005). "Palmitoylation is a sorting determinant for transport to the myelin membrane." *J Cell Sci* 118(Pt 11): 2415-2423.

Schneider, A., P. Montague, I. Griffiths, M. Fanarraga, P. Kennedy, P. Brophy and K. A. Nave (1992). "Uncoupling of hypomyelination and glial cell death by a mutation in the proteolipid protein gene." *Nature* 358(6389): 758-761.

Schulte, S. and W. Stoffel (1993). "Ceramide UDPgalactosyltransferase from myelinating rat brain: purification, cloning, and expression." *Proc Natl Acad Sci U S A* 90(21): 10265-10269.

Seitelberger, F. (1995). "Neuropathology and genetics of Pelizaeus-Merzbacher disease." *Brain Pathol* 5(3): 267-273.

Shimomura, O., F. H. Johnson and Y. Saiga (1962). "Extraction, purification and properties of aequorin, a bioluminescent protein from the luminous hydromedusan, *Aequorea*." *J Cell Comp Physiol* 59: 223-239.

Siegel GJ, Agranoff BW, Albers RW, *et al.*, editors. *Basic Neurochemistry: Molecular, Cellular and Medical Aspects*. 6th edition. Philadelphia: Lippincott-Raven; 1999.

Simons, M., E. M. Kramer, P. Macchi, S. Rathke-Hartlieb, J. Trotter, K. A. Nave and J. B. Schulz (2002). "Overexpression of the myelin proteolipid protein leads to accumulation of cholesterol and proteolipid protein in endosomes/lysosomes: implications for Pelizaeus-Merzbacher disease." *J Cell Biol* 157(2): 327-336.

Smith, P. K., R. I. Krohn, G. T. Hermanson, A. K. Mallia, F. H. Gartner, M. D. Provenzano, E. K. Fujimoto, N. M. Goeke, B. J. Olson and D. C. Klenk (1985). "Measurement of protein using bicinchoninic acid." *Anal Biochem* 150(1): 76-85.

Stockard, J. E., M. D. Saste, V. J. Benford, L. Barness, N. Auestad and J. D. Carver (2000). "Effect of docosahexaenoic acid content of maternal diet on auditory brainstem conduction times in rat pups." *Dev Neurosci* 22(5-6): 494-499.

Stoffel, W., D. Boison and H. Bussow (1997). "Functional analysis *in vivo* of the double mutant mouse deficient in both proteolipid protein (PLP) and myelin basic protein (MBP) in the central nervous system." *Cell Tissue Res* 289(2): 195-206.

Stoffel, W., H. Giersiefen, H. Hillen, W. Schroeder and B. Tunggal (1985). "Amino-acid sequence of human and bovine brain myelin proteolipid protein (lipophilin) is completely conserved." *Biol Chem Hoppe Seyler* 366(7): 627-635.

Stoffel, W., H. Hillen and H. Giersiefen (1984). "Structure and molecular arrangement of proteolipid protein of central nervous system myelin." *Proc Natl Acad Sci U S A* 81(16): 5012-5016.

Stoffel, W., B. Holz, B. Jenke, E. Binczek, R. H. Gunter, C. Kiss, I. Karakesisoglou, M. Thevis, A. A. Weber, S. Arnhold and K. Addicks (2008). "Delta6-desaturase (FADS2) deficiency unveils the role of omega3- and omega6-polyunsaturated fatty acids." *EMBO J* 27(17): 2281-2292.

Stoffel, W., W. Schroeder, H. Hillen and R. Deutzmann (1982). "Analysis of the primary structure of the strongly hydrophobic brain myelin proteolipid apoprotein (lipophilin). Isolation and amino acid sequence determination of proteolytic fragments." *Hoppe Seylers Z Physiol Chem* 363(9): 1117-1131.

Stroud, C. K., T. Y. Nara, M. Roqueta-Rivera, E. C. Radlowski, P. Lawrence, Y. Zhang, B. H. Cho, M. Segre, R. A. Hess, J. T. Brenna, W. M. Haschek and M. T. Nakamura (2009).

"Disruption of FADS2 gene in mice impairs male reproduction and causes dermal and intestinal ulceration." *J Lipid Res* 50(9): 1870-1880.

Swanton, E., S. High and P. Woodman (2003). "Role of calnexin in the glycan-independent quality control of proteolipid protein." *EMBO J* 22(12): 2948-2958.

Tanimoto, Y., S. Iijima, Y. Hasegawa, Y. Suzuki, Y. Daitoku, S. Mizuno, T. Ishige, T. Kudo, S. Takahashi, S. Kunita, F. Sugiyama and K. Yagami (2008). "Embryonic stem cells derived from C57BL/6J and C57BL/6N mice." *Comp Med* 58(4): 347-352.

Thomas, K. R. and M. R. Capecchi (1986). "Introduction of homologous DNA sequences into mammalian cells induces mutations in the cognate gene." *Nature* 324(6092): 34-38.

Tinoco, J. (1982). "Dietary requirements and functions of alpha-linolenic acid in animals." *Prog Lipid Res* 21(1): 1-45.

Trapp, B. D. and J. Bernsohn (1978). "Essential fatty acid deficiency and CNS myelin. Biochemical and morphological observations." *J Neurol Sci* 37(3): 249-266.

Uschkureit, T. (2000). Struktur-Funktionsanalyse der Myelinmembran von Axonen des zentralen Nervensystems durch Gen-Ablation mittels homologer Rekombination. Mat-Nat faculty, Universität zu Köln.

Uschkureit, T., O. Sporkel, J. Stracke, H. Bussow and W. Stoffel (2000). "Early onset of axonal degeneration in double (plp^{-/-}mag^{-/-}) and hypomyelinoses in triple (plp^{-/-}mbp^{-/-}mag^{-/-}) mutant mice." *J Neurosci* 20(14): 5225-5233.

Vinot, N., M. Jouin, A. Lhomme-Duchadeuil, P. Guesnet, J. M. Alessandri, F. Aujard and F. Pifferi (2011). "Omega-3 fatty acids from fish oil lower anxiety, improve cognitive functions and reduce spontaneous locomotor activity in a non-human primate." *PLoS One* 6(6): e20491.

Wahle, S. and W. Stoffel (1998). "Cotranslational integration of myelin proteolipid protein (PLP) into the membrane of endoplasmic reticulum: analysis of topology by glycosylation scanning and protease domain protection assay." *Glia* 24(2): 226-235.

Wallace, J. E., E. E. Krauter and B. A. Campbell (1980). "Motor and reflexive behavior in the aging rat." *J Gerontol* 35(3): 364-370.

Webster, H. D., C. G. Palkovits, G. L. Stoner, J. T. Favilla, D. E. Frail and P. E. Braun (1983). "Myelin-associated glycoprotein: electron microscopic immunocytochemical localization in compact developing and adult central nervous system myelin." *J Neurochem* 41(5): 1469-1479.

Weimbs, T., T. Dick, W. Stoffel and E. Boltshauser (1990). "A point mutation at the X-chromosomal proteolipid protein locus in Pelizaeus-Merzbacher disease leads to disruption of myelinogenesis." *Biol Chem Hoppe Seyler* 371(12): 1175-1183.

- Weimbs, T. and W. Stoffel (1992). "Proteolipid protein (PLP) of CNS myelin: positions of free, disulfide-bonded, and fatty acid thioester-linked cysteine residues and implications for the membrane topology of PLP." *Biochemistry* 31(49): 12289-12296.
- Weisinger, H. S., A. J. Vingrys and A. J. Sinclair (1996). "The effect of docosahexaenoic acid on the electroretinogram of the guinea pig." *Lipids* 31(1): 65-70.
- Werner, H., M. Jung, M. Klugmann, M. Sereda, I. R. Griffiths and K. A. Nave (1998). "Mouse models of myelin diseases." *Brain Pathol* 8(4): 771-793.
- Werner, H. B., K. Kuhlmann, S. Shen, M. Uecker, A. Schardt, K. Dimova, F. Orfaniotou, A. Dhaunchak, B. G. Brinkmann, W. Mobius, L. Guarente, P. Casaccia-Bonnel, O. Jahn and K. A. Nave (2007). "Proteolipid protein is required for transport of sirtuin 2 into CNS myelin." *J Neurosci* 27(29): 7717-7730.
- Wight, P. A., C. S. Duchala, C. Readhead and W. B. Macklin (1993). "A myelin proteolipid protein-LacZ fusion protein is developmentally regulated and targeted to the myelin membrane in transgenic mice." *J Cell Biol* 123(2): 443-454.
- Wood, D. D. and M. A. Moscarello (1989). "The isolation, characterization, and lipid-aggregating properties of a citrulline containing myelin basic protein." *J Biol Chem* 264(9): 5121-5127.
- Yehuda, S., S. Rabinovitz, R. L. Carasso and D. I. Mostofsky (2002). "The role of polyunsaturated fatty acids in restoring the aging neuronal membrane." *Neurobiol Aging* 23(5): 843-853.
- Yehuda, S., S. Rabinovitz and D. I. Mostofsky (1999). "Essential fatty acids are mediators of brain biochemistry and cognitive functions." *J Neurosci Res* 56(6): 565-570.
- Yool, D. A., J. M. Edgar, P. Montague and S. Malcolm (2000). "The proteolipid protein gene and myelin disorders in man and animal models." *Hum Mol Genet* 9(6): 987-992.
- Youdim, K. A., A. Martin and J. A. Joseph (2000). "Essential fatty acids and the brain: possible health implications." *Int J Dev Neurosci* 18(4-5): 383-399.
- Zimmerman, L., B. Parr, U. Lendahl, M. Cunningham, R. McKay, B. Gavin, J. Mann, G. Vassileva and A. McMahon (1994). "Independent regulatory elements in the nestin gene direct transgene expression to neural stem cells or muscle precursors." *Neuron* 12(1): 11-24.

Zusammenfassung

Myelinscheiden des zentralen Nervensystems werden von Oligodendrozyten gebildet und bestehen zu 80% aus Lipiden und zu 20% aus Proteinen. Die Myelinbildung stellt einen komplexen und konservierten Prozeß dar. Kommt es zu pathologischen Veränderungen im Ablauf, die eine fehlerhafte Zusammensetzung der Protein- oder Lipidkomponente bedingen, kann dies zu funktionalen Störungen des Myelins führen.

Die hier vorgestellte Arbeit kann in zwei Kerngebiete aufgeteilt werden:

A) Die Untersuchung der Rolle der Cys-Reste des Proteolipid Protein (PLP/Dm20) auf die Myelinstruktur und -funktion.

B) Die Rolle von PLP/Dm20 und den mehrfach ungesättigten Fettsäuren (polyunsaturated fatty acids, PUFAs) bei der Morphologie und der Physiologie des Myelins im ZNS.

A) Das PLP ist stark konserviert und macht den größten Proteinanteil des ZNS Myelins aus. Punktmutationen im PLP sind bekannt dafür, verschiedene Formen von PMD/SPG2 dysmyelinisierende Leukodystrophien in Mensch und Maus zu verursachen. Einige Punktmutationen in PLP werden im Zusammenhang mit einem gestörten Plasmamembrantransport von PLP/Dm20 in den Oligodendrozyten und dem jeweiligen Krankheitsgrad der PMD diskutiert.

PLP und seine Isoform Dm20 besitzen 14 beziehungsweise 12 Cys-Reste, die in die posttranslationale S-Acylierung und die Bildung von zwei Disulfid Brücken einbezogen sind. Diese Arbeit sollte zum besseren Verständnis der Bedeutung der Cys-Reste in PLP/Dm20 führen. Dafür wurde eine PLP/Dm20 Mutante verwendet, in der die Cys- durch Ser-Reste ausgetauscht wurden (i.e. Mut-PLP/Dm20). *In silico* Analysen zeigten, dass Mut-PLP und Mut-Dm20 sowohl verminderte Transmembran-Strukturen als auch reduzierte hydrophobe Eigenschaften besitzen, während mit Hilfe der *in vivo* und *in vitro* Analysen ein verringertes Zelloberflächen Targeting nachgewiesen wurde.

Um die Rolle von Mut-PLP in der Myelinisierung früher embryonaler Stadien zu verstehen, sollte durch Vorkerninjektion eine Mauslinie generiert werden, die einen Nestin Enhancer und ein MBP Promotor regulatorisches Element zusammen mit der Mut-PLP cDNA trägt. Zudem sollte eine knock-in Mausmutante generiert werden, die keine Disulfidbrücken in PLP/Dm20 trägt, um die Rolle der Disulfid-Brücken in PLP zu verstehen.

B) PLP ist ein integrales Myelinmembranprotein, PUFAs sind Bestandteile von Phospholipiden, den beiden kritischen strukturellen Komponenten der ZNS Myelinmembran. Zum besseren Verständnis der signifikanten Rolle von PLP und den PUFAs und deren Auswirkung auf das ZNS wurden Untersuchungen an der *plp*^{-/-} *fads*^{-/-} transgenen Doppelmutante (DM) durchgeführt. Die DM wurde durch Kreuzung generiert und auf genomischer-, sowie Transkriptions- und Translationsebene bestätigt.

Die DM zeigt einen schweren kataleptischen Zustand mit einem milden Tremor und Krämpfen ab dem fünften Lebensmonat, sowie eine drastisch verkürzte Lebensdauer im Vergleich zu den Einzelknockout Mutanten (*plp*^{-/-} und *fads*^{-/-}) und dem Wildtyp.

Die Fettsäureanalyse des Gehirns der DM und des ZNS Myelins zeigten nur teilweise verminderte Docosahexaensäure (DHA) Konzentration (40-50%), was andeutet, dass DHA stark konserviert ist und deswegen in den Membranstrukturen des ZNS zurückbehalten wird.

Erstaunlicherweise wurde eine ungewöhnliche PUFA, die Eisosatriensäure (20:3) gefunden, die möglicherweise die nicht mehr vorhandene Arachidonsäure ersetzt. Weitere Analysen des DM Genexpressionsprofils zeigten keine signifikanten Unterschiede der Myelinproteine und Desaturasen. Das erlaubt den Schluß, dass die Abwesenheit von PLP und den PUFAS zu keiner Veränderung der myelinbezogenen Proteine führt.

Die Morphologie des ZNS Myelins ist in der DM Maus stark verändert, und weist Hypomyelinisierung und Verlust der Kompaktheit des Myelins auf.

Das retinale Pigmentepithel zeigt keinerlei morphologischen Veränderungen. Die durch das ERG nachgewiesene retinale Funktion zeigt einen Abfall im a-Wellen Signal, was auf Veränderungen der visuellen Funktionen hinweist.

Verhaltensphysiologische Studien, die unter anderem mit Hilfe des Rota Rod und der Water Maze durchgeführt wurden, zeigten partielle, aber keine signifikanten Defekte in der neuromotorischen Koordination/Funktion. Durch die Water Maze wurden zudem signifikante Defekte in den kognitiven Fähigkeiten (i.e. die Raumkognition/Lernfähigkeit und Erinnerungsvermögen) nachgewiesen. Die Veränderungen in der Verhaltensphysiologie und der reduzierten Lebensdauer korrelieren möglicherweise mit der gestörten Myelinmorphologie und der Hypomyelinisierung des ZNS.

Abstract

The CNS myelin sheath is an extension of the oligodendrocyte plasma membrane and is composed of 80% lipid and 20% protein. Myelin formation is a very sophisticated and highly conserved process, any disturbance of myelin protein or lipid composition has a strong impact on myelin biogenesis and myelin phenotype, which often results in CNS myelin pathology. The work presented here is divided into two parts: A. An investigation of the role of proteolipid protein (PLP/Dm20) Cys residues in myelin structure and function, and B. The role of PLP/Dm20 and polyunsaturated fatty acids (PUFAs) in CNS myelin morphology and CNS physiology.

A. PLP is highly conserved and is the most abundant protein of CNS myelin. Also, point mutations in PLP are known to cause a variety of mild to severe PMD/SPG2 dysmyelinating leukodystrophies both in human and in mice. Some PLP point mutations are directly correlated to the perturbed plasma membrane trafficking of PLP/Dm20 in oligodendrocytes and correlate with the severity of PMD. PLP and its isoform Dm20 have 14 and 12 Cys residues, respectively, and are involved in post-translational S-acylation and the formation of two disulfide bridges. The work presented within this thesis furthers the understanding of the role of the Cys residues in PLP/Dm20. We analysed PLP/Dm20 Cys residue function by replacing Cys residues in PLP/Dm20 with Ser residues (i.e., Mut-PLP/Dm20). *In silico* analyses predicted that the Mut-PLP and Dm20 have impaired transmembrane structure and reduced hydrophobic properties, supported by our *in vivo* and *in vitro* analysis which revealed perturbed cell surface targeting of the mutant proteins. Furthermore, in order to understand the role of Mut-PLP in CNS at early embryonic stages, a transgenic mouse mutant is being generated via pronuclear injection of a transgene composed of a Nestin enhancer and MBP promoter regulatory elements along with Mut-PLP cDNA, on a PLP negative genomic background. In addition, to understand the role of di-sulfide bridges in PLP; a knock-in mouse mutant is being generated in which the disulfide bridges of PLP/Dm20 have been deleted.

B. PLP is an integral myelin membrane protein, and PUFAs are constituents of phospholipids, which are critical structural components of the CNS myelin membrane. In this thesis, we have expanded the understanding of the significant role of PLP and PUFAs and their impact in the CNS by phenotyping the *plp*^{-/-}*fads2*^{-/-} double knock-out mouse model (DM). The DM has been generated and validated on a genomic, RNA and protein level confirming lack of PLP and *Fads2* which is a key enzyme for endogenous PUFAs synthesis. The DM exhibited a profound behavioral cataleptic state with mild tremor and seizures starting from 5 months age, and had a significantly reduced life span, compared to the single mutants (*plp*^{-/-} and *fads2*^{-/-}) and wild-type counterparts.

In the brain and CNS myelin of the DM mice, PUFAs analysis revealed only partially depleted docosahexanoic acid (DHA) levels (40-50%) suggesting that DHA is highly regulated and/or is compensated for depleted PUFAs and was retained tenaciously in membrane structures of the CNS. Intriguingly, an unusual PUFA, eicosatrienoic acid (20:3) was detected, which may substitute for the observed depletion of arachidonic acid. Further analyses of the gene expression profile in the DM brain revealed no significant differences among myelin membrane proteins, desaturases and other myelin specific proteins, thus suggesting no alteration of these proteins in the absence of PLP and PUFAs.

The DM mice showed a massive alteration in morphology of the CNS myelin manifesting as hypomyelination and a loss of myelin compaction around axons. In retinal electron micrographs, the retinal pigment epithelium (RPE) region showed no major significant morphological alterations. Retinal function, as assessed by ERG, revealed a decrease in a-wave signals suggesting defects in visual functions. Behavioral physiology studies, as assessed by the rota-rod task and Morris water maze and other similar tasks, showed partial but significant defects in neuromotor coordination/functions. The Morris water maze also revealed significant defects in cognitive ability (i.e., spatial acquisition/learning and in the reference memory). Alterations in behavioral physiology and the reduced lifespan in DM mice may be correlated with the disrupted myelin morphology and hypomyelination of CNS.

Erklärung

Ich versichere, dass ich die von mir vorgelegte Dissertation selbständig angefertigt, die benutzten Quellen und Hilfsmittel vollständig angegeben und die Stellen der Arbeit – einschließlich Tabellen, Karten und Abbildungen –, die anderen Werken im Wortlaut oder dem Sinn nach entnommen sind, in jedem Einzelfall als Entlehnung kenntlich gemacht habe; dass diese Dissertation noch keiner anderen Fakultät oder Universität zur Prüfung vorgelegen hat; dass sie noch nicht veröffentlicht worden ist sowie, dass ich eine solche Veröffentlichung vor Abschluss des Promotionsverfahrens nicht vornehmen werde. Die Bestimmungen der Promotionsordnung sind mir bekannt. Die von mir vorgelegte Dissertation ist von Prof. Dr. Dr. Dr. h.c. mult. Stoffel betreut worden.

Keine Teilpublikationen.

Raju Chintha

Köln, den 15.10.2012

Curriculum vitae

Name	Raju Chintha
Current Address (During PhD)	Gleueler Straße 88A, 50931 Koeln, Germany
Place of birth	Warangal, AP, India
Date of Birth, Family status	Aug.1983, Single
Nationality	Indian

Academic Qualification

- (1999 - 2001)** **PUC (Board of Intermediate Education)**
Lal Bahadur College, Warangal Dist., A.P, INDIA
- (2001 - 2004)** **Bachelor of Science** (Biotechnology, Zoology, Chemistry)
Kakatiya University, A.P, INDIA
- (2004 - 2006)** **Master of Science** (Organic Chemistry)
Kakatiya University, AP, INDIA
(M.Sc Thesis Title: Synthesis, Characterization and Biological evaluation, of some 2, 3 substituted -1, 3-Thiazolidin-4-one Derivatives)
- (11/2008 – 12/2012)** **PhD / Doctorate**
University of Cologne, Germany
Supervisor: Prof. Dr. Dr. Dr. h.c. mult. Wilhelm Stoffel.
PhD dissertation title: Role of proteolipid protein (PLP/Dm20) and polyunsaturated fatty acids (PUFAs) in normal and pathological central nervous system (CNS)

Research experience

- 10/2006 - 10/2007 University of Bonn, Germany
M.Sc in Life Science Informatics (Completed only 1st Year)
- 12/2006 - 02/2007 Infill Communications, Bonn, Germany
(Assistant/Student Medical Writer on cardiovascular drugs)
- 07/2007 - 03/2008 Max-Planck Institute for Plant Breeding, Koeln, Germany
(Research Fellow, Project title: Sub-classification of Arabidopsis and tomato papain-like proteases by activity-based profiling and homology modeling)
- 03/2008 - 11/2008 Max-Planck Institute for Neurological Research, Germany
(Research Fellow, Project title: Small Molecule Inhibitors identification and High throughput screening for treating Non-Small Cell Lung Cancer)
- 11/2008 - 12/2012 Molecular Neuroscience Group, Biochemistry Department,
Medical Faculty, University of Cologne, Germany
PhD dissertation research and academic work